Journal of Electroceramics, 11, 5–66, 2003

Ferroelectric Materials for Microwave Tunable Applications

A.K. TAGANTSEV, V.O. SHERMAN, K.F. ASTAFIEV, J. VENKATESH & N. SETTER
Ceramics Laboratory, Swiss Federal Institute of Technology, EPFL, 1015 Lausanne, Switzerland

Submitted June 26, 2003; Revised November 16, 2003; Accepted November 18, 2003

Abstract. A review of the properties of ferroelectric materials that are relevant to microwave tunable devices is presented: we discuss the theory of dielectric response of tunable bulk materials and thin films; the experimental results from the literature and from own work are reviewed; the correspondence between the theoretical results and the measured properties of tunable materials is critically analyzed; nominally pure, real (defected), and composite bulk materials and thin films are addressed. In addition, techniques for characterization of tunable ferroelectrics and applications of these materials are briefly presented.

Keywords: microwave, ferroelectrics, tunability, dielectric loss, tunable materials

TABLE OF CONTENTS

1. Introduction

The recognition of the potential usefulness of ferroelectric materials in tunable high-frequency devices dates back over 40 years [1]. However, due to various reasons related to both device electronics and materials technology, it is only in the past decade that intensive development efforts are being made in this direction. The main driving force for this resurgent interest is the potential for substantial miniaturization of microwave (MW) components and systems (accompanied also by a large cost reduction) and the potential for integration with microelectronic circuits due to the development of thin and thick film ferroelectric technology. A number of review papers [2–5] have appeared recently, covering different aspects of tunable ferroelectric materials and their applications. However, the recent theoretical, experimental and technical developments (e.g. investigations of tunable composites) necessitate revisiting the subject. In the present work, we present a comprehensive updated discussion of the main issues of tunable ferroelectric materials.

The desired material properties are quite well known: a high tunability and low dielectric losses are required. The underlying physics has been already developed (see e.g. [2, 6]), but its applicability to present day problems is not straight forward; While materials are being developed, questions arise such as: Is it preferable to use the tunable material in its paraelectric phase, in its ferroelectric phase or at about the phase transition temperature? What is the interplay between dielectric constant and tunability? Is it possible to have a material with an intermediate permittivity yet a high tunability? Can a material be of a high permittivity yet of low losses? Are high tunability and low loss contradictory? What is the low-loss limit one can expect and how will it vary with frequency and temperature? Can mixing of a low loss dielectric and a ferroelectric result in an overall low loss without deteriorating strongly the tunability of the composite? Why are thin films often more lossy than bulk materials of similar compositions? Are loss mechanisms similar in thin films and in bulk single crystals? Why do films often exhibit lower permittivity and tunability than bulk materials of a similar composition and is this phenomenon general and inevitable? Other questions are related to the significance of the measurement results: Is the measurement of losses at kHz frequencies useful for the evaluation of the performance of the material at GHz frequencies? Is the measured tunability at kHz frequencies indicative of the tunability at MW frequencies? Are losses measured at zero bias field indicative of losses under field?

In the following review some considerations and answers to the above questions are presented: First, we summarize the principal applications of tunable ferroelectrics in order to estimate the needed performance and through it the details of the needed properties. Next, the theory of dielectric response in tunable ferroelectrics (permittivity, tunability and dielectric

losses) without and under dc field is presented and discussed, first for ideal ferroelectrics, then for real materials (including defects) and for multiphase materials (composites). The evaluation methods of the relevant properties are described and the significance of the obtained results is assessed. Experimental work on properties of modern tunable ferroelectrics is summarized, based on results reported in the literature and on results at the authors' laboratory. These results are discussed in the context of the theory.

2. Applications

The applications of tunable ferroelectrics in microwave devices are summarized below in order to estimate the performance that is required from the materials. A detailed discussion of designs and applications of ferroelectric based microwave components can be found in Refs. [2, 3, 5, 7, 8].

For a microwave engineer the main attraction of ferroelectric materials is the strong dependence of their dielectric permittivity ε on the applied bias electric field E_0. This characteristic is commonly described by the *tunability n* defined as the ratio of the dielectric permittivity of the material at zero electric field to its permittivity at some non-zero electric field, as expressed by Eq. (2.1). The *relative tunability* (n_r) is defined by Eq. (2.2).

$$n = \frac{\varepsilon(0)}{\varepsilon(E_0)} \tag{2.1}$$

$$n_r = \frac{\varepsilon(0) - \varepsilon(E_0)}{\varepsilon(0)} = 1 - \frac{1}{n} \tag{2.2}$$

An example of dielectric constant—electric field dependence for a bulk ferroelectric material ((Ba,Sr)TiO_3 [9]) is presented in Fig. 1.

The dielectric loss in ferroelectrics is not as small as that of common microwave dielectric materials and the loss tangent ($\tan\delta$) is an important characteristic of the material, which should be taken into account in the device design. The temperature dependence of the dielectric permittivity over the operating temperature interval is another important issue: this is of particular concern in the vicinity of the ferroelectric transition temperature, in which the material exhibits a high but strongly temperature dependent tunability. The trend "the higher the dielectric constant, the higher the tunability, loss, and temperature dependence of the dielectric permittivity" is observed for many dielectrics [10, 11]. This trend can be traced across different materials, it is illustrated in Table 1.

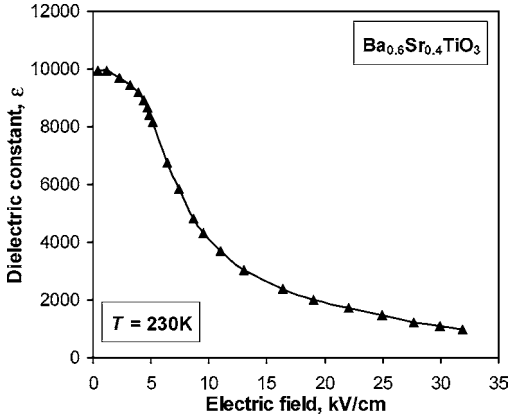

Fig. 1. Typical field dependence of the dielectric permittivity of a tunable ferroelectric material $Ba_{0.6}Sr_{0.4}TiO_3$ [9].

The correlation between the tunability and the loss tangent forces designers to choose the material with the optimal trade-off between these two parameters for best device performance. This optimal trade-off is found by an integral parameter called the Commutation Quality Factor (K). The commutation quality factor was originally introduced to characterize the switching properties of semiconductor two-state microwave switches (*p-i-n* diodes [15] and field effect transistors). It was shown that this parameter does not depend on the characteristics of the passive network that is used together with the switchable element in the microwave circuit designs. In other words, the factor K can be considered as an invariant that characterizes the tunable performance of the material. Later this theory was adapted to other switchable and tunable components including ferroelectrics [16]. The Commutation Quality Factor for ferroelectrics is given by:

$$K = \frac{(n-1)^2}{n \cdot \tan\delta(U_{\min}) \cdot \tan\delta(U_{\max})}, \tag{2.3}$$

where $U_{\max}$ and $U_{\min}$ are the voltages applied in the two states of the ferroelectric capacitor and n is the tunability of the capacitor determined as the ratio $\varepsilon(U_{\min})/\varepsilon(U_{\max})$.

In theory, all forms of ferroelectric materials, bulk single crystals, bulk ceramics, thin films, and thick films can be used in RF and microwave tunable elements. Each of these forms has its advantages and shortcomings.

Table 1. Permittivity, temperature coefficient of permittivity and quality factor of some linear dielectrics and ferroelectrics used as the microwave resonators.

Material	ε_r @ 25°C	TCE (ppm/K) @ 25°C	$Q = 1/\tan\delta$ @ 25°C	Loss measured @ f (GHz)
Ba-Zn-Ta-O [(1)]	30	$-18\ldots-26$	12600	10
Zr-Sn-Ti-O [(1)]	37	$-7\ldots-45$	5800	9
Ba-Nd-Ti-O [(1)]	88	$-8\ldots-46$	1100	5
TiO_2 [(4)]	100	-900	14500	3
$SrTiO_3$	300 [(2)]	-2000 [(2)]	1000 [(5)]	10 [(5)]
$Ba_{0.6}Sr_{0.4}TiO_3$	4000 [(3)]	-40000 [(3)]	50 [(5)]	10 [(5)]

(1) Values taken from the datasheet of Morgan Electro Ceramics company. (2) Values calculated based on the data reported in Refs. [12, 13] (3) Values calculated based on the data reported in Ref. [14]. (4) Values are taken from Ref. [10]. (5) Values taken from Ref. [2]. The temperature dependence of the dielectric permittivity is given in term of $TCE = \varepsilon^{-1}\partial\varepsilon/\partial T \times 10^6$.

2.1. Bulk Ferroelectrics

Cylinders or cubes of ferroelectric single crystals and ceramics can be used in *tunable dielectric resonators* and *tunable filters* [17]. The linear dimensions of these filters and correspondingly their mass are proportional to the length of the electromagnetic wave propagating in the ferroelectric medium which in turn is related to the dielectric permittivity of the material according to the relation:

$$l = \frac{c}{f_0 \cdot \sqrt{\varepsilon}} \tag{2.4}$$

where $c = 3 \times 10^8$ m/s is the speed of light in vacuum, and f_0 and l are the frequency and length of the electromagnetic wave, respectively. The potential reduction in dimensions and mass from using a ferroelectric material is proportional to $\sqrt{\varepsilon}$.

These elements can be used at radio frequencies (RF) as parallel plate *tunable capacitors* or *varactors*. Presently, the high loss of ferroelectrics (compared to that of semiconductor varctors at these frequencies) and mainly the high voltage needed for tuning limit the use of this kind of bulk varactors in comparison to the semiconductor ones.

Bulk ferroelectrics can also be used in *lens antennas* [8, 18]. Shown in Fig. 2, a lens antenna is a stack of electroded ferroelectric slabs [18]. The dielectric constant of each slab is controlled by varying the dc electric field applied. As a result an electromagnetic beam can be steered by passing through the antenna.

The use of ferroelectric single crystals or bulk ceramics as dielectric substrates for tunable *microstrip or strip line structures* is limited because their high and field dependent permittivity requires an adaptive impedance matching to 50 Ω in addition to the high operation voltage. Some of these problems can be minimized by an appropriate design as shown by Flaviis et al. [19].

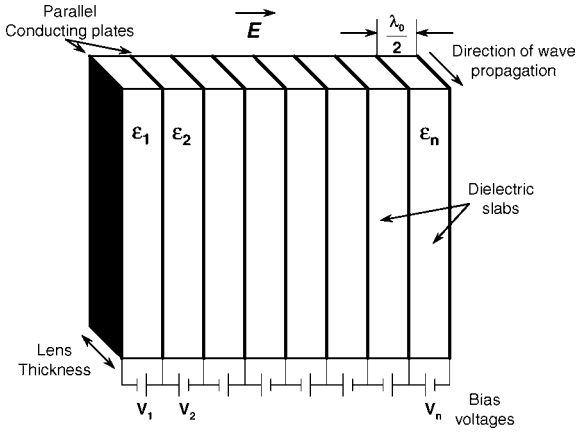

Fig. 2. Sketch of ferroelectric lens antenna [18].

At microwave frequencies, the loss in ferroelectrics can be significanly lower than that in semiconductor varactors. However, the use of relatively thick bulk ferroelectric materials still requires very high voltages for the tuning, of the order of hundreds of volts to tens of kilovolts. This limits the applicability of bulk ceramics and single crystals in tunable devices.

2.2. Ferroelectric Thin Films

Thin films are very attractive for microwave tunable applications due to the low tuning voltages and the relatively low production cost. Sapphire, MgO, and

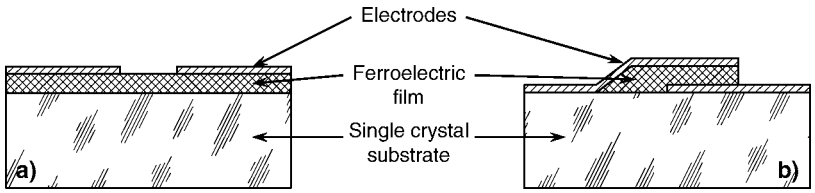

Fig. 3. Planar (a) and trilayer (b) planar capacitors based on ferroelectric film [2, 20].

$LaAlO_3$ substrates which are frequently used in microwave circuits are also used as substrates in ferroelectric film based components. These substrates provide good lattice matching to the perovskite ferroelectrics whereas the standard Si wafers, which are attractive substrates when the requirement of 100% compatibility with IC technology is imposed, do not provide lattice matching, resulting in inferior properties of the deposited ferroelectric films. Another problem with the use of Si for substrates for tunable devices is too high conductivity of poly-Si.

The simplest tunable passive component based on thin ferroelectric films is a *varactor* which can be made as a planar structure, the co-called "planar capacitor" (Fig. 3(a)), or as a tri-layer "sandwich" structure (Fig. 3(b)) [2, 20].

For the tri-layer capacitor the dc voltage is applied across the film thickness and as a result relatively small dc voltages (1–20 V) are sufficient for effective tuning. However, because of the high dielectric permittivity and the small thickness, the varactors have large capacitance which limits their high frequency applications. Moreover, in the parallel plate configuration, the electrodes contribute to the loss tangent of the device much more than in the case of the planar structure.

For the planar structures, the electric field is applied along the film across the gap, which is typically more than an order of magnitude larger than the film thickness. This makes the capacitance smaller, however, the voltage needed for tuning increases.

Microwave ferroelectric phase shifters are the most widely studied tunable ferroelectric components. Their importance stems from the role they could play in phased array antennas. A phased array antenna consists of thousands of radiating elements which should be served by thousands of phase shifters. The phase shifters are used to modify and control the width and angle of the steered radar beam. At present each phase shifter is a housed microwave semiconductor module. The use of ferroelectric films enables the integration of the phase shifters with the microwave circuits on one substrate thus substantially reducing the size, mass, and cost of the antennas.

A simple coplanar line structure patterned on a ferroelectric thin film coated substrate makes a phase shifter (Fig. 4(a)) in which the phase velocity of the electromagnetic wave that passes through the line is controlled by the applied dc electric field, U_{dc} (via changing the permittivity of the film, which in turn controls the wave velocity) [21]. It is also possible to tune the phase velocity of the electromagnetic wave passed through the coplanar line by loading this line with tunable ferroelectric capacitors (by contrast to the previous case where the coplanar line is homogeneously loaded with a ferroelectric film) [22].

Another possibility is the so-called digital phase-shifter which is used only at two values of the tuning voltage providing a fixed phase shift (e.g. 45° or 90°). Examples of this kind of phase shifters are presented in Fig. 4(b) and (c). Figure 4(b) shows a layout of a periodically loaded line digital phase shifter with two planar capacitors connected in parallel to the line as flip chip elements [23]. Another solution is presented in Fig. 4(c) [24] showing a phase shifter that consists of a transforming circuit that is terminated by a coplanar 3-electrode capacitor. The advantage of the digital phase shifters compared to those based on the simple coplanar line is that the former can be better optimized. Namely, better impedance matching with the 50 Ω external wave impedance and lower amplitude modulation distortions at switching can be reached in the digital phase shifters.

The figure of Merit (F_{ph}) of microwave phase shifters is the ratio of the phase shift produced by the phase shifter ($\Delta\phi_{\mathrm{ph}}$) to its insertion loss (L_{dB}). The upper bound of the figure of Merit F_{ph} for an optimally designed one-bit digital phase shifter (not taking into account conductor and interconnections losses) can be determined as [25, 26]:

$$F_{\mathrm{PH}}^{\max} = 6.6\frac{\Delta\varphi/2}{\sin(\Delta\varphi/2)} \cdot \sqrt{K}, \qquad (2.5)$$

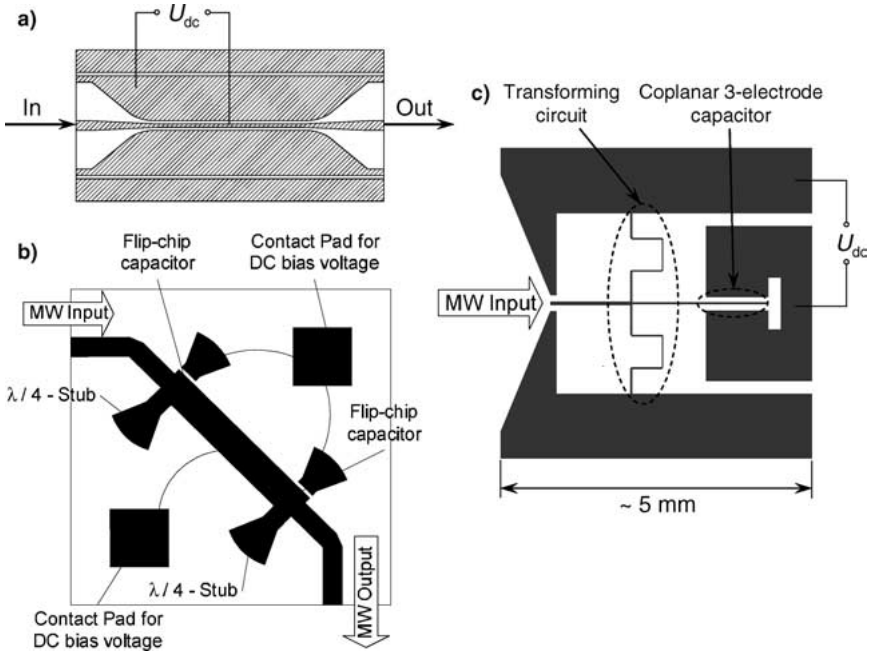

Fig. 4. Ferroelectric microwave phase shifters: (a) coplanar line analog phase shifter [21], (b) periodically loaded line phase shifter [23], (c) reflection type digital phase shifter [24].

where K is the commutation quality factor of the ferroelectric capacitor used in the circuit and $\Delta\varphi$ is the desired phase shift.

Values of F_{ph} in the range of 30–100 (for frequencies of 1–30 GHz) were reported [19, 21–24, 27, 28] for phase shifters based on ferroelectric films with tunability 1.5–2, loss tangent 0.02–0.05, and with copper or gold as the conducting layers.

Microwave tunable filters based on ferroelectric thin films have also been recently demonstrated [29, 30]. The figure of Merit for the tunable band pass filter (F_{BPF}) is characterized by the ratio between the shift of the central frequency due to the tuning and the average bandwidth of the filter. The figure of Merit of the tunable N-pole filter as a function of the K-factor can be found in the following form [31]:

$$F_{\text{BPF}} = \frac{\omega_{02} - \omega_{01}}{\sqrt{\Delta\omega_1 \Delta\omega_2}} = \frac{1}{2N^2} \cdot \sqrt{K}. \qquad (2.6)$$

where ω_{01}, ω_{02}, $\Delta\omega_1$, and $\Delta\omega_2$ are the central frequencies and the band widths of the filter in two inter-switchable states. The layout of a 3-pole filter and its simulated frequency characteristics are shown in Fig. 5 [31].

The designs of other microwave active and passive ferroelectric thin film based components such as microwave *voltage controlled oscillator* [27], *frequency modulators* [32], *parametric amplifiers* [9] and *tunable power divider* [33] were also reported recently.

2.3. Ferroelectric Thick Films

Screen printed or tape cast thick films are regarded as promising ferroelectric elements for hybrid RF/microwave circuits because of their low production costs. The principles of design and operation of ferroelectric thin film based microwave components can be applied to the thick film devices with only minor modifications [34]. However, to date, high loss and technological limitations on the linear dimensions associated with the thick film technology still impede the use of ferroelectric thick films in tunable microwave devices. In addition, the planar microwave devices made of thick ferroelectric films are expected to have worse tunability compared to thin film devices. The reason is that only a thin upper layer of the thick ferroelectric film contributes to the effective tuning whereas the contribution of the rest of the film can be regarded as that of a

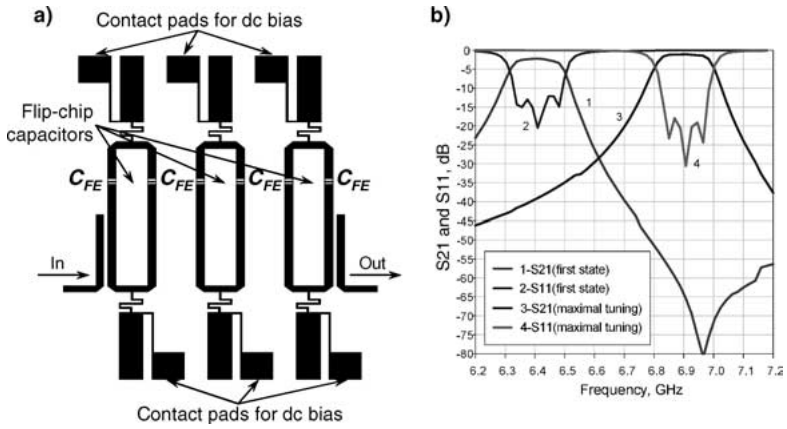

Fig. 5. Layout of a tunable 3-pole filter based on ferroelectric planar capacitors (a) and its simulated characteristics at different values of dc bias voltage (b) where S21 and S11 are the transmission and reflection coefficients, respectively [31].

non-tunable capacitance connected in parallel with the upper tunable part of the film.

2.4. *Requirements Imposed on the Material by the Device Performance Needs*

Generalizing the above discussion, it is of interest to estimate the needed properties of the ferroelectric varactors for various potential applications.

Figure 6(a) shows the calculated dependence of F_{ph}, the figure of merit for a phase shifter, on the commutation quality factor of the material. For practical applications, in order to be competitive with semiconductor devices, $F_{\text{ph}} \geq 200$ is required, which implies $K > 900$. Of course this requirement depends also on the frequency used and on the specifics of the application of the device.

Figure 6(b) shows the dependence of F_{BPF} (figure of merit for band-bass filter) on the commutation quality factor. One can see that, for example, to have a filter which can be tuned for 5 pass bands ($F_{\text{BPF}} = 5$), the commutation quality factor of the capacitors should be more than 8000 for a 3-pole band-pass filter ($N = 3$) and more than $6 \cdot 10^4$ for a 5-pole band-pass filter ($N = 5$).

This means that a competitive ferroelectric varactor should have loss tangent on the level of 0.005–0.01 and tunability $n > 1.5$ at the frequencies of the interest. However, it should be noted that the commutation quality factor is not the only parameter representing the properties of the switchable microwave

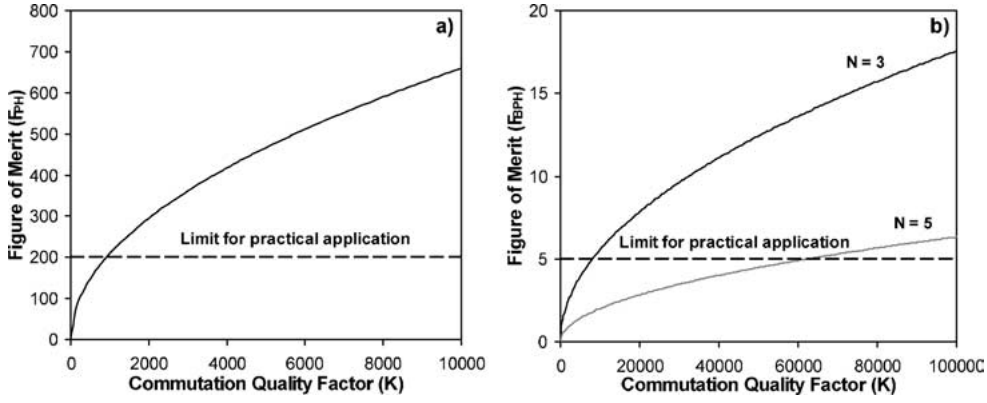

Fig. 6. Calculated dependences of the figure of merit of: (a) phase shifters and (b) band-pass filters on the commutation quality factor of switchable component. (N in figure (b) corresponds to the order of filter).

element. It is more a qualitative than a quantitative characteristic of the ferroelectric varactor. It tells us qualitatively whether the ferroelectric capacitor is potentially suitable for the design of a microwave tunable component with the required characteristics. Keeping the commutation quality factor constant it is possible to have an infinite number of values of the tunability and loss tangent (see Eq. (2.3)); it may be a combination of a high loss with a high tunability as well as that of a low loss with a low tunability. For almost all designs of microwave controllable components, the first case is preferable because the higher the tunability, the easier it is to combine the varactor with the passive microwave circuit to get a better performance. In addition, there are many methods to reduce the effective loss tangent and tunability of a varactor by loading it with various kinds of microwave passive elements. This also gives an advantage to the more tunable materials. Another issue is a rather high absolute value of the relative dielectric permittivity of the ferroelectrics, which is often not desirable for high frequency devices (too small dimensions are required). For this reason, for the same value of the commutation quality factor, materials with lower permittivity may be preferable. The typically high *TCE* of materials with high permittivity also suggests a preferable use of materials with lower permittivity. The main parameters of a tunable material (tunability, loss tangent, dielectric permittivity, and *TCE*) are dependent one on the other so that the material optimization has to be done with great care. The interplay among these parameters is the center of the rest of this paper.

3. Theory of Dielectric Response of Tunable Materials

3.1. Dielectric Constant and Tunability of Ferroelectric Materials

Ferroelectrics are known for their high dielectric constant and high tunability. These features of ferroelectrics are linked and the general trend "the higher the dielectric constant, the higher the tunability" generally holds in ferroelectric materials. It holds for an "ideal ferroelectric" where the dielectric response is controlled by the lattice dynamics of the material as well as for situations where the dielectric response is essentially influenced by the presence of defects or inclusions of a low-dielectric-constant non-tunable material. Below we will discuss these situations separately. The effects of dielectric anisotropy do not usually play an essential role in the performance of tunable materials. For this reason, these effects are not addressed here so that we will always consider the situation where the polarization and electric fields are collinear.

3.1.1. Ideal Ferroelectric

Dielectric Permittivity. The origin of the high dielectric permittivity of ferroelectrics in the paraelectric phase is a delicate compensation of various kinds of microscopic forces that maintains the material in a non-poled state in the absence of a microscopic electric field. Because of this compensation, the restoring force opposing the poling action of the applied field is relatively weak. This results in a high dielectric permittivity of the material. In the ferroelectric phase, the newly appeared spontaneous polarization is not very stable either. This makes the dielectric permittivity high in the ferroelectric phase. In addition to this, the permittivity may be further increased by contributions stemming from ferroelectric domains. Since the present paper is devoted to microwave materials, in the following discussion, we will address only the paraelectric phase of ferroelectrics (normal or incipient) of the displacive type; it is believed that only for this case will a material exhibit a high tunability and a relatively low dielectric loss at microwave frequencies, a combination of interest for microwave application. Order-disorder materials are inappropriate since they exhibit a much smaller permittivity at microwave frequencies,[1] which implies a smaller tunability. The situation with the ferroelectric phase of the displacive ferroelectrics is not so clear. Though, in the ferroelectric phase, additional mechanisms (domain related, see e.g. [35], and quasi-Debye mechanisms, see Section 3.2.1) of the loss are active, their contributions might not be decisive in the case of real materials. Thus, the tunable materials in the ferroelectric phase should not be ruled out outright.

The most straightforward description of the dielectric response of ferroelectrics is given by the conventional Landau theory and is based upon an expansion of the Helmholtz free energy F with respect to the vector macroscopic polarization $\mathbf{P}$. For the situation where the polarization is collinear with the macroscopic electric field $\mathbf{E}$ in the material, the first two terms of this

expansion read:

$$F = \frac{\alpha}{2}P^2 + \frac{\beta}{4}P^4. \tag{3.1}$$

The equation of state $\partial F/\partial P = E$ then leads to a relation between the polarization and electric field:

$$E = \alpha P + \beta P^3. \tag{3.2}$$

Equation (3.2) enables us to present the relative dielectric permittivity of the material in the form:

$$\varepsilon = \frac{1}{\varepsilon_0}\frac{\partial P}{\partial E} = \frac{1}{\varepsilon_0}\frac{1}{\alpha + 3\beta P^2} = \varepsilon(0)\frac{1}{1 + 3\beta\varepsilon(0)\varepsilon_0 P^2} \tag{3.3}$$

where $\varepsilon(0) = (\varepsilon_0\alpha)^{-1}$ and $\varepsilon_0 = 8.85 \times 10^{-12}$ F/m. This expression describes the dielectric permittivity both in the absence of a bias field and under it. In the first case, one sets $P = 0$ in Eq. (3.3) to obtain:

$$\varepsilon = \varepsilon(0) = \frac{1}{\varepsilon_0\alpha}, \tag{3.4}$$

whereas, for the situation under the bias, one sets $P = P_{\mathrm{dc}}$ in Eq. (3.3) (P_{dc} is the polarization induced by the bias field).

According to the Landau theory, the coefficient α is assumed to be a linear function of temperature and vanishes at the Curie-Weiss temperature T_0, the ferroelectric instability temperature of the material

$$\alpha = \alpha_L = \frac{1}{\varepsilon_0}\frac{T - T_0}{C}. \tag{3.5}$$

where C is the Curie-Weiss constant. This assumption of the Landau theory[2] can be always justified for $|T - T_0|/T_0 \ll 1$. However, for displacive ferroelectrics, it has been shown [36] that the coefficient α can be taken with a good precision in the form given by Eq. (3.5) for a much wider temperature range: starting from the temperature of about a fraction of the Debye temperature θ of the material and up to its melting point. For real materials, this statement has been checked for the incipient ferroelectrics $SrTiO_3$ and $KTaO_3$, with the Debye temperatures of about 400 K, and it was shown that Eq. (3.5) applies with a reasonable accuracy from 50–80 K up to very high temperatures [12].

Equation (3.5) ceases to work at $T \ll \theta$ where the quantum statistics of the lattice vibration should be taken into account. In this regime, the temperature dependence of α strongly slows down. In terms of simple models, several explicit forms have been suggested for this dependence. The Barrett theory [37], which models the lattice dynamics of the ferroelectric with a system of identical oscillators, yields:

$$\alpha = \alpha_B = \frac{T_B}{\varepsilon_0 C}\left[\coth\left(\frac{T_B}{T}\right) - \frac{T_0}{T_B}\right]. \tag{3.6}$$

whereas according to Vendik [38] (who models the lattice dynamics of the ferroelectric with a system of spatially coupled oscillators) the following formula can be used for a description of the temperature dependence of α:

$$\alpha = \alpha_V = \frac{T_V}{\varepsilon_0 C}\left[\sqrt{\frac{1}{16} + \left(\frac{T}{T_V}\right)^2} - \frac{T_0}{T_V}\right]. \tag{3.7}$$

Here T_B and T_V are parameters decreasing the slowing down of the temperature dependence of α on decreasing temperature. Calculations performed in a more precise model [36] give a temperature dependence of α similar to these given by Eqs. (3.6) and (3.7).

An essential feature of displacive ferroelectrics is the typical value of the Curie-Weiss constant C of about 10^5 K. Such a value of C implies high values of the dielectric permittivity even far from the Curie-Weiss temperature T_0. Indeed, at $T = T_0 + 200$ K, Eqs. (3.4) and (3.5) implies $\varepsilon \cong 500$.

Tunability. The dependence of the dielectric permittivity on the applied dc bias electric field E_0 can be determined from Eq. (3.3). There are two parameters used for characterization of this dependences: tunability

$$n = \frac{\varepsilon(0)}{\varepsilon(E_0)}, \tag{3.8}$$

and relative tunability

$$n_r = \frac{\varepsilon(0) - \varepsilon(E_0)}{\varepsilon(0)} = \frac{n - 1}{n}. \tag{3.9}$$

The aforementioned trend—the higher permittivity $\varepsilon(0)$, the higher the tunability (for a given value of the bias field E_0) can be clearly traced. In the limit of weak nonlinearity, i.e. at $n_r \ll 1$, this trend is really strong. Indeed, in this case, according to (3.3), we have:

$$n = \frac{\varepsilon(0)}{\varepsilon(E_0)} = 1 + 3\beta\varepsilon(0)\varepsilon_0 P_{\mathrm{dc}}^2 \approx 1 + 3\beta(\varepsilon(0)\varepsilon_0)^3 E_0^2. \tag{3.10}$$

That means that the relative tunability is a very fast function of $\varepsilon(0)$, specifically, $n_r \propto \varepsilon(0)^3$. With increasing bias fields this dependence slows down. In the limit of ultrahigh fields where $n \gg 1$, one readily finds $\varepsilon(E_0) \approx \beta^{-1/3} E_0^{-2/3}/(3\varepsilon_0)$. This implies $n \propto \varepsilon(0)$. It is instructive to give an expression for the field E_n needed to achieve a given tunability n:

$$E_n = \frac{\sqrt{n-1}(2+n)}{\varepsilon_0\sqrt{27\beta\varepsilon_0}} \frac{1}{\varepsilon(0)^{3/2}}. \tag{3.11}$$

Thus, it is seen that a high dielectric permittivity of the material is really essential for its tunable behavior.

For the description of the dielectric non-linearity at an arbitrary dc field, one can use equation (3.3) where the polarization P is calculated from the solution of cubic equation (3.2). A convenient form for calculation of the dependence of the permittivity on the dc bias field has been suggested by Vendik [38, 39]:

$$\varepsilon(T, E_0) = \frac{\varepsilon_{00}}{[(\xi^2+\eta^3)^{1/2}+\xi]^{2/3} + [(\xi^2+\eta^3)^{1/2}-\xi]^{2/3} - \eta}; \tag{3.12}$$

$$\varepsilon_{00} = \frac{C}{T_0}; \quad \eta = \varepsilon_{00}\,\alpha\varepsilon_0;$$

$$\xi = \xi_B = \frac{E_0}{E_N}; \tag{3.13}$$

$$E_N = \frac{2}{\sqrt{27\beta\varepsilon_{00}^3}}.$$

The field dependence of dielectric permittivity discussed above is illustrated in Fig. 7 for two values of $\varepsilon(0)$ and the value of $\beta = 8 \times 10^9$ JC^{-4} m^{-5} (typical for $SrTiO_3$). The regimes of small and high tunability are shown together with the asymptotic dependences of $\varepsilon(E)$ in these regimes.

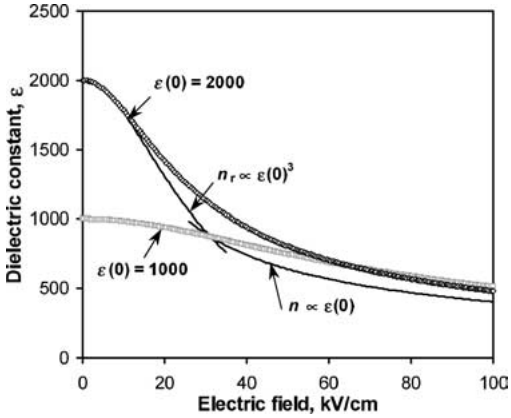

Fig. 7. Field dependence of the dielectric permittivity according to Eq. (3.12) plotted for $\beta = 8 \times 10^9$ JC^{-4} m^5 and for the values of $\varepsilon(0)$ 2000 and 1000. The regimes of small and high tunability are shown together with the asymptotic dependences of $\varepsilon(E)$ in these regions.

3.1.2. Ferroelectric with Random Field Defects

The thermodynamic model discussed in the previous subsection was extended by Vendik and Zubko [40] to the case of materials containing random built-in electric fields (or random built-in polarization). These fields can naturally come from the presence of dipolar or charged defects and should result in a suppression of local dielectric permittivity. The calculation of the dielectric response of a ferroelectric containing random electric field is a difficult task for an exact theoretical treatment. Vendik and Zubko treated the problem in an approximation equivalent to a model where the material is presented as a system of layers perpendicular to the applied field. The layers differ by the values of their built-in random electric fields, a Gaussian distribution of the latter being assumed. It was shown that the results obtained this way for the temperature and field dependence of the dielectric permittivity can be reasonably well approximated by Eq. (3.12) where the parameter ξ, which controls the field effect, is set in the form:

$$\xi = \sqrt{\xi_B^2 + \xi_{St}^2}. \tag{3.14}$$

In this framework, parameter ξ_{St} controls the suppressing effect of the random fields on the dielectric permittivity of the ferroelectric material. The ratio ξ_B/ξ_{St} has the physical meaning of the ratio between the applied field and the typical value of the random field.

This model was used for the description of the dielectric response in a number of materials of interest for tunable applications. For these maratials, the model parameters entering Eqs. (3.7) and (3.12–14) are listed in Table 2.

3.1.3. Ferroelectric Containing Inclusions of Low-Dielectric-Constant Non-Tunable Material

There are some situations where the tunable material can be treated as a ferroelectric/dielectric composite.

Table 2. Parameters of the Vendik's model for $KTaO_3$ and $SrTiO_3$ crystals and $(Ba_x\ Sr_{1-x})TiO_3$ ceramics [2, 41].

	$SrTiO_3$	$Ba_xSr_{1-x}TiO_3$	$KTaO_3$
T_0 (K)	42	$T_c(x) = 42 + 439.37 \cdot x - 95.95 \cdot x^2$	32.5
$C \times 10^{-5}$	0.86	$C(x) \times 10^{-5} = 0.86 + 1.1 \cdot x^2$	0.45
T_v (K)	175	175	170
ε_{00}	2080	$\varepsilon_{00}(x) = C(x)/T_c(x)$	1390
E_N (kV/cm)	19	$E_N(x) = 8.4/(\varepsilon_0(3\varepsilon_{00}(x))^{3/2})$	15.6
ξ_s	0.018	0.3	0.02

These situations occur due to the presence of near by–electrode layers or secondary phases at grain boundaries as well as when a ferroelectric/dielectric composite is deliberately used as a tunable material. The dielectric permittivity and tunability of the materials are strongly affected by the presence of the "passive" component. Since no exact general theory of the dielectric constant and tunability of composites is available,[3] we will overview some results obtained for three models of bi-component ferroelectric-dielectric composites. These models correspond to different structures illustrated in Fig. 8. In addition to the models shown in this figure, the so-called "brick-wall" model is often addressed in the literature (see e.g. [44]). It consists of a regular structure of cubes of one phase equally separated in three dimensions by thin layers of another phase. We will not specifically address this model since, in the case of the ferroelectric tunable composite (the cubes are of a ferroelectric and the layers are of a dielectric), this model is very close to the layered model (shown in Fig. 8(a)) with a 3 times reduced concentration of the dielectric.

We start from the layered model (Fig. 8(a)). This case can be described as the in-series connection of several capacitors corresponding to the different layers of the composite. Electrically, this system is equivalent to the in-series connection of only two capacitors which correspond to the two components of the mixture. The effective dielectric permittivity of such a composite can be found as:

$$\frac{1}{\varepsilon_{\text{mix}}(q)} = \frac{1-q}{\varepsilon_f} + \frac{q}{\varepsilon_d} \tag{3.15}$$

where q is the volume concentration of the dielectric phase in the composite. ε_{mix}, ε_f, and ε_d are the dielectric constants of the composite, ferroelectric and dielectric, respectively.

The field dependence of the composite dielectric constant originates from that of the dielectric constant $\varepsilon_f(E_f)$ of the ferroelectric component, where E_f is the electric field in the ferroelectric. This dependence $\varepsilon_f(E_f)$ can be obtained by applying Eqs. (3.2)–(3.4) to the ferroelectric component of the composite to get

$$\varepsilon_f^{-1}(E_f) = \varepsilon_0\alpha + 3\beta\,\varepsilon_0\,P_f^2 \tag{3.16}$$

$$\beta\,P_f^3 + \alpha\,P_f - E_f = 0. \tag{3.17}$$

To find the dielectric constant of the composite material as a function of the bias field E_0 and concentration q one appends Eqs. (3.15–17) with the condition of continuity of electrical displacement:

$$\varepsilon_0\varepsilon_b E_f + P_f = \varepsilon_0\varepsilon_d\,E_d \tag{3.18}$$

and the equation for the voltage drops across the composite components:

$$E_f\,(1-q) + E_d\,q = E_0. \tag{3.19}$$

Here E_d is the electric field in the dielectric and ε_b is the background dielectric constant[4] of the ferroelectric, which describes the contribution of the hard ("non-ferroelectric") optical phonon modes and the electronic degrees of freedom to the permittivity of the material.

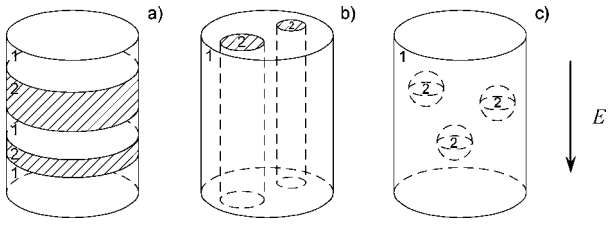

Fig. 8. Schematic of models of bi-component composite: (a)—layered model, (b)—columnar model and (c)—spherical inclusion model. 1—ferroelectric component, 2—dielectric component.

Using Eqs. (3.15–19) the solution of the problem can be presented in the form [45]:

$$\beta P_f^3 + \alpha^* P_f - E_f^* = 0, \tag{3.20}$$

$$\begin{cases} \alpha^* = \alpha + \dfrac{q}{\varepsilon_0 \varepsilon_b q + \varepsilon_0 \varepsilon_d (1-q)} \\ E_f^* = E_0 \dfrac{\varepsilon_d}{\varepsilon_b q + \varepsilon_d (1-q)} \end{cases}, \tag{3.21}$$

$$\varepsilon_{\text{mix}}^{-1}(q, E_0) = \varepsilon_0 \alpha^* + 3\beta\varepsilon_0 P_f^2 - \frac{q^2(\varepsilon_b - \varepsilon_d)}{\varepsilon_d[\varepsilon_b q + \varepsilon_d(1-q)]} - q\varepsilon_0(\alpha + 3\beta P_f^2). \tag{3.22}$$

In the limit of small concentration of the dielectric material in the mixture ($q \ll 1$) and when $\varepsilon_f/\varepsilon_d \gg 1$, the last three terms in the Eq. (3.22) can be neglected and the renormalized electric field E^* in Eq. (3.20) becomes equal to the electric field E_0. Thus, Eqs. (3.20) and (3.22) become identical to the equations for the permittivity and polarization of the pure ferroelectric material, Eqs. (3.2) and (3.3), but with the coefficient α replaced by α^*. One can easily see that, in this case, the behavior of the composite is identical to that of the pure ferroelectric whose coefficient α is increased, which corresponds to an effective decrease of the Curie-Weiss temperature of the material.

The second model, the columnar structure shown in Fig. 8(b), is clearly much simpler to analyze [43]. This system is equivalent to the parallel connection of two capacitors corresponding to the two components of the mixture. The effective dielectric permittivity of such composite can be presented as:

$$\varepsilon_{\text{mix}}(q) = \varepsilon_f (1-q) + \varepsilon_d q. \tag{3.23}$$

In the case of parallel connection of the composite components, the electric field is the same in all parts of the composite, being equal to the applied field E_0. This means that the field dependence of dielectric constant of the composite is simply given by Eq. (3.23) where ε_f is given by Eqs. (3.2) and (3.3).

The spherical inclusion model shown in Fig. 8(c) consists of a random distribution of dielectric spheres in the ferroelectric host medium. The well-known electrostatic solution of the problem for a dielectric sphere embedded into a dielectric medium gives the electric field distribution in the sphere and in the medium. This solution also enables the calculation of the effective dielectric permittivity of a two-component material in the limit of low concentration of the spherical inclusions ($q \ll 1$) [46]. For this dielectric-ferroelectric bicomponent system, the dielectric constant ε_{mix} and the electric field in the ferroelectric matrix $\vec{E}_f$ read [46]:

$$\varepsilon_{\text{mix}}(q) = \varepsilon_f + 3q\,\varepsilon_f \frac{\varepsilon_d - \varepsilon_f}{\varepsilon_d + 2\varepsilon_f}, \tag{3.24}$$

$$\vec{E}_f(\vec{r}) = \vec{E} + \sum_i^N \frac{\varepsilon_d - \varepsilon_f}{\varepsilon_d + 2\varepsilon_f} \frac{R^3}{|\vec{r} - \vec{r}_i|^3} \overleftrightarrow{G} \vec{E}, \tag{3.25}$$

where R is the radius of the dielectric inclusions, N is the total number of the dielectric spheres distributed in the composite, and $\vec{r}_i$ is the radius-vectors pointing to the center of the ith spherical inclusion. The matrix $\overleftrightarrow{G}$ reads

$$G_{ts} = 3n + ns - \delta_{ts}$$

where $\vec{n} = (\vec{r} - \vec{r}_i)/|\vec{r} - \vec{r}_i|$ and δ is the Kroneker symbol. where φ and θ are the azimuthal and polar angles of the vector $\vec{r} - \vec{r}_i$.

In the limit where $\varepsilon_d \ll \varepsilon_f$ these expressions can be reduced to:

$$\varepsilon_{\text{mix}}(q) = \varepsilon_f \left(1 - \frac{3}{2}q\right), \tag{3.24a}$$

$$\vec{E}_f(\vec{r}) = \vec{E} - \frac{1}{2}\sum_i^N \frac{R^3}{|\vec{r} - \vec{r}_i|^3} \overleftrightarrow{G} \vec{E}. \tag{3.25a}$$

This solution takes into account a non-uniform distribution of the electric field in the host material but does not take into account its dielectric nonlinearity. Once this nonlinearity is taken into account, the problem becomes much more complicated. A very rough solution of this problem, in the case of weak dc fields corresponding to a small relative tunability, $n_r \ll 1$ (a typical situation in bulk ceramics), is available in Ref. [45]. In this solution, when calculating the dielectric nonlinearity of the composite the second term in Eq. (3.27) is neglected so that in the ferroelectric matrix one set $\vec{E}_f \approx \vec{E}$. Thus, in this approximation, to calculate the effective dielectric permittivity at a non-zero E_0 one still use Eq. (3.24a), where $\varepsilon_f = \varepsilon_f(E_0)$. This implies that, at small q, the concentration dependence of the relative tunability is very weak (the linear term in q is absent)). Further calculations performed beyond this approximation (analytical and finite element analysis FEMLAB$^{\text{TM}}$) confirmed the weakness of this dependence, however, with a non-vanishing linear term in q.

Specifically, it is obtained [47] for the relative tunability of the composite $n_{r,\mathrm{mix}}$ that

$$n_{r,\mathrm{mix}} = (1 + 0.2q)n_r. \tag{3.26}$$

where $n_{r,\mathrm{mix}}$ is the tunability of the ferroelectric at the same value of the applied field. This result is quite unexpected since it predicts an increase (though weak) of the tunability as of a ferroelectric with delusion it with a non-tunable dielectric. However, it agrees with the prediction that could be drawn from the theories of other authors on the optical [48] and dielectric [49] nonlinearity of composites.

The presented above analysis enables a comparison of the concentration dependences of the tunability for the three model for the ferroelectric/dielectric composite. These dependences are shown in Fig. 9(a) (the results for the spherical inclusion model being valid in the limit $n_r \ll 1$ and $q \ll 1$). Here it is of interest to note that the tunability calculated for the spherical inclusion model does not lay between the results obtained for the "in-series" and "parallel" models. This fact might be considered as unexpected, however, in contrast to the case of dielectric permittivity, there is no reason to consider the "in-series" and "parallel" models as those giving upper and lower bound for the tunability of the composite.

3.1.4. Tunability as a Function of the Permittivity

When discussing the tunability of the ideal ferroelectric we have seen that the tunability is an increasing function of the permittivity of the material. This trend does not always hold for ferroelectric materials containing imperfections or inclusions of non-tunable dielectrics substantially varying from one system to another. The knowledge of this dependence for a given system may be useful for various purposes. First, when working with a "non-ideal" ferroelectric, the comparison of the measured n vs. ε dependence with those simulated for various models may provide information on the character of the imperfection of the material. Second, depending on the application, a combination of a high tunability with larger ε or smaller ε is desirable. Thus, the knowledge of possible n vs. ε dependences may help in tailoring properties of the material.

In Fig. 9(b), the results of simulation of the n vs. ε dependence for a pure ferroelectric, a ferroelectric with random field impurities, and various ferroelectric/dielectric composites are shown. It is seen that these dependences may be very different from each other (for material parameters use in the simulation see Table 5). A feature to mention is that the behavior of the layered composite is very close to that of pure ferroelectric in the whole interval of the permittivity. Remarkable is the behavior of the columnar composite

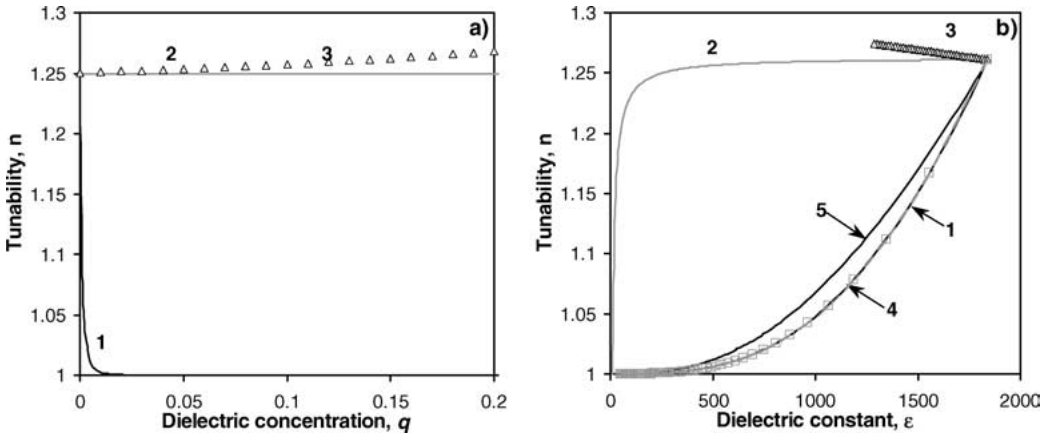

Fig. 9. Tunability n of ferroelectric/dielectric composites as a function of dielectric concentration q (a) and dielectric constant of the material ε (b) (black solid line 1—layered model, grey solid line 2—columnar model, and triangles 3—spherical inclusions model). For comparison, the ε dependence of tunability n is also given for a pure ferroelectric (grey dashed line 4 with squares) and ferroelectric with random-field impurities (black solid line 5). Modeling was performed for material parameters of $SrTiO_3$ given in Table 2. In the case of a pure ferroelectric; the permittivity is influenced by a temperature variation, in the case of a ferroelectric with random-field impurities it is influenced by a variation of the random-field intensity, and in the case of composites it is influenced by a variation of the concentration of dielectric inclusions.

(and the spherical model composite in the limit of small q and n_r) where an essential reduction of the permittivity may take place without essential reduction of the tunability or even with a slight increase of the latter.

3.2. Dielectric Loss in Ferroelectrics

Materials used for microwave tunable applications are incipient or regular ferroelectrics (in the paraelectric phase) of displacive type. For the frequencies of interest both fundamental phonon loss mechanisms and extrinsic mechanisms (owing to the coupling of the microwave field with defects) are relevant. Below we discuss these contributions as well as the loss in ferroelectric/dielectric composites and the impact of dc bias electric field on the loss.

3.2.1. Intrinsic Loss

The origin of the fundamental loss is the interaction of the ac field with the phonons of the material. The theory of the loss stemming from this interaction has been developed for crystalline materials with a well defined phonon spectrum (see for a review [6]), i.e., for materials where the damping of phonons (average frequency of the inter-phonon collisions), Γ, is much smaller than their frequencies. According to this theory, in terms of quantum mechanics, the fundamental loss mainly corresponds to the absorption of the energy quantum of the electromagnetic field $\hbar\omega$(ω is the ac field frequency) in collisions with the thermal phonons, which have much higher energies. This large difference in the energies makes it difficult to satisfy the conservation laws in these collisions. In such a complicated situation there exist three efficient schemes of absorption of the $\hbar\omega$-quanta, which correspond to the three main fundamental loss mechanisms: (1) three-quantum, (2) four-quantum, and (3) quasi-Debye.

Three-Quantum Mechanism. The three-quantum mechanism corresponds to a process involving a $\hbar\omega$-quantum and two phonons. The theory of this contribution has been developed by different authors [6, 50–53]. Owing to a very big difference between the energy quantum of the electromagnetic field $\hbar\omega$ and those of the thermal phonons, the three-quantum processes can take place only in the regions of the wave-vector space ($\vec{k}$-space) where the difference between the frequencies of two different phonon branches is small, specifically, of the order of ω and/or of the phonon damping Γ. These regions are usually located in the vicinity of the degeneracy lines of the spectrum, i.e. the lines in $\vec{k}$-space where the frequencies of different branches are equal. In the materials of interest for tunable applications, the phonon spectrum contains low-lying (soft) optical modes controlling their high dielectric permittivity and the degeneracy lines formed with participation of these modes are of primary importance for the loss. Since the degeneracy of the spectrum is mainly controlled by the symmetry of the crystal, the explicit temperature dependence (which does not take into account the temperature dependence of the dielectric permittivity) and frequency dependence of the three-quantum loss are very sensitive to the symmetry of the crystal. Depending on crystalline symmetry, temperature interval, frequency range and some parameters of the phonon spectrum, the temperature and frequency dependence of the imaginary part of the dielectric permittivity can be described by power laws [6], i.e:

$$\varepsilon'' \propto \omega^n T^m \tag{3.27}$$

where $n = 1$–5; $m = 1$–9.

For microwave high-ε and tunable materials, which are typically centrosymmetric, cubic or pseudocubic, the T-, ω-, and ε-dependence of the three-quantum loss can be evaluated in an analytical form. The calculations made for a model, in which the dielectric response is assumed to be controlled only by the lowest polar transverse optical (TO) mode (Ω_{TO} is the frequency of this mode at $\vec{k} = 0$), give for $T \geq \hbar\Omega_{\mathrm{TO}}/k_B$ [52, 54, 55]:

$$\varepsilon'' \cong A\omega\left[\ln\left(\frac{\Omega_{\mathrm{LO}}^2}{\omega^2 + 4\Gamma^2}\right) + \frac{\omega}{\Gamma}\tan^{-1}\left(\frac{\omega}{2\Gamma}\right)\right];$$
$$A = \frac{\mu\Gamma\varepsilon^2}{12\Omega_{\mathrm{LO}}^2}\left(\frac{\varepsilon}{\varepsilon_\infty}\right)^{x-2}, \tag{3.28}$$

where Γ is the damping of these phonons ($\Gamma \propto T$) and Ω_{LO} is the typical frequency of longitudinal optical phonons; ε_∞ is the optical permittivity; μ is the small anharmonicity parameter [6, 56], which can be evaluated as $k_B T/Mv^2$ (M and v are the average mass of the atoms and the average sound velocity in the crystal). The parameter x has been calculated for two limiting cases: (i) for the case of a strong dispersion of the TO mode (the typical case for ferroelectric soft modes) and (ii) for the case of a negligible TO mode dispersion (the case close to the situation in non-ferroelectric

crystals). In these cases, $x = 2.5$ and $x = 5$ have been found, predicting a fast growth of dielectric loss with increasing permittivity.[5]

For high-ε but non-ferroelectric materials, the theoretical result has been compared to the data of submillimeter frequency studies of dielectric loss in a system of complex perovskites $Ba(M^{(I)}_{1/2}\, M^{(II)}_{1/2})O_3$ ($M^{(I)}$ = Mg, In, Y, Gd, Nd and $M^{(II)}$ = W, Ta, Nb) [55, 57]. These are cubic non-ferroelectric (pseudo-cubic) centrosymmetric materials with the relative dielectric permittivity ranging from 20 to 40. In this frequency range the imaginary part of dielectric permittivity is expected to be controlled by the intrinsic contribution given by Eq. (3.28). A value of x close to 5 is expected due to the non-ferroelectric nature of these materials. The comparison of the theory to the experiment is shown in Fig. 10. This figure shows that the experimental data on ε'' measured at 300 GHz do reveal a strong correlation between ε'' and ε, which can be approximated as a power law with the exponent close to 4. This value is close to the upper theoretical bound for this exponent. The difference between the upper bound for x and its measured value is attributed to a small but appreciable dispersion of the optical modes in the studied materials.

For the case of a tunable material with the ferroelectric soft mode, the theory was tested [6, 54] by using the experimental data on microwave dielectric loss in $SrTiO_3$. In this case, Eq. (3.28) with $x = 2.5$ and $\omega \ll \Gamma$ leads to $\tan\delta \equiv \varepsilon''/\varepsilon \propto \omega T^2 \varepsilon^{1.5}$. As shown in Fig. 11, this expression is in good agreement with experimental data reported for crystalline $SrTiO_3$ by Buzin [58].

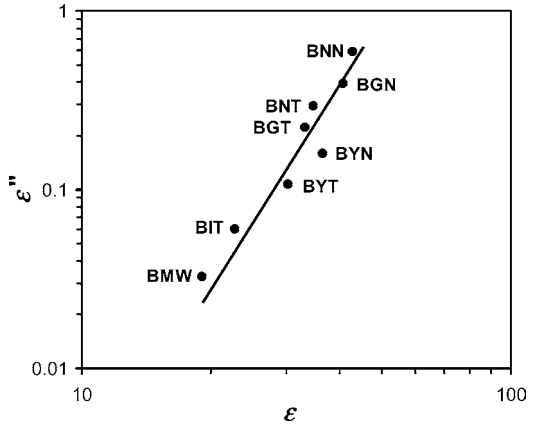

Fig. 10. Imaginary part of the dielectric permittivity plotted vs. its real part for $Ba(Mg_{1/2}W_{1/2})O_3$ (BMW), $Ba(In_{1/2}Ta_{1/2})O_3$ (BIT), $Ba(Y_{1/2}Ta_{1/2})O_3$ (BYT), $Ba(Y_{1/2}Nb_{1/2})O_3$ (BYN), $Ba(Gd_{1/2}Ta_{1/2})O_3$ (BGT), $Ba(Nd_{1/2}Ta_{1/2})O_3$ (BNT), $Ba(Gd_{1/2}Nb_{1/2})O_3$ (BGN), and $Ba(Nd_{1/2}\, Nb_{1/2})O3$ (BNN) measured at $\omega = 300$ GHz. The best fit $\varepsilon'' \propto \varepsilon^x$; $x = 4.1$ K [55, 57].

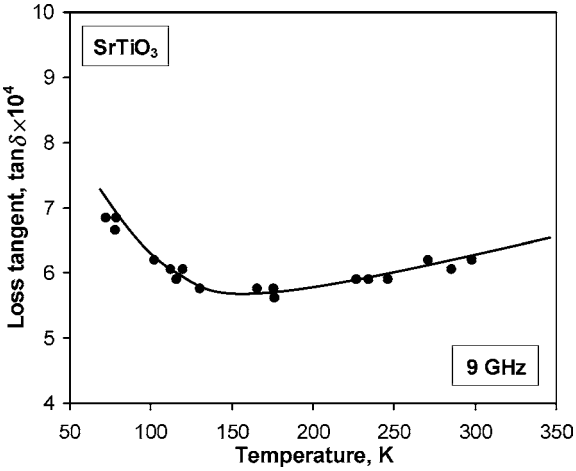

Fig. 11. Temperature dependence of the loss tangent in $SrTiO_3$ crystals at the ac electric field frequency 9 GHz: points—experimental data [58], curve—the prediction of the phonon theory [54] $\tan\delta \propto \omega T^2 \varepsilon^{1.5}$. The theory also correctly predicts the order of magnitude for the proportionality coefficient in this relation.

Four-Quantum Mechanism. The four-quantum mechanism corresponds to the field-quantum absorption processes involving three phonons [59–61]. The conservation (energy and quasi-momentum) laws do not impose strong restrictions on the type and energy of the phonons participating in these processes. For this reason, in contrast to the three-quantum processes, not only the degeneracy lines but also the whole thermally excited part of the $\vec{k}$-space nearly homogeneously contributes to the loss. Due to this fact, the explicit temperature and frequency dependence of the contribution of this mechanism to the imaginary part of the dielectric permittivity appears to be insensitive to the symmetry of the crystal. For $T \geq \hbar\Omega_{TO}/k_B$, this mechanism provides $\varepsilon'' \propto \omega T^2$; whereas at lower temperatures its contribution to the loss drastically decreases with decreasing temperature, e.g., for $T \ll \hbar\Omega_{TO}/k_B$, this mechanism provides [6] $\varepsilon'' \propto \omega T^9$.

This theory is quite applicable to the materials of interest for tunable applications. In this case, for the high temperature situation of practical importance where $T \geq \hbar\Omega_{TO}/k_B$, one finds [60, 61] $\tan\delta \equiv \varepsilon''/\varepsilon \propto \omega T^2 \varepsilon^{1.5}$ for the four quantum contribution to the loss.

This dependence is identical, to within a logarithmic factor, to result for the three-quantum contribution at $\omega \leq \Gamma$ (see Eq. (3.28) with $x = 2.5$). However, based on order-of-magnitude estimates [6, 54], one expects that, in these materials, the three-quantum contribution is still leading in the total balance of the intrinsic loss.

Fundamental Loss Mechanism in Centrosymmetric Crystal. The three- and four-quantum mechanisms are the only two mechanisms which control the intrinsic loss in centrosymmetric crystals [6]. In the case of practical interest of the low-microwave-loss materials, the theory of phonon transport, which has been used to obtain the results reviewed in the two previous sections, is applicable with quite good accuracy. This means that, possessing the complete information on the phonon spectrum and the constants of inter-phonon and ac field-phonon couplings, one can calculate the intrinsic dielectric loss with an accuracy equal to the relative damping of the typical phonons participating in the absorption of the ac field [6]. Thus, the result that the intrinsic loss in centrosymmetric crystals is given by the sum of the three- and four-quantum contribution can be considered as perfectly justified. However, in practice, when discussing the intrinsic microwave loss, two models differing from that discussed above are often used. These two models are the Vendik model [38, 61] and the so-called damped oscillator model [62]. Let us discuss the correspondence between the results of the phonon transport theory and of these models.

The Vendik model, as was mentioned in the original paper [61], is a version of the theory of the four-quantum mechanism. It gives correct dependences of the four-quantum-contribution to the loss tangent on frequency, temperature and dielectric permittivity for the temperature range of practical importance.

In the damped oscillator model, the loss is calculated by using the expression for the shape of the far-infrared absorption lines (associated with transverse optical branches) at the ac field frequency, which is much below the resonance frequencies. In this framework, the contribution to the complex dielectric permittivity from one branch (with frequency Ω_{TO}) is presented in the form [62]:

$$\varepsilon^* \propto \frac{1}{\Omega_{\mathrm{TO}}^2 - \omega^2 + 2i\omega\Gamma} \tag{3.29}$$

and used at $\omega \ll \Omega_{\mathrm{TO}}$ for the description of the dielectric loss. The analysis in terms of the phonon transport theory shows that the use of this formula for calculating the dielectric loss at $\omega \ll \Omega_{\mathrm{TO}}$ is not justified [6], except for crystals of symmetry $\frac{4}{m}$ and $\frac{6}{m}$. Thus, the damped oscillator model, in general, is not supported by the comprehensive theory. Table 3 compares the predictions of the two aforementioned models with these of the phonon transport theory. The comparison is performed for the case of a cubic incipient ferroelectric at $T \geq \hbar\Omega_0/k_B$ where Ω_0 is the soft-mode frequency (like $SrTiO_3$ or $KTaO_3$ at $T \geq$ 20–30 K). One concludes from this table that, for the frequency range $\omega \leq \Gamma$ (for $SrTiO_3$ or $KTaO_3$ that means $\omega \leq 100$ GHz), to within the logarithmic factors, the Vendik model gives correct functional dependences of the loss tangent on the frequency, temperature and the dielectric permittivity,[6] whereas the prediction of damped oscillator model substantially differs from that of the comprehensive phonon theory.

Table 3. Functional dependence of the loss tangent $\tan\delta = \varepsilon''/\varepsilon$ of a cubic incipient ferroelectric according to different models used for the description of the intrinsic loss.

Frequency range	Phonon transport theory	Vendik model	Damped oscillator
$\omega \leq \Gamma$	$\omega T^2 \varepsilon^{3/2} [1 + b \ln(\Omega_{\mathrm{TO}}/\Gamma)]$	$\omega T^2 \varepsilon^{3/2}$	$\omega T \varepsilon$
$\omega \gg \Gamma$	$\omega^2 T \varepsilon^{3/2}$	–	$\omega T \varepsilon$

Quasi-Debye Loss Mechanism. The origin of this mechanism is the relaxation of the phonon distribution function of the crystal [6, 51, 62, 63]. In non-centrosymmetric crystals, the phonon frequencies are linear functions of a small electric field applied to the crystal [51]. Thus, the oscillations of the ac field result in time modulation of the phonon frequencies; the latter in turn induces a deviation of the phonon distribution function from its equilibrium value. A relaxation of the phonon distribution functions gives rise to dielectric loss in a similar way as a relaxation of the distribution function of the dipoles gives rise to the loss in the Debye theory [64]. This analogy is expressed by the name "quasi-Debye". The frequency dependence of the quasi-Debye contribution to the loss factor is of the Debye type, the average relaxation time of the phonon distribution function playing the role of the Debye relaxation time. The contribution of the quasi-Debye mechanism to the tensor of the imaginary part of the relative dielectric permittivity of a crystal, $\varepsilon''_{\alpha\beta}$, can be expressed in terms of phonon dispersion curves,

$\Omega_j(\vec{k})$ phonon damping, $\Gamma_j(\vec{k})$, and the so-called vector of electrophonon potential, $\vec{\Lambda}_j(\vec{k})$. Here the index j designates the phonon branches and $\vec{k}$ is the phonon wave-vector. Calculated in the relaxation-time approximation $\varepsilon''_{\alpha\beta}$ can be presented in quadratures [6]:

$$\varepsilon''_{\alpha\beta} = \varepsilon_0^{-1} \sum_j \int \frac{d^3k}{(2\pi)^3} N_j(N_j+1) \times \frac{\hbar^2 \Omega_j^2 \Lambda_j^{(\alpha)} \Lambda_j^{(\beta)}}{k_B T} \frac{2\Gamma_j \omega}{4\Gamma_j^2 + \omega^2} \qquad (3.30)$$

where ε_0 and $N_j = [\exp(\hbar\Omega_j/k_BT) - 1]^{-1}$ are the permittivity of free space and the Planck distribution function; the integration volume is the first Brillouin zone. The electrophonon potential $\vec{\Lambda}_j(\vec{k})$ is defined as the relative change of the phonon frequencies per unit of the applied electric field [6]:

$$\Delta\Omega_j(\vec{k}) = \Omega_j(\vec{k}) \Lambda_j^{(\alpha)}(\vec{k}) E^{(\alpha)} \quad \text{or} \quad \Lambda_j^{(\alpha)}(\vec{k}) = \frac{1}{\Omega_j(\vec{k})} \frac{\partial \Omega_j(\vec{k})}{\partial E_\alpha}. \qquad (3.31)$$

One can notice an analogy between Eq. (3.30) and the expression for the Debye loss contribution [64]:

$$\varepsilon'' \propto \frac{p^2}{k_B T} \frac{\tau\omega}{1 + (\tau\omega)^2} \qquad (3.32)$$

(p is the dipole moment of the Debye dipoles) as well as between Eq. (3.31) and the expression for the change of energy of a dipole in an electrical field:

$$\Delta U = -p^{(\alpha)} E^{(\alpha)}, \qquad (3.33)$$

with a correspondence $p \Leftrightarrow -\hbar\Lambda\Omega$ and $\tau \Leftrightarrow 1/2\Gamma$. Apparently, in non-centrosymmetric crystal, the phonons behave similarly to the Debye dipoles, as far as the dielectric loss is concerned [51].

An important feature of the quasi-Debye mechanism is that, once allowed by symmetry, it can be easily a few orders of magnitude greater than that of three- and four-quantum mechanisms. To give an idea about the strength of this mechanism, rough estimates for the three-, four-quantum and quasi-Debye contributions to the loss tangent $\tan\delta = \varepsilon''/\varepsilon'$ are presented in Fig. 12. Specifically, this figure schematically shows the contributions arising from the interaction of the ac field

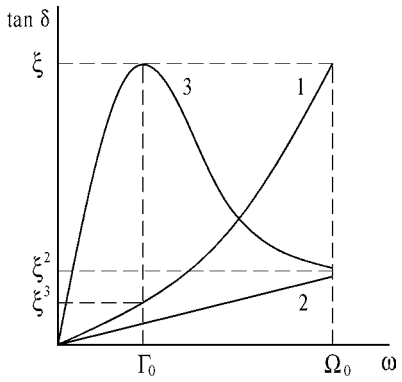

Fig. 12. Results of phonon transport theory. Schematic off-scale plot of the frequency dependence of the three-quantum (1), four-quantum (2), and quasi-Debye (3) contributions to the loss tangent due to interaction of the ac electric field with the phonons of the soft mode of a displacive type ferroelectric. Ω_0 and Γ_0 are the soft-mode frequency and damping, respectively. $\xi = \Gamma_0/\Omega_0$. The range of applicability of the theory is $\Gamma_0 \ll \Omega_0$ and $\omega \ll \Omega_0$ (at ω tending to Ω_0, the curves are only shown to guide the eye).

with the soft-mode phonons of a perovskite-type ferroelectric in the ferroelectric phase. It is seen that in this material the quasi-Debye contribution dominates the intrinsic loss in the frequency range $\omega \leq \Gamma$ (for $SrTiO_3$ and $KTaO_3$ at $T \geq 20$–30 K that means $\omega \leq 100$ GHz).

In microwave materials for tunable application, which are typically centrosymmetric, the quasi-Debye mechanism does not contribute to the loss in the absence of the tuning bias. However, under a dc bias field, $\vec{E}_0$, it becomes active due to the breaking of the central symmetry so that one is dealing with the *dc-field-induced quasi-Debye mechanism*. The contribution of this mechanism has been modeled for $SrTiO_3$, $(Ba,Sr)TiO_3$ and $KTaO_3$ using the above formulae and the available information on the material parameters and parameters of the phonon spectrum of these materials [65–67]. It was shown that for not too high frequencies ($\omega \leq \Gamma$), the contribution in question can be presented as:

$$\tan\delta_{\mathrm{QD}}(E_0) = A\,\omega \cdot I(E_0) \cdot n_r \qquad (3.34)$$

where the function $I(E_0) \to 1$ in the limit of small relative tunability $n_r = \frac{\varepsilon(0) - \varepsilon(E_0)}{\varepsilon(0)} \ll 1$. The theoretical estimates for the parameter A are given in Table 4 together with the experimental data available in the literature [2, 7] (see also Section 5 of the present paper). The agreement between the theory and experiment can be considered as reasonable despite significant spread

Table 4. Experimental and simulated data for A in Eq. (3.34) for $KTaO_3$, $SrTiO_3$ and $Ba_{0.6}Sr_{0.4}TiO_3$.

	$A \times 10^{-3}(\mathrm{GHz}^{-1})$		
	$KTaO_3$ ($T = 50$ K)	$SrTiO_3$ ($T = 80$ K)	$Ba_{0.6}Sr_{0.4}TiO_3$ ($T = 300$ K)
Experiment [2, 7]	23	17	–
Calculation	8–27	5–19	0.7–1.4

of the theoretical estimates, which is related, first of all, to the lack of reliable information on the damping of the phonons participating in the microwave absorption.

For dc fields corresponding to small relative tunability n_r, Eq. (3.34) suggests a quadratic field dependence of the dc field induced contribution to the loss tangent, $\tan\delta_{QD}(E_0)$. For higher fields, the $\tan\delta_{QD}$ vs. E_0 dependence deviates from this simple law and appears to be different for different materials. The result of simulations of this dependence for $SrTiO_3$ and $Ba_{0.6}Sr_{0.4}TiO_3$ crystals is shown in Fig. 13. In this simulation, only $\tan\delta_{QD}(E_0)$ was modeled whereas $\tan\delta\,(0)$ was taken from experimental data [2, 68]. For the case of $SrTiO_3$, the value of the A parameter was set to fit the experimental $\tan\delta\,(E_0)$ dependence [2] at smallE_0.

The striking difference between the field dependences of the loss in $SrTiO_3$ and $Ba_{0.6}Sr_{0.4}TiO_3$ shown in Fig. 13 is attributed to the difference in the strength of the flexoelectric coupling between the soft mode and acoustic branches in these materials. The nonmonotonic field dependence of the loss tangent in $SrTiO_3$ is related to the contribution of the acoustic phonon to the quasi-Debye loss, which is activated by this flexoelectric coupling [65, 66]; in $Ba_{0.6}Sr_{0.4}TiO_3$, where the flexoelectric coupling is much smaller, this contribution is small and cannot be seen.

The above analysis implies that the contribution of the field-induced quasi-Debye loss can be a major contribution to the total loss in a material, especially in the case of thin films where high dc fields are readily achievable. For instance, for $SrTiO_3$ at and $Ba_{0.6}Sr_{0.4}TiO_3$ @ $E_{dc} = 100$ kV/cm & $\omega = 25$ GHz, according to Fig. 13 and Eq. (3.34) one expects $\tan\delta_{QD}$ about 0.1 and 0.02 at $T = 80$ K and $T = 300$ K, respectively.

An important feature of the quasi-Debye loss is that as a function of frequency, similar to the Debye loss, its contribution to the loss tangent passes through a maximum at $\omega \cong \Gamma$ (see Fig. 11) For the aforementioned materials, where the phonon damping Γ is of the order of 10^2 GHz , this means a certain slowing down of the linear frequency dependence of $\tan\delta_{QD}$, Eq. (3.34), in the higher part of the microwave-frequency range.

3.2.2. *Extrinsic Loss*

The role of the intrinsic mechanisms in the total balance of the dielectric loss of a material is strongly dependent on the dielectric permittivity of the material and the measuring frequency: typically, the higher the frequency and permittivity, the more important the intrinsic loss. In the case of tunable ferroelectric materials

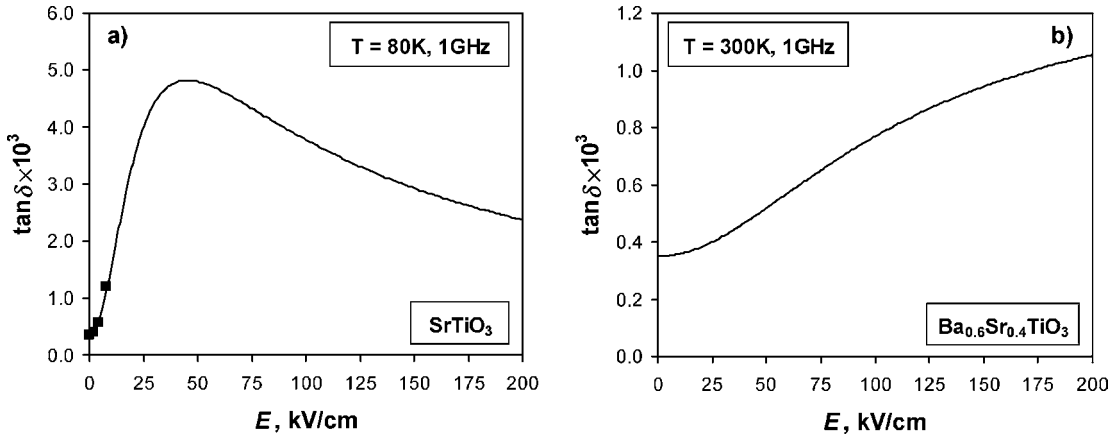

Fig. 13. Simulated field dependence of the loss tangent (solid lines) plotted together with experimental data [2] (black squares) for $SrTiO_3$ (a) and $Ba_{0.6}Sr_{0.4}TiO_3$ (b) crystals; $A_{SrTiO_3} = 17 \times 10^{-3}$ GHz^{-1}, $A_{Ba_{0.6}Sr_{0.4}TiO_3} = 0.7 \times 10^{-3}$ GHz^{-1}. The values of $\tan\delta(0)$ are taken from Refs. [2] and [68], respectively.

at microwave frequencies, the intrinsic and extrinsic contributions are comparable so that the dominating contribution to the loss may be extrinsic or intrinsic depending on the quality of the material. A kind of extrinsic/intrinsic crossover in loss may also take place under the action of a dc bias field, i.e. without the field, the extrinsic contribution dominates the loss, whereas under the field the intrinsic one does. Among the known extrinsic loss mechanisms those listed below are considered as significantly contributing to the loss in tunable microwave materials: (i) loss owing to charged defects, (ii) universal relaxation law mechanism, (iii) quasi-Debye contribution induced by random-field defects.

Loss Owing to Charged Defects. Motion of charged defects caused by an ac electric field results in a generation of acoustic waves at the frequency of the applied field. This brings about an additional loss mechanism that was proposed by Schlöman [69], formulated for high-dielectric-constant materials by Vendik and Platonova [70], and developed by Garin [71]. The contribution of this mechanism to the loss tangent can be approximated as follows:

$$\tan\delta_{\text{ch}} = F\varepsilon\frac{n_d}{\rho v_t^3}\frac{Z^2}{4\pi}\,\omega\cdot\left[1-\frac{1}{\left(1+\omega^2/\omega_c^2\right)^2}\right] \quad (3.35)$$

where Z and n_d are the effective charge of the defects and their atomic concentration; ρ and v_t are the density and average transversal sound velocity of the material; F is a material-dependent numerical constant of the order of unity; $\omega_c = v_t/r_c$ where r_c is the correlation length of the charge distribution in the material. The physical meaning of r_c is the minimal distance at which the elecroneutrality is maintained. For Schottky defects r_c is of the order of the typical distance between the positively and negatively charged defects. This mechanism may play an essential role in thin film based tunable capacitors, where an elevated defect concentration compared to the bulk material is expected. In this case, the effect of semiconductor depletion of the carriers from the deep traps (caused by ferroelectric/electrode contact) [72, 73] will further increase the contribution of this mechanism via a strong reduction of $\omega_c = v_t/r_c$. This occurs in the depleted areas due to a strong increase of r_c up to the depletion length. An essential feature of this mechanism is that its contribution to the loss tangent is proportional to the permittivity of the material. This implies that this contribution is inversely dependent on the applied dc field.

Universal-Relaxation-Law Mechanism. For all of the loss mechanisms discussed above, a linear frequency dependence of the loss tangent is typical at least for microwave frequencies and below. In reality, this dependence is usually observed at the microwave and higher frequencies. For lower frequencies, a much weaker frequency dependence is usually observed, which is consistent with the so-called universal-relaxation law which in turn corresponds to the following expression for the complex dielectric permittivity ε^* [74]:

$$\varepsilon^* = G(i\omega)^{n-1} = G(\cos(n\pi/2) - i\sin(n\pi/2))(\omega)^{n-1} \quad (3.36)$$

where G is a frequency-independent constant and $0 < n < 1$. In perovskite thin films in both frequency and time domains, dielectric relaxation corresponding to this equation (for n close to but smaller than unity) has been reported up to the microwave frequency range, e.g. in (Ba,Sr)TiO_3 [75]. The physical origin of this behavior is attributed to a variation in charge transport barriers, e.g. at the grain boundaries [76], or to creep of the boundary of the near-by-electrode depletion layer [77]. No information is available on the dependence of G on the dielectric constant of the material.

Impact of Local Polar Regions. The typically centrosymmetric tunable materials may have local polar regions induced by various defects and structural imperfections. For example, recent infrared reflectivity investigations of $SrTiO_3$ ceramics revealed a clear presence of grain-boundary-induced polar phase inclusions [78]. Random field defects can also be responsible for the appearance of local polar regions (see e.g. [4]). In all these polar inclusions, the quasi-Debye mechanisms is expected to be active. Though the volume fraction of the polar phase is typically small, this "defects-induced" quasi-Debye mechanism may be important due to its large (compared to other intrinsic loss mechanisms) contribution per unit of volume. Though the theory of the "defect-induced" quasi-Debye mechanism is not developed, using the results on the quasi-Debye loss in the ferroelectric phase [54] one can conclude that the contribution of the "defect-induced" quasi-Debye

mechanism should be strongly ε-dependent. According to Ref. [54] in the ferroelectric phase of a displacive ferroelectric $\tan\delta_{\rm QD} \propto \varepsilon^{3/2} P_S^2$ where P_S is the spontaneous polarization. In the case of non-polar tunable material with polar inclusions one can substitute the volume average of the local polarization squared, $\langle P_{\rm loc}^2 \rangle$, for P_S^2 to evaluate the contribution of the "defect-induced" quasi-Debye mechanism as

$$\tan\delta_{\rm dQD} \propto \varepsilon^{3/2} \cdot \left\langle P_{\rm loc}^2 \right\rangle. \tag{3.37}$$

We can also use the relation between the ferroelectric correlation length ξ and $\langle P_{\rm loc}^2 \rangle$ [78]: $\langle P_{\rm loc}^2 \rangle \propto \xi^{3-d}$ where d is the dimension of the defect, i.e. $d = 2$ for a planar defects like grain boundaries, $d = 1$ for linear defects, and $d = 0$ for point defects. Finally, making allowance that $\xi \propto \sqrt{\varepsilon}$ we arrive at a rather strong ε-dependence of the contribution of this mechanism, namely:

$$\tan\delta_{\rm dQD} \propto \varepsilon^{4.5-d}. \tag{3.38}$$

3.2.3. Loss in Tunable Composites

As we have mentioned above there are some situations where the tunable material can be treated as a ferroelectric/dielectric composite (see Section 3.2.2). Clearly, not only the dielectric permittivity and tunability of the materials are strongly affected by the presence of the "passive" component but the dielectric loss is affected as well. Since "normal" low-ε dielectrics typically exhibit much lower loss tangent than ferroelectrics, a reduction of the loss in composites may be expected with increasing volume fraction of the dielectric. Recently performed simulation of the problem for a number of simple models of the composite showed that this trend does not necessarily take place [45]. In what follows we will review the results of these simulations which were performed for the layered, columnar and spherical inclusion models already discussed in Section 3.1.3 and illustrated in Fig. 8.

First of all an important remark should be made. Mixing a tunable ferroelectric with a linear dielectric modifies the electrical properties of the material due to following effects: (i) the effect of mutual doping of the composite components (inter-diffusion), (ii) effects of inter-component bondaries, (iii) effects of mixing-induced modification of microstructure of the ferroelectric component, and (iv) the effect of the electric field redistribution between the different components of the mixture. In the following we will address the last but not least effect, which can be treated in terms of electrostatic considerations. Thus, when discussing the composite effects on the electric parameters of a real material, the result presented below should be applied together with arguments related to the other aforementioned effects.

The calculation of the imaginary part of the permittivity of the composite, $\varepsilon''_{\rm mix}$, can be performed based on the equation of the balance of the dissipated energy in the material[7]

$$\frac{\omega}{2}\varepsilon''_f\left\langle \tilde{E}_f^2 \right\rangle (1-q) + \frac{\omega}{2}\varepsilon''_d\left\langle \tilde{E}_d^2 \right\rangle q = \frac{\omega}{2}\varepsilon''_{\rm mix}\tilde{E}^2 \tag{3.39}$$

where $\tilde{E}$ is the applied ac field amplitude whereas $\langle \tilde{E}_f^2 \rangle$ and $\langle \tilde{E}_d^2 \rangle$ stand for the averaged squared amplitudes of the ac field in the ferroelectric and dielectric, respectively; q is the volume fraction of the dielectric.

In the case of columnar and layered composites, where the ac fields in the ferroelectric and dielectric remain homogeneous, the loss tangent of the mixture can be readily expressed (using Eqs. (3.39), (3.15), and (3.23)) in term of the volume fraction and permittivity of the components, namely:

$$\tan\delta_{\rm mix}^{\rm col} = \frac{\tan\delta_f \varepsilon_f (1-q) + \tan\delta_d \varepsilon_d q}{(1-q)\varepsilon_f + \varepsilon_d q} \tag{3.40}$$

for the columnar composite and

$$\tan\delta_{\rm mix}^{\rm lay} = \frac{\tan\delta_f \varepsilon_d\,(1-q) + \tan\delta_d \varepsilon_f q}{(1-q)\,\varepsilon_d + \varepsilon_f q} \tag{3.40a}$$

for the layered composite. Here $\tan\delta_f$ and $\tan\delta_d$ are the loss tangent of the ferroelectric and dielectric. These expressions can also be used for calculation of the loss tangent of the composites in the presence of a dc bias field E_0. In the case of the columnar composite under dc bias, the permittivity and loss tangent of the ferroelectric in Eq. (3.40) should be set equal to their values corresponding to dc field equal E_0, i.e. $\varepsilon_f(E_0)$ and $\tan\delta_f(E_0)$. In the case of the layered composite, these parameters should be set equal to $\varepsilon_f(E_f)$ and $\tan\delta_f(E_f)$ where the field seen by the ferroelectric E_f is to be calculated by taking into account the field redistribution between the components (see Section 3.1.3). Due to this, in the latter case, the fraction q dependence

of the loss tangent is more complicated than the explicit q-dependence of Eq. (3.40a).

In the case of the spherical inclusion model, the field in the ferroelectric matrix is not homogeneous (see Eqs. (3.25) and (3.25a)) so that the extra contribution to $\langle \tilde{E}_f^2 \rangle$ arises due to the inhomogeneous component of the field. This essentially complicates the problem. Below we will present some results of calculations performed for the case of small volume concentration of the dielectric spherical inclusions (i.e. $q \to 0$) and small relative tunability of the composite. In these calculations, it was also assumed that the real and imaginary parts of permittivity are much greater in the ferroelectric matrix than in the dielectric inclusions (i.e. $\varepsilon_d \ll \varepsilon_f$, $\varepsilon_d'' \ll \varepsilon_f''$), which is true to the real experimental situation. In this case, using Eqs. (3.39) and (3.25a) one finds for the imaginary part of the composite permittivity [45]:

$$\varepsilon''_{\text{mix,sph}} \approx \varepsilon''_f \left(1 - \frac{3}{2} q\right), \tag{3.41}$$

This result essentially differ from those for columnar and layered models which give in the same limiting case ($\varepsilon_d \ll \varepsilon_f$, $\varepsilon_d'' \ll \varepsilon_f''$, and $q \to 0$):

$$\varepsilon''_{\text{mix,col}} \approx \varepsilon''_f (1 - q), \tag{3.42}$$

$$\varepsilon''_{\text{mix,lay}} \approx \varepsilon''_f \left(1 - 2\frac{\varepsilon_f}{\varepsilon_d} q\right), \tag{3.43}$$

respectively. It is instructive to compare the above results for the imaginary part of permittivity with the predicted concentration dependences of the real part of permittivity

$$\varepsilon_{\text{mix,col}} \approx \varepsilon_f (1 - q), \tag{3.44}$$

$$\varepsilon_{\text{mix,lay}} \approx \varepsilon_f \left(1 - \frac{\varepsilon_f}{\varepsilon_d} q\right), \tag{3.45}$$

$$\varepsilon_{\text{mix,sph}} \approx \varepsilon_f \left(1 - \frac{3}{2} q\right). \tag{3.46}$$

and loss tangent

$$\tan \delta^{\text{col}}_{\text{mix}} \approx \tan \delta_f, \tag{3.47}$$

$$\tan \delta^{\text{lay}}_{\text{mix}} \approx \tan \delta_f \left(1 - \frac{\varepsilon_f}{\varepsilon_d} q\right), \tag{3.48}$$

$$\tan \delta^{\text{sph}}_{\text{mix}} \approx \tan \delta_f. \tag{3.49}$$

which are evaluated in the same limiting case. A remarkable feature of these results is that the dilution effect on the loss tangent can be much less pronounced than for the real part of the permittivity as it is seen in the columnar and spherical inclusion models. That actually means a rather weak $\tan\delta$ vs. ε dependence which is absolutely untypical for the loss mechanisms in "non-composite" materials discussed in the preceding sections. This result holds for the case of higher concentrations of the dielectric as it is seen from the modeling performed in a wide range of the permittivity variation. The results of this modeling are presented in Fig. 14 where the loss tangent of the composites is plotted as a function of their permittivity and the concentration of the dielectric. The material parameters used in the modeling are listed in Table 5.

Table 5. Characteristics of the composite components.

Material	Dielectric constant ε		Loss tangent ($\tan\delta$)
	$E = 0$	$E = 7.3$ kV/cm	
Ferroelectric ($\beta = 7.37 \times 10^9$ JC^{-4} m^{-5})	3300	2640	$10^{-2} \frac{\varepsilon(E)}{\varepsilon(0)}$
Linear dielectric	8.4	8.4	10^{-4}

3.3. *Commutation Quality Factor of Tunable Materials*

As was discussed in Section 2 the Vendik's Commutation Quality Factor of the ferroelectric K (introduced by Eq. (2.3) is a most suitable parameter for characterization of performance of tunable ferroelectric materials. It is instructive to consider the implication of the theoretical results reviewed above on the K-factor of tunable materials. Two issues will be addressed below: the limitation on the K-factor imposed by the dc field induced quasi-Debye mechanism and the expected impact on the K-factor of the dilution of ferroelectrics with a low-permittivity-low-loss dielectric.

The dc-field-induced increase of the loss tangent of a tunable material imposes intrinsic limitations on the K factor. Since the field induced contribution to the loss tangent may be comparable to its typical values, this contribution ought to be taken into account when evaluating the intrinsic limitations on the K-factor of various materials. The intrinsic limit for the K-factor can be evaluated by using the result on tunability from Section 3.1.1, Eq. (3.34) for the contribution of the field induced quasi-Debye mechanism to the loss, and

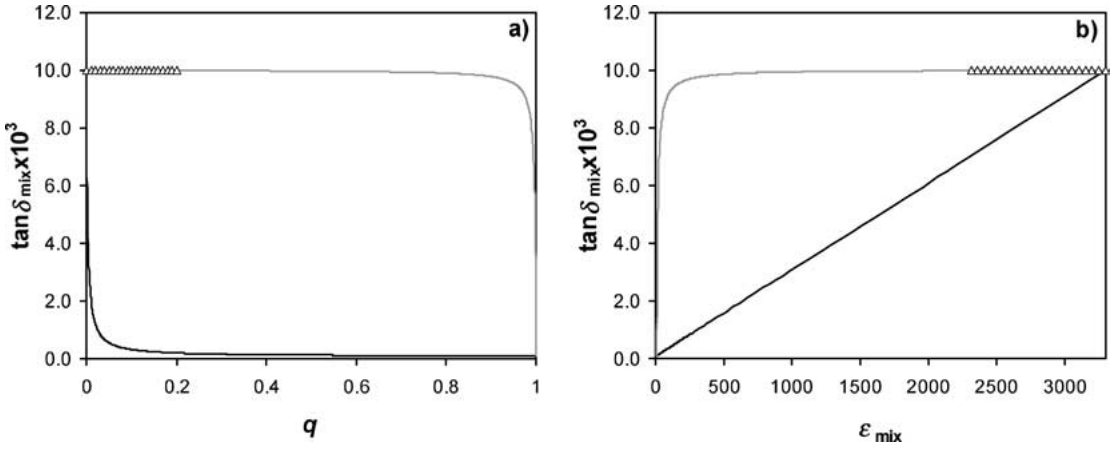

Fig. 14. Calculated loss tangent of ferroelectric/dielectric composites, $\tan\delta_{\rm mix}$, as a function of volume concentration of dielectric q (a) and dielectric constant of the composite material $\varepsilon_{\rm mix}$ (b). (Black lines—layered model; grey lines—columnar model; triangles—spherical inclusion model) [45].

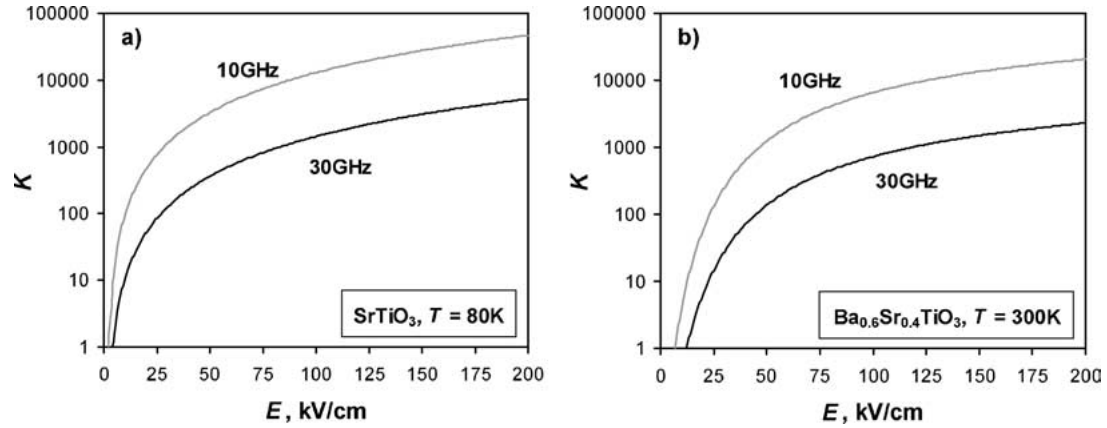

Fig. 15. Calculated field dependences of the quality factor K for $SrTiO_3$ (a) and $Ba_{0.6}Sr_{0.4}TiO_3$ (b) ferroelectrics at frequencies of 10 GHz (grey lines) and 30 GHz (black lines). The calculations were performed for the same material parameters as those used for plotting the graphs in Fig. 13 [67].

the data on the intrinsic component of loss tangent. The latter can be presented as $\tan\delta\,(0) = A_0\omega$ where A_0 is a frequency independent constant. This gives

$$K = \frac{n-1}{A_0 A\omega^2 I(E_0)}. \tag{3.50}$$

The K-factor calculated this way for $SrTiO_3$ (a) and $Ba_{0.6}Sr_{0.4}TiO_3$ (b) [67] is presented in Fig. 15 as a function of the tuning bias dc field E_0.

The modeling of impact of the dilution of ferroelectrics with a low-permittivity-low-loss dielectric on the K-factor is motivated by the current activity on the tunable performance of ferroelectric/dielectric composites [68, 79, 80]. The calculations performed in Sections 3.1.3 and 3.2.3 enable such modeling. Figure 16 shows the results of this modeling performed for a ferroelectric/dielectric composite whose parameters are listed in Table 5. The three types of the composite illustrated in Fig. 8 are addressed. The field dependence of the loss in the ferroelectric is set as $\tan\delta_f(E) = \tan\delta_f(0)\frac{\varepsilon_f(E)}{\varepsilon_f(0)}$, which is consistent with the trend known for the extrinsic contributions to the loss in real materials as will be discussed in Section 5.2.

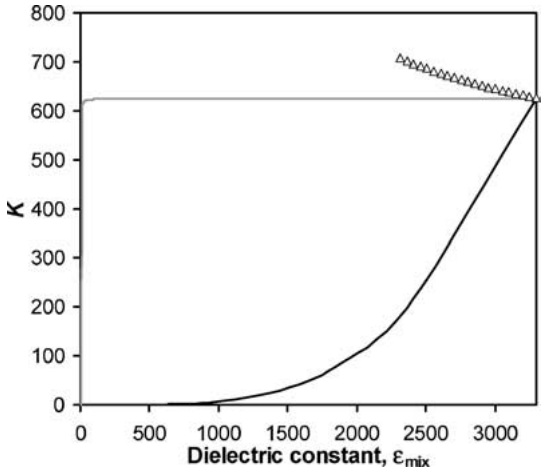

Fig. 16. Calculated quality factor of composite, K, as a function of its dielectric constant ε_{mix}. (Black lines—layered model; grey lines—columnar model; triangles—spherical inclusion model).

Several features of the results shown in Fig. 16 are to be commented upon.

First, in contrast to the case of linear dielectric response, the result for the spherical inclusion model does not lay between those for the layered and columnar models. Second, the results for the spherical inclusion model shows that the composite effect may result in an increase (though slight) of the K-factor owing to dilution of a ferroelectric with non-tunable dielectric. Of interest is that this effect takes pace due to an increase of tunability rather than decrease of the loss tangent. Concerning these results one should also mentioned that these were obtained only for a very limited case of small relative tunability and small concentration of the dielectric. Thus, the problem of tunability of a ferroelectric composite remains open for theoretical studies. Third, considering the above results of modeling from the practical point of view, one can state that, in ferroelectric/dielectric composites, the dilution of the ferroelectric may lead to a substantial reduction of the composite permittivity having, at the same time, a minute effect on the K-factor.

The above analysis enables us to conclude that, at least due to the considered effect of the field redistribution, it is difficult to expect a substantial improvement of the tunable performance of a ferroelectric material by using a composite. At the same time, one cannot exclude an appreciable increase of the K-factor caused by the addition of a dielectric in the ferroelectric, which is due to a kind of doping effect, e.g. due to a doping induced reduction of the loss in the ferroelectric matrix. In addition, the composite effect may be advantageous for the tunable applications where a lower dielectric permittivity of the active material is desirable. This advantage is coming from the aforementioned possibility to have in composites a lower permittivity for the same value of the K-factor.

3.4. Dielectric Response of Tunable Thin Films

The theory reviewed in the preceding section is equally applicable to bulk and film forms of tunable materials. However, in the case of films, there exist additional effects that may substantially influence the tunable performance of the material. These effects are responsible for the difference between the tunable performance of the films and bulk samples having nominally the same chemical composition. Specifically, the films typically exhibit lower dielectric permittivity and higher loss than the bulk materials of similar composition (see Section 5 for a discussion of experimental results). In the case of films thinner than a few micrometers, which are commonly called *thin films* and which we are going to approach below, this difference is always significant, at least when the permittivity of the material exceeds 1000. The origin of this difference relates to two groups of factors. First, the processing conditions for bulk materials and thin films are different (e.g., a difference in the processing temperature, a possibility for a substantial loss of a volatile component, etc). Second, even if the bulk and film counterparts are chemically identical (the same compositions and defect populations), one can expect a difference in their properties due to several physical size effects. In the present section we give an overview the physics behind these effects.

3.4.1. Passive Layer Effects

Several reasons may cause a ferroelectric thin film to exhibit identical or similar dielectric response to that of a perfect ferroelectric film with a thin dielectric layer at its surfaces. The simplest possibility is the presence of a secondary phase at the surface of the films. This situation can be excluded by proper processing control. In addition, there exist two intrinsic reasons for this kind of dielectric behavior of the films. The first one is a near-by-surface variation of the polarization (field induced or spontaneous). This situation was theoretically addressed by Kretschmer and Binder [81] in a general

manner and further analyzed by Vendik and Zubko [40, 82]. Second, if the dielectric response of a film is monitored by using a parallel plate capacitor, this response is affected by the fact that the free charges in the electrode form a finite thickness layer that behaves as a capacitor connected in-series with the material of the films [83, 84]. Treatment of the electron gas in the electrode in the Thomas-Fermi approximation [85] shows that this capacitor has the capacitance per unit area of ε_0/l_s where l_s is the Thomas-Fermi screening length. This evidentially leads to the following expression for the apparent out-of-plane dielectric permittivity in the film:

$$\varepsilon_{\text{eff}}^{-1} = \varepsilon^{-1} + \frac{2l_s}{h}. \tag{3.51}$$

The two models mentioned above have an essential common feature, namely, the in-plane and out-of-plane components of the dielectric permittivity are differently affected by the considered effects. In the case of the "electrode effect", only the out-of-plane component is affected since it is this component that is measured using the plate-capacitor set up. For the "near-by-surface variation effect", the out-of-plane component is more strongly affected than the in-plane one, however this is less obvious than in the case of the "electrode effect". This issue will be addressed below following the results from Refs. [40, 81, 82]. However, these results will be corrected by the impact of the background dielectric permittivity of the ferroelectric, which was ignored in these papers.

The starting point of the model is the assumption that the surface value of the polarization in a ferroelectric is not affected by the electric field as strongly as that in the bulk. This is consistent with the microscopical arguments that the ferroelectric softness of the lattice is somehow suppressed near to the surface. The simplest modeling of this point is performed in the framework of the continuous Landau theory for a situation where the polarization at the two surfaces of the film is completely blocked. This corresponds to the equation for the polarization:

$$E = \alpha P - \kappa \frac{\partial^2 P}{\partial x^2} \tag{3.52}$$

with the boundary conditions

$$P(0) = 0 \quad \text{and} \quad P(h) = 0, \tag{3.53}$$

the surfaces of the film being at $x = 0$ and $x = h$. In the following treatment we will also take into account that the relative dielectric permittivity of the material is always large, i.e. $\varepsilon = (\alpha\varepsilon_0)^{-1} \gg 1$.

In the case of the in-plane component of the effective permittivity of the system, which is actually monitored in the planar capacitor setup (shown in Fig. 3a) having the gap g much greater than the film thickness h, the expected inhomogeneity of polarization across the film does not create depolarizing field. Thus, the field E entering Eq. (3.52) is equal[8] to the "applied field" $E_{\text{ext}} = U/g$, where U is the voltage applied to the gap. In this case, the distribution of the polarization across the film (i.e. in the direction of the film normal) can be readily found in the form

$$P(x) = \frac{E_{\text{ext}}}{\alpha}\left(1 - \frac{\cosh\frac{x-h/2}{\xi}}{\cosh\frac{h}{2\xi}}\right) \tag{3.54}$$

where

$$\xi = \sqrt{\frac{\kappa}{\alpha}} \tag{3.55}$$

is the so-called correlation length having the meaning of the scale on which the polarization changes near the surfaces. Typically, ξ rarely exceeds a few nm. For the case of practical interest where $h \gg \xi$, Eq. (3.54) leads to the following value of the average polarization in the films:

$$\bar{P} = \frac{1}{h}\int_0^h P(x)\,dx = \frac{E_{\text{ext}}}{\alpha}\left(1 - \frac{2\xi}{h}\right). \tag{3.56}$$

This corresponds to effective dielectric permittivity of the system:

$$\varepsilon_{\text{eff}} = \varepsilon\left(\frac{h - 2\xi}{h}\right). \tag{3.57}$$

This equation means that, effectively, two layers of thickness ξ have the dielectric constant much smaller than ε so that they, actually, do not contribute to the polarization response. Alternatively, these layers can be considered as connected in parallel with ferroelectric films of thickness $h - 2\xi$.

In the case of the out-of-plane component of the effective permittivity of the system, which corresponds to the situation in the parallel plate ("through thickness") capacitor, the polarization is normal to the plane of the

films so that its variation *does create a depolarizing field*. This is a crucial difference compared to the preceding case. The relation between the "applied field" $E_{\text{ext}} = U/h$, where U is the voltage applied across the films, and the field seen by the ferroelectric can be found from the Poisson equation. Taking into account the background contribution to the displacement $\varepsilon_0\varepsilon_b E$, where $\varepsilon_b \ll \varepsilon$ is the contribution to the electric permittivity of the non-ferroelectric lattice modes of the crystal, the Poisson equation reads in our case as $d(\varepsilon_0\varepsilon_b E + P)/dx = 0$ leading to the sought relation:

$$E = E_{\text{ext}} - \frac{1}{\varepsilon_0\varepsilon_b}(P - \bar{P}). \tag{3.58}$$

Using this relation, Eq. (3.52) can be rewritten as

$$E_{\text{ext}} = \alpha P - \kappa\frac{\partial^2 P}{\partial x^2} + \frac{1}{\varepsilon_0}(P - \bar{P}). \tag{3.59}$$

The solution of this equation that satisfies the boundary conditions Eq. (3.53) reads

$$P(x) = \frac{E_{\text{ext}}}{\alpha}\left(1 - \frac{\cosh\frac{x-h/2}{\xi_1}}{\cosh\frac{h}{2\xi_1}}\right)\frac{1}{1 + 2\varepsilon\frac{\xi_1}{h}\tanh\frac{h}{2\xi_1}} \tag{3.60}$$

where $\xi_1 = \xi/\sqrt{1+\varepsilon/\varepsilon_b} \approx \xi/\sqrt{\varepsilon/\varepsilon_b} = \sqrt{\varepsilon_b}\sqrt{\kappa\varepsilon_0}$ has the meaning of the scales on which, in this geometry, the polarization changes near the surfaces. Note that ξ_1 is yet smaller than ξ so that, for any case of practical interest, $\xi_1/h \ll 1$. Under this conditions, Eq. (3.60) leads to the expression for the effective dielectric permittivity of the film:

$$\varepsilon_{\text{eff}}^{-1} = \varepsilon^{-1} + \frac{2\xi_1}{h}. \tag{3.61}$$

This relation corresponds to the in-series connection of the ferroelectric film with two dielectric layers of thickness ξ_1 and dielectric permittivity $\varepsilon_d = 1$.

Thus we see that the surface region with partially suppressed dielectric response behaves as a passive layer, however in contrast to a real dielectric layer its thickness is essentially different for in-plane and out-of-plane geometries.

The above theoretical treatment of the problem has been presented for the situation where the polarization at the surfaces of the films is completely blocked. The more general situation where the blocking is not complete can be simulated by using the mixed boundary conditions

$$P(0) - \lambda\frac{\partial P}{\partial x}\bigg|_{x=0} = 0 \quad \text{and} \quad P(h) + \lambda\frac{\partial P}{\partial x}\bigg|_{x=h} = 0 \tag{3.62}$$

instead of (3.53). These conditions interpolate the situation between the blocked (at $\lambda = 0$) and free (at $\lambda \to \infty$) polarization at the surfaces of the films. Under this modification the above results, Eqs. (3.57) and (3.61) hold however with the substitutions

$$\xi \Rightarrow \frac{\xi}{1+\lambda/\xi} \quad \text{and} \quad \xi_1 \Rightarrow \frac{\xi_1}{1+\lambda/\xi_1}. \tag{3.63}$$

Thus, as one can expect, a weakening of the surface blocking leads to a reduction of the effective passive layer thickness, the effect vanishing in the limit of free polarization at the film surface ($\lambda \to \infty$).

It is instructive to illustrate schematically the difference between the spatial distribution of the polarization for the "in-plane" and "out-of-plane" situations (Fig. 17). In the "in-plane" situation where there is no impact of the depolarizing effects, the polarization reaches exponentially fast the value that is expected

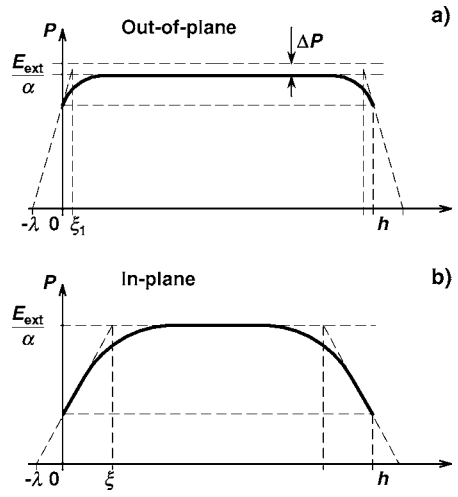

Fig. 17. Schematic distribution of polarization across a film of thickness h for out-of-plane (a) and in-plane (b) cases. $\Delta P\alpha/E_{\text{ext}} = 2\varepsilon\xi_1/h$ where $\xi_1 = \xi\sqrt{\varepsilon_b/\varepsilon}$ (see Eq. (3.60)). Here, ε is the dielectric constant of the material, ε_b its background dielectric constant, h is the thickness of the film, ξ is the correlation length, and E_{ext}/α is the "bulk value" of the polarization.

in the bulk sample for the same value of the applied filed. On the other hand, in the "out-of-plane" situation, due to the depolarizing effects the polarization changes yet faster with the distance from the electrode, however finally reaching a value which is smaller than the polarization reached in the bulk situation. This figure also illustrates the geometrical meaning of parameter λ as the so-called extrapolation length.

All in all, the two models predict an increasing thickness dependence of the dielectric permittivity of the films, Eqs. (3.51), (3.57), and (3.61). Let us now address the applicability of these predictions to a real experimental situation in (Ba,Sr)TiO_3. To do so, some information on the correlation length ξ in the material is needed in addition to its known dielectric parameters. This information may be extracted from data on the dispersion of the soft mode. Using the data from Refs. [86, 87], the temperature independent parameter $\xi/\sqrt{\varepsilon} = \sqrt{\kappa\varepsilon_0}$ is evaluated[9] as 0.03 Å for $BaTiO_3$ and 0.08 Å for $SrTiO_3$. For $\varepsilon = 1600$, this leads to the estimates for the correlation length 1.2 Å for $BaTiO_3$ and 3.2 Å for $SrTiO_3$.This estimate enables us to make important conclusions:

(i) For situations of practical interest, the expected thickness dependence of the in-plane component of the measured permittivity is very weak. According to Eq. (3.57) the expected relative correction to the bulk permittivity is about $2\xi/h$. For 200 nm thick films, this makes a 1% correction at most. However, this result may be taken only as quantitative since the theoretical situation corresponds to the limit of the range of applicability of the continuous Landau theory; the latter is applicable if the typical scale of the polarization variation (ξ in this case) is essentially larger than the lattice constant of the material (4 Å in the case of (Ba,Sr)TiO_3).

(ii) For the out-of-plane component of the measured permittivity, a much stronger impact of the surface blocking of the polarization is found. According to Eq. (3.61) the expected relative correction to the bulk permittivity is about $2\xi_1\varepsilon/h$, that is some $\sqrt{\varepsilon/\varepsilon_b}$ times stronger than in the case of the in-plane component. On the other hand, assuming $\varepsilon_b \cong 10$ the scale $\xi_1 = \sqrt{\varepsilon_b}\sqrt{\kappa\varepsilon_0}$ (i.e. 0.1–0.2 Å) is much below the value of the lattice constant of the material, so that the use of the theoretical prediction, even as an order-of-magnitude estimate, cannot be justified. However, the physics behind Eq. (3.61), namely the in-series connection of the surface passive layer with the "bulk" ferroelectric part of the film looks reasonable. In this context, Eq. (3.61) might be used as a semi-empirical relation, ξ_1 being a fitting parameter. An analysis of the thickness dependence of the in-plane component of dielectric constant in terms of Eq. (3.61) performed by Vendik and Zubko [82] for (Ba,Sr)TiO_3 thin films yields the values of ξ_1 in the range 0.2–2.5 Å.

One more useful qualitative conclusion can be done on the basis of the above modeling for the out-of-plane component of the permittivity. Namely, its thickness dependence may be sensitive to the electrode material since the effective thickness of the surface dead layer is a function of the boundary condition at the electrodes, which in turn may be dependent on the electrode material. Here two hypotheses for the relation between the boundary condition in question and the electrode material should be mentioned. First, it was suggested that the surface blocking of polarization is much less pronounced in the case of a similarity between the ferroelectric and electrode, specifically, when the electrode is oxide and the ferroelectric is an oxide perovskite [40]. The second hypothesis is that in the case of oxide electrode, the effective surface passive layer is short-circuited [88]. Thus, both hypotheses imply that ferroelectric capacitors with oxide electrodes are expected to exhibit a weaker thickness dependence of the measured dielectric constant compared to those with metallic electrodes, which according to Vendik and Zubko is compatible with the existing experimental data [40].

Thus, though not being quantitatively justified, the mechanism relating the size effect to the surface blocking of the polarization looks relevant to the experimental situation in ferroelectric thin films. On the other hand, the "electrode" mechanism should not be discarded. Its prediction Eq. (3.51), which is strictly justified mathematically, is identical to that of the "surface blocking" model where ξ_1 is replaced by screening length l_s. The experimental data [82] for (Ba,Sr)TiO_3 thin films correspond to l_s in the range 0.2–2.5 Å, which is comparable to the typical value of Thomas-Fermi screening length, ≈ 0.5 Å.

The presented analysis is readily extended to the description of the tunability of a ferroelectric capacitor containing the aforementioned effective or real passive layers. In the case of a real dielectric layer or the "electrode" effect, the film will obviously exhibit the tunable behavior of a layer composite, which was

discussed in Section 3.1.3. In the case of the "surface polarization blocking" scenario, the situation with the out-of-plane component of the permittivity is also of this type of tunable behavior. The physical reason[10] for that is that the spatial scale ξ_1 weakly depends on ε which is the only field dependent parameter of the system. Thus, in all these cases, the field dependence of the measured permittivity of the films is controlled by the simple "in-series-capacitor" formula:

$$\varepsilon_{\text{eff}}^{-1}(E) = \varepsilon^{-1}(E_f) + \frac{l}{h} \tag{3.64}$$

where l is a constant that is independent of E and h (c.f. Eqs. (3.15) and (3.21)). As was mentioned in Section 3.1.3, the impact of the passive layer on the polarization response (permittivity and tunability) is identical to that of a lowering of the Curie-Weiss temperature of the material. Thus, all the passive layer models addressed above predict the polarization response of the films identical to that of an ideal film with a modified value of the Curie-Weiss temperature.

Concluding the discussion of the passive layer effects it is instructive to give a table for the thickness of a dielectric layer with $\varepsilon_d = 1$, which influence the dielectric permittivity of the film identically to a given passive layer effect.

3.4.2. *Depletion Effect*

Electrochemical interaction of conductive electrodes with electronic carriers of the ferroelelectric may result in the so-called depletion effect i.e. the removal of the carriers from narrow near-by-electrode regions so that charged regions of bare impurities are formed near the electrodes. In the case of a wide gap and heavily compensated semiconductor, which is the case of typical ferroelectrics used for tunable applications, this built-in charge is related to deep trapping centers and oxygen vacancies [72]. It can be considered as immobile during electrical measurements at room temperatures and homogeneous inside the depletion layers [73]. The depletion phenomenon is characterized by the parameter W called *depletion layer thickness*, which is a function of the electrochemical parameters of the electrode-ferroelectric interface. If the film thickness h is larger than $2W$, the film contains two space-charge layers at the two electrodes and a neutral region in the middle. This is the case of *partial depletion*. If $h < 2W$, the film is homogeneously filled with space charge. This is

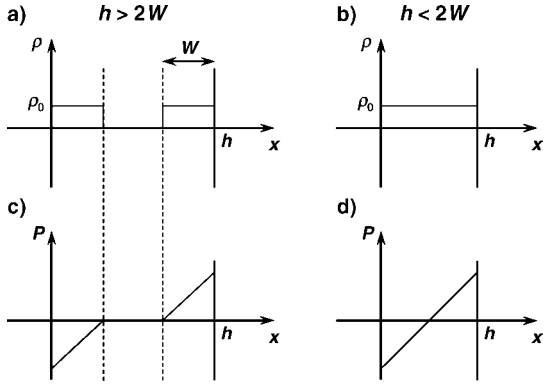

Fig. 18. Space charge distributions of partially (a) and fully (b) depleted films. The distributions of the build-in polarization (c) and (d), in these cases, respectively.

the case of the so-called *full depletion*. For the two case discussed above, the charge density distribution $\rho_d(x)$ across the films is shown in Fig. 18(a) and (b).

This space charge can influence the ferroelectric and dielectric properties of the films [89, 90]. The impact of the depletion effect on the effective dielectric permittivity of a parallel plate capacitor containing a ferroelectric which is subjected to the depletion effect of the electrodes can be elucidated using the following simple arguments. The built-in depletion charge results in a certain built-in electric field which in turn creates the built-in x-dependent polarization $P_b(x)$, x being the coordinate normal to the plane of the film. For the dielectric response of the film, this implies a local x-dependent permittivity of the films whose out-of-plane component according to Eq. (3.3) reads:

$$\varepsilon_{\text{loc}}(x) = \frac{1}{\varepsilon_0}\frac{1}{\alpha + 3\beta P_b^2(x)}. \tag{3.65}$$

Taking into account the "in-series" geometry of the problem the effective dielectric constant of the system can be found by averaging $1/\varepsilon_{\text{loc}}(x)$ across the film thickness, namely

$$\begin{aligned}\frac{1}{\varepsilon_{\text{eff}}} &= \frac{1}{h}\int_0^h \frac{dx}{\varepsilon_{\text{loc}}(x)} \\ &= \frac{1}{\varepsilon} + \frac{3\beta\varepsilon_0}{h}\int_0^h P_b^2(x)\,dx.\end{aligned} \tag{3.66}$$

The exact value of $P_b(x)$ can be obtained form a rather cumbersome solution of a set of equations: the Poisson

equation

$$d(\varepsilon_0\varepsilon_b E + P_b(x))/dx = \rho(x), \tag{3.67}$$

where $\rho(x)$ is the density of the built-in charge and the equation of state for the ferroelectric, Eq. (3.2). This solution should also obey the condition

$$\int_0^h E dx = 0. \tag{3.68}$$

A good approximation for the built-in polarization can be readily obtained if, in Eq. (3.67), one neglects the term $\varepsilon_0\varepsilon_b E$. This approximation is justified by a large value of the dielectric permittivity of the ferroelectric (i.e. $\varepsilon \gg \varepsilon_b$). Then, Eqs. (3.67) and (3.68) yield

$$P_b(x) = (x - h/2)\rho_0 \tag{3.69}$$

for the full-depletion case and

$$\begin{aligned} &P_b(x) = (x - W)\rho_0 \quad 0 < x < W \\ &P_b(x) = 0 \quad \text{for } W < x < h - W \\ &P_b(x) = (x - h + W)\rho_0 \quad h - W < x < h \end{aligned} \tag{3.70}$$

for the case of partial depletion. Here ρ_0 is the space charge density in the depleted regions. The profiles given by Eqs. (3.69) and (3.70) are illustrated in Fig. 18(c) and (d).

Using this result for the built-in polarization and Eq. (3.66) we find that the depletion leads to a reduction of the effective dielectric permittivity of the film. In the cases of the full and partial depletion, one finds

$$\frac{1}{\varepsilon_{\text{eff}}} = \frac{1}{\varepsilon} + \frac{4\varepsilon_0\beta\rho_0^2 W^3}{h} \tag{3.71}$$

and

$$\frac{1}{\varepsilon_{\text{eff}}} = \frac{1}{\varepsilon} + \frac{\varepsilon_0\beta\rho_0^2 h^2}{2}, \tag{3.72}$$

respectively. Equations (3.71) and (3.72) imply that, for the effective dielectric permittivity of the film, the depletion effect is equivalent to the in-series connection of the ferroelectric with a linear capacitor. In the case of the partial depletion, this capacitance is independent of the film thickness so that the film behaves like a film with a real passive layer. However, in the case of the full depletion, according to Eq. (3.72) this series capacitance goes up with decreasing thickness as h^3. Comparison of the "passive layer" performance of the depletion effects with that of other passive layer effects is presented in Table 6.

Table 6. Thickness of a dielectric layer with $\varepsilon_d = 1$, which impacts the dielectric permittivity of the film identically to a given passive layer effect or depletion effect.

	In-plane permittivity	Out-of-plane permittivity
Real layer with $\varepsilon_d = 1$	d	d
Full surface blocking of polarization	ξ	$\xi_1 = \xi\sqrt{\frac{\varepsilon_b}{\varepsilon}}$
Partial surface blocking of polarization	$\frac{\xi}{1+\lambda/\xi}$	$\frac{\xi_1}{1+\lambda/\xi_1}$
Electrode effect	–	l_s
Partial depletion effect, $h > 2W$	–	$h_d = 2\varepsilon_0\beta\rho_0 W^3$
Full depletion effects $h < 2W$	–	$h_d\left(\frac{h}{2W}\right)^3$

h—film thickness; d—thickness of the layer; ξ—correlation length; ε and ε_b—permittivity and background permittivity of the ferroelectric; λ—extrapolation length for the polarization boundary conditions; l_s—Thomas-Fermi screening length; β—coefficient of the dielectric non-linearity, ρ_0—space charge density in the depletion layer; W—depletion layer width.

It is instructive to evaluate the possible impact of the depletion effect on the permittivity. Numerically, it is not strong but, it is, however, comparable with that of the effective passive layers discussed in the previous section. For values of W and ρ_0 compatible with the data on ferroelectric perovskite with metallic electrodes, $W = 0.2\ \mu$m and $\rho_0 \cong 1.6 \times 10^{-19} \times 10^{18}$ Ccm^{-3} = 0.16 Ccm^{-3} [72, 89, 91] one finds that, in the case of partial depletion (where $h > 2W$), a single depletion layer works as a dielectric layer with $\varepsilon_d = 1$ and thickness $h_d = 2\varepsilon_0\beta\rho_0^2 W^3 \approx 0.2$ Å . In the case of full depletion, the depletion effect on the permittivity can be readily identified by a drastic reduction of the effect with decreasing film thickness (see Eq. (3.72)). It is also worth mentioning that, as for any "in-series model", the impact of the depletion on the dielectric constant of a ferroelectric material in paraelectric phase is formally equivalent to a lowering of its Curie-Weiss temperature [90].

The modification of tunability by the depletion effect has not been addressed theoretically so that, at present, it is not clear whether under a dc bias electric field a depleted film still behaves as in-series connection of ferroelectric and a dielectric layers.

There is another obvious effect of the depletion: the built-in polarization will induce the quasi-Debye loss mechanism. However, theoretical treatment which can provide reliable estimates for the magnitude of the dielectric loss induced by this effect is not available in the literature.

3.4.3. Strain Effects

Ferroelectric films deposited onto dissimilar substrates are subjected to in-plane deformation. This deformation modifies the dielectric permittivity of the films as well as its temperature dependence due to the electrostrictive coupling. This effect can be readily described in terms of the Landau expansion for the free energy of the material. Let us address it for the case of a (001) film of a cubic ferroelectric perovskite in the paraelectric phase. To do that we will generalize Eq. (3.1) by making allowance for the electrostrictive coupling and crystalline anisotropy of the material:

$$\begin{aligned} F = {} & \frac{\alpha}{2}\left(P_1^2 + P_2^2 + P_3^2\right) - q_{11}\left(u_{11}P_1^2 + u_{22}P_2^2\right. \\ & \left. + u_{33}P_3^2\right) - q_{12}\left[u_{33}\left(P_1^2 + P_2^2\right) + u_{22}\left(P_3^2 + P_1^2\right)\right. \\ & \left. + u_{11}\left(P_2^2 + P_3^2\right)\right] - 4q_{44}(u_{12}P_1P_2 + u_{23}P_3P_2 \\ & + u_{13}P_1P_3) + \cdots \end{aligned} \tag{3.73}$$

where u_{ij} are the components of the strain tensor. Typically, the films are isotropically strained laterally so that $u_{11} = u_{22} \equiv u_m$ and $u_{12} = 0$ whereas in other directions they are mechanically free, the latter implying $u_{13} = u_{23} = 0$ and $u_{33} = -u_m\eta/(1-\eta)$ where η is the Poisson ratio of the ferroelectric. In this case, on the lines of Section 3.3 one readily finds:

$$\varepsilon_{11}^{-1} = \varepsilon_{22}^{-1} = \varepsilon^{-1} - 2\varepsilon_0 u_m\left[q_{11} + q_{12} - \frac{2\eta}{1-\eta}q_{12}\right] \tag{3.74}$$

for the in-plane and

$$\varepsilon_{33}^{-1} = \varepsilon^{-1} - 2\varepsilon_0 u_m\left[2q_{12} - \frac{2\eta}{1-\eta}q_{11}\right] \tag{3.75}$$

for the out-of-plane components of the dielectric permittivity of the film, where $\varepsilon = (\alpha\varepsilon_0)^{-1}$ is the dielectric permittivity of the non-strained ferroelectric. The in-plane deformation of the film, usually called misfit strain, is mainly controlled by two contributions: the strain that appears during the film crystallization and the thermal strain due to the difference between the thermal expansion coefficients of the substrate and ferroelectric.[11] In the simplest case of liner thermal expansion of the substrate and ferroelectric, the temperature dependence of u_m reads

$$u_m = u_{mR} + (\alpha_s - \alpha_f)(T - T_R) \tag{3.76}$$

where α_s and α_f are the thermal expansion coefficients of the substrate and ferroelectric, u_{mR} being the misfit strain at a certain temperature T_R. When the dielectric permittivity of the ferroelectric obeys the Curie-Weiss law $\varepsilon = C/(T - T_0)$, relations (3.74)–(3.76) imply a renormalization of the Curie-Weiss constant and Curie-Weiss temperature of the films [93, 94]. Clearly, the renormalized values of C and T_0 will be different for the in-plane (C_{in}, T_{in}) and out-of-plane (C_{out}, T_{out}) components of the permittivity:

$$C_{\text{in}}^{-1} = C^{-1} - 2\varepsilon_0\left[q_{11} + q_{12} - \frac{2\eta}{1-\eta}q_{12}\right](\alpha_s - \alpha_f), \tag{3.77}$$

$$C_{\text{out}}^{-1} = C^{-1} - 2\varepsilon_0\left[2q_{12} - \frac{2\eta}{1-\eta}q_{11}\right](\alpha_s - \alpha_f), \tag{3.78}$$

$$\begin{aligned} T_{\text{in}} = {} & T_0\frac{C_{\text{in}}}{C}\left[1 + 2C\varepsilon_0\left(q_{11} + q_{12} - \frac{2\eta}{1-\eta}q_{12}\right)\right. \\ & \left. \times [u_{mR} + (\alpha_s - \alpha_f)T_R]\right], \end{aligned} \tag{3.79}$$

$$\begin{aligned} T_{\text{out}} = {} & T_0\frac{C_{\text{out}}}{C}\left[1 + 2C\varepsilon_0\left(2q_{12} - \frac{2\eta}{1-\eta}q_{11}\right)\right. \\ & \left. \times [u_{mR} + (\alpha_s - \alpha_f)T_R]\right]. \end{aligned} \tag{3.80}$$

The strength of the impact of the mechanical effect on the dielectric response of the ferroelectric films can be assessed from the relations for the value of misfit strain u_R that is required to shift the Curie-Weiss temperature to a given temperature, namely

$$u_R = \frac{T_R - T_0}{2C\varepsilon_0\left[q_{11} + q_{12} - \frac{2\eta}{1-\eta}q_{12}\right]} \tag{3.81}$$

for the in-plane and

$$u_R = \frac{T_R - T_0}{2C\varepsilon_0\left[2q_{12} - \frac{2\eta}{1-\eta}q_{11}\right]} \tag{3.82}$$

for the out-of-plane polarization instabilities.

Let us evaluate the strength of the effects discussed above using the numerical values of the parameters for $SrTiO_3$ ($T_0 = 42$ K, $C = 86000$ K, $q_{11} = 2.2 \times 10^{10}\,\mathrm{m}/F$, $q_{12} = 0.2 \times 10^{10}\,\mathrm{m}/F$, $\alpha_f = 11 \times 10^{-6}$ K, $\eta = 0.24$ [95]) and typical substrates (MgO $\alpha_s = 13 \times 10^{-6}$ K; Al_2O_3 $\alpha_s = 6 \times 10^{-6}$ K; Si $\alpha_s = 4 \times 10^{-6}$ K).

From Eqs. (3.81) and (3.82) we find that to shift the in-plane ferroelectric instability temperature up to room temperature, the in-plane tensile deformation of some 0.7% is required whereas, for the out-of-plane instability, it is the out-of-plane compressive deformation of some 1.5%. Note that the in-plane deformation results in opposite shifts the Curie-Weiss temperatures of the in-plane and out-of-plane components of the permittivity. This seems to be a general feature of perovskite thin films (see also Refs. [96, 97]).

The impact of the mechanical effects on the Curie-Weiss constant depends on the relation between α_s and α_f. If $\alpha_s > \alpha_f$, the in-plane Curie-Weiss constant is larger whereas the out-of-plane Curie-Weiss constant is smaller than the original value of the Curie-Weiss constant. This is the case of MgO substrate where $(C_{\mathrm{in}} - C)/C_{\mathrm{in}} \approx 0.07$ and $(C_{\mathrm{out}} - C)/C_{\mathrm{out}} \approx -0.03$. If $\alpha_s < \alpha_f$, the opposite relation takes place. This is the case of Al_2O_3 and Si substrates, for which $(C_{\mathrm{in}} - C)/C_{\mathrm{in}} \approx -0.17$ and $(C_{\mathrm{out}} - C)/C_{\mathrm{out}} \approx 0.08$ and $(C_{\mathrm{in}} - C)/C_{\mathrm{in}} \approx -0.24$ and $(C_{\mathrm{out}} - C)/C_{\mathrm{out}} \approx 0.11$, respectively.

All these estimates show that the mechanical effects in tunable thin films are large enough to be measured experimentally and to influence the behavior of film based tunable devices.

Concluding this section, important reservations are to be made:

(i) The above consideration was aiming at the elucidation of the basic trend related to the impact of the misfit strain effects on the dielectric permittivity of the ferroelectric thin films. On the other hand, the real parameter of interest of thin films is their tunability. To obtain information on the latter, an analysis of the impact of the mechanical effects on the coefficient of the dielectric non-linearity is required. Such analysis is available in recent papers on the subject [96–98]. It predicts a certain renormalization of these coefficients which, for tunable materials of interest like $(Ba,Sr)TiO_3$ does not seem to be significant. Thus, the impact of mechanical effects on the tunability of the films is actually reduced to a change of the initial permittivity. This corresponds to the replacement of α in the equation of state Eq. (3.2) with the $1/(\varepsilon_0\varepsilon_{\mathrm{cor}})$ where $\varepsilon_{\mathrm{cor}}$ is the permittivity of the films in the absence of a dc field corrected by the mechanical effects, i.e. ε_{11} or ε_{33} in Eqs. (3.74) and (3.75).

(ii) The relations derived above are quantitatively valid when the permittivity of the ferroelectric obeys the Curie-Weiss law; the validity of Eqs. (3.77)–(3.80) also requires the linearity of the thermal expansion in the ferroelectric and the film. If it is not the case, e.g. at low temperatures, Eqs. (3.74) and (3.75) still can be used , however using the real temperature dependence of ε(e.g. from Eq. (3.7)) and values of u_m evaluated taking into account the temperature dependence of α_s and α_f.

(iii) The mechanical effects may also influence other structural instabilities of the ferroelectric which in turn can modify the dielectric response of the system. This is the case for $SrTiO_3$ where an antiferrodistorsive phase transition at 105 K takes place. A theoretical treatment of the resulting two-instability system has been offered in Ref. [98]. Though, a focused theoretical treatment of the tunability in this situation is still missing, the analysis of the result obtained in this paper suggests that the additional instability does not affect the tunable behavior of the material in a crucial manner.

4. Measurement Techniques

In this section we address the methods and techniques that enable the measurements of the complex dielectric permittivity and tunability of different forms of ferroelectric materials.

All measurement techniques require two steps. First, the electrical characteristic of a ferroelectric containing device is monitored. Second, the dielectric permittivity and loss tangent of the material are evaluated from the obtained data. Thus, the problem of determination

of the complex dielectric permittivity of the material can be divided into two: measurement problems and evaluation problems.

All measurement methods can be divided into three groups:

– *direct methods* where either the capacitance and loss tangent of a capacitor containing the investigated material are measured using an impedance analyzer, or else the scattering matrix [99] of the ferroelectric capacitor is measured by a network analyzer,
– *waveguide methods* in which the scattering matrix of the ferroelectric containing waveguide is measured using a network analyzer.
– *resonance methods* where the characteristics of a resonator which contains the investigated material are measured.

The choice of the measurement method and correspondingly the type of the measurement setup strongly depends on the frequency range and on the form of the ferroelectric material (thin film, thick film or bulk sample). For frequencies below some tens or hundreds of megahertz (radio frequencies), the tunable capacitor which is made of any form of ferroelectric material is regarded as a lumped element since its dimensions are much less than the wavelength of the electromagnetic signal. The capacitance and loss tangent of this capacitor can be measured directly by a standard impedance analyzer.

At higher frequencies, direct measurements of the capacitances are less applicable because, at higher frequencies, the dimensions of the capacitors become comparable with the length of the electromagnetic wave and they cannot be considered any more as lumped elements. Moreover, the impedance of the capacitors becomes very small in comparison to the resolution of the impedance analyzer. Thus, these methods are to be replaced by filled-waveguide characterization techniques and resonance methods.

4.1. Lumped Capacitance Measurement Methods

Capacitors used for the characterization of tunable materials can be fabricated by depositing electrodes onto the parallel sides of a ferroelectric bulk sample (Fig. 19(a)) or by making a set of small top electrodes on a ferroelectric film with a common bottom electrode (Fig. 19(b)). Capacitors with lower capacitance values, which are more suitable for high frequency measurements, can be made from thick- or thin-ferroelectric films by forming an interdigital electrode pattern (Fig. 19(c)) or rectangular electrodes with an air gap in between (Fig. 19(d)). In the two last types of capacitors, often called *"planar capacitors"*, only the top side of the film is subjected to metallization.

Parallel Plate Capacitors. At low frequencies the ferroelectric parallel plate capacitor (Fig. 19(a) and (b)) is described by a simple electrical equivalent circuit consisting of a capacitance (C_p), a frequency dependent resistance (R_p) connected in parallel, and a series resistance (R_s) corresponding to the conducting losses in the electrodes [100–102]. Measurements up to a few megahertz can be done by an impedance analyzer, directly giving the values of the capacitance and loss tangent. Higher frequencies require the use of a network analyzer to measure the complex reflection coefficient (S_{11}). In this case, the loss tangent and capacitance of the ferroelectric capacitor are calculated using the following equation:

$$\tan\delta \cdot \omega C + j\omega C = \frac{1}{Z_0}\left(\frac{1 - S_{11}}{1 + S_{11}}\right) \tag{4.1}$$

where ω is the angular frequency of the a.c. field, C and $\tan\delta$ are the measured capacitance and loss tangent, respectively; $Z_0 = 50\ \Omega$.

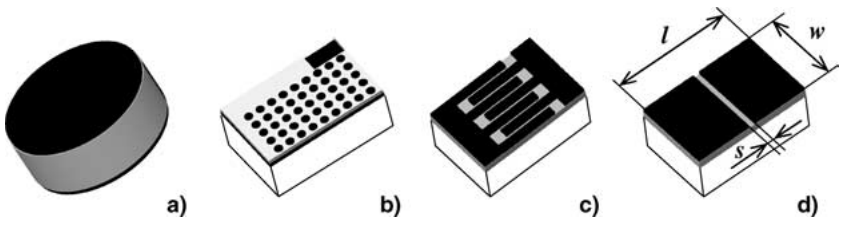

Fig. 19. Different types of ferroelectric capacitors: (a) parallel plate capacitor, (b) array of thin/thick film parallel plate capacitors, (c) interdigital capacitor, (d) air gapped planar capacitor (in all pictures black color represents conducting electrodes, grey—ferroelectric material and white color-substrate).

The loss in the electrodes (represented by R_s), which is often not negligibly small, is to be taken into account. This can be done by subtracting the conducting loss using the following equation:

$$\frac{\varepsilon''}{\varepsilon} = \tan\delta_e = \tan\delta_{\text{meas}} - \omega R_s C_p \qquad (4.2)$$

where $\tan\delta_e$ and $\tan\delta_{\text{meas}}$ are the loss tangent of the ferroelectric material and measured loss tangent of the capacitor, respectively. The parameter R_s can be evaluated analytically [100, 101] or determined experimentally [102]. For parallel plate capacitors, the relative dielectric permittivity of the ferroelectric material can be extracted from the measured capacitance using the simple formula:

$$\varepsilon = \frac{Ct}{\varepsilon_0 S}, \qquad (4.3)$$

where C is the measured capacitance, t is the thickness of the sample and S is the electrode area.

The so-called quasi-lumped approach to the characterization of a capacitor made of a ferroelectric bulk ceramics was proposed by Li [103]. This approach allows expanding the frequency range of the measurements up to 2 GHz, while the conventional lumped approach does not work at so high frequencies because the dimensions of the sample are comparable to the wavelength in the ferroelectric material. In this approach, the measured sample is modeled as an equivalent electrical circuit consisting of two parts: the first part of this circuit is a lossy transmission line of a length equal to the thickness of the sample. This line is terminated by a lumped capacitor. Measuring the reflection coefficient from the sample, one can calculate its complex dielectric permittivity.

Planar Capacitors. Modeling of the planar capacitor structures (Fig. 19(c) and (d)) is more complicated and should take into account the electric field distribution between the ferroelectric layer, substrate and air. Based on the conformal mapping technique, mathematical models for the capacitance of the interdigital structure [104] and air-gapped electrodes structures [105] were developed. For the latter case (Fig. 19(d)), the capacitance can be calculated as [105]:

$$C = \varepsilon_0 w\left[\frac{2}{\pi}\ln\left(\frac{4l}{s}\right) + \frac{\varepsilon_3 - 1}{\pi}\ln\left(16\frac{h_3 + h_2}{\pi s}\right) + \frac{\varepsilon_2 - \varepsilon_3}{\frac{s}{h_2} + \frac{4}{\pi}\ln 2}\right], \qquad (4.4)$$

where ε_2 and ε_3 are the relative dielectric permittivities of the ferroelectric film and the substrate respectively, h_2 and h_3 are the thicknesses of the ferroelectric film and the substrate, respectively, l is the length of the capacitor, s is the gap between the electrodes, and w is the capacitor width (see Fig. 19(d)). This equation was derived for a situation typical for ferroelectric capacitors. According to Vendik et al. [105] it provides some 1–2% accuracy on condition that $h_2 < s \leq 10\,h_2$, $s \leq 0.25\,l$, $s \leq 0.5\,h_3$, $\frac{\varepsilon_2}{\varepsilon_3} > 100$. However, a numerical simulation of the problem performed by Delinev [106] showed that this formula still can be used with an accuracy better than 5% on a relaxed condition $s \leq 100\,h_2$.

4.2. Waveguide and Transmission Line Methods

Filled Waveguide. The waveguide method is one of the first developed methods for characterization of dielectric materials at microwave frequencies. This method, described in detail by Altschuler in Ref. [107], involves the measurements of the scattering matrix of a waveguide filled with the investigated dielectric. This method can be readily used for the characterization of materials with relatively low dielectric permittivity but it is less suitable in the case of very high dielectric permittivity materials, because of the problem of impedance matching.

Transmission Line. The transmission line method is a special case of the waveguide method. It consists of the measurement of the scattering matrix of a transmission line which is patterned onto the ferroelectric film. The coplanar transmission line structure shown in Fig. 20(a) is often used for the characterization of both thick and thin ferroelectric films. The microstrip line structure with the bottom electrode shown in Fig. 20(b) can be used only for the characterization of thick ferroelectric films (thicker than 50 μm). Only in this case can the microstrip line have a value of the wave impedance comparable to 50 Ω.

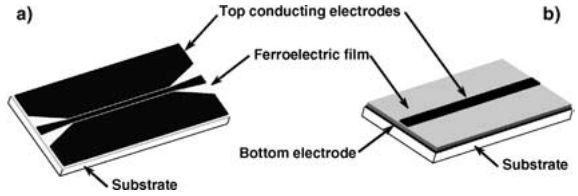

Fig. 20. Coplanar line (a) and microstrip line (b) structures patterned on the ferroelectric films (black color represents conducting layers).

The full wave analysis of such structures [108] or models developed by the conformal mapping technique [109] enable the extraction of the parameters of the ferroelectric material from the measured scattering matrix. To minimize the error in the determination of the loss tangent of the ferroelectric, the conduction loss of the electrodes is to be taken into account when calculating the parameters of the material from the measured frequency characteristics [110, 111].

4.3. Resonance Methods

Hakki-Coleman Method and Its Modifications. The last group of measurement techniques is represented by various resonance methods. These methods are well developed for both bulk samples and films (thick and thin).

The classical Hakki-Coleman method [112] consists of the measurement of the resonance frequency and quality factor of the TE_{01n} mode, excited in a dielectric rod which is placed between two metal discs ($L = h$ in Fig. 21(a)). To reduce the influence of loss in the metal discs, Krupka [113] proposed to keep the distance between the discs much greater than the sample thickness ($L \gg h$ in Fig. 21(a)).

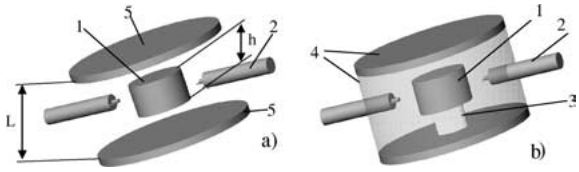

Fig. 21. Sketch of resonance measurement setups for characterization of dielectric bulk materials: Hakki-Coleman setup (Fig. 21(a), $L = h$), modified Hakki-Coleman setup (Fig. 21(a), $L \gg h$), and metal cavity with the dielectric resonator (b). 1—dielectric resonator, 2—coaxial cables terminated with coupling loops, 3—dielectric support, 4—metal cavity, 5—metal plates with the diameter much bigger than that of the sample [113].

Another frequently used modification of this method is shown in Fig. 21(b). It employs a metal cavity with dimensions 2–3 times greater than those of the dielectric sample. The cavity has two coupling loops to feed the microwave power to the resonator. It was shown that in this structure the resonance frequency and the quality factor of the system are identical to those of the dielectric resonator in a free space [114].

Measuring the parameters of the resonator, the dielectric permittivity (ε) and loss tangent ($\tan\delta$) of the sample can be evaluated [112, 113].

As in the case of the waveguide method, the dielectric resonator method is very difficult to use for ferroelectrics because their high dielectric constant and relatively high loss impede effective excitation of the resonator.

Characterization Techniques Based on the Excitation of the Transverse Magnetic Field (TM) Resonance Modes. Another resonance technique was used by Vendik et al. [115]. It consists of excitation and characterization of the TM_{mn0} resonances in a cylindrical sample placed in a break of the central conductor of a coaxial line. To match the impedance of this line with that of the network analyzer a set of quarter-wavelength coaxial lines with different wave impedances is used (Fig. 22). The dielectric permittivity and loss tangent can be simply evaluated from the resonance frequency and Q-value of a TM_{mn0} mode of the resonator using the following equation [115–117]:

$$\varepsilon = \left(\frac{k_{0n}c}{2\pi r f_0}\right)^2, \quad \tan\delta = \frac{1}{Q_0} - \frac{R_{sur}c}{120\pi^2 h f_0}, \quad (4.5)$$

where k_{0n} is the n-th root of the Bessel function, $c = 3 \cdot 10^8$ m/s, r is the radius of the cylinder, R_{sur} is the surface resistance of the electrode, h is the thickness of

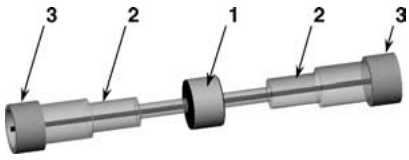

Fig. 22. Sketch of the coaxial line based measurement setup (1—both sides metallized dielectric resonator, 2—set of quarter-wavelength coaxial impedance transformers, 3—microwave connectors).

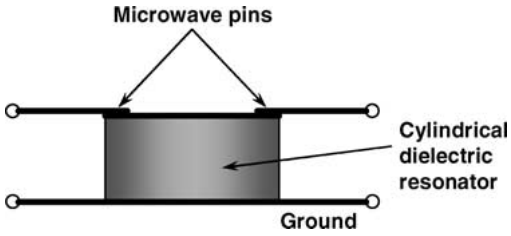

Fig. 23. Measurement setup for excitation of resonator by using microwave pins [119].

the resonator, f_0 is the resonance frequency, and Q_0 is the unloaded quality factor.

The unloaded quality factor (Q_0) can be calculated from the loaded (or measured) one either analytically or numerically. An alternative simple and fast numerical method of determination of the unloaded quality factor has been proposed by Kaifez [118]. This method enables the evaluation of the loaded and unloaded quality factors as well as the coupling coefficient only from the measured scattering matrix of the resonator, not involving an analysis of the resonator itself.

The excitation of the lowest TM_{mn0} modes in the cylindrical resonator can also be done through galvanic couplings where the pins of the microwave connectors are in direct contact with the top conductive electrode [119] while the bottom electrode is grounded (Fig. 23). This method, potentially, can be applied to the characterization of thick films deposited on conductive substrates.

4.4. Resonance Perturbation Techniques

Another group of resonance measurement techniques employs the resonance perturbation approach. In these methods the sample is introduced into a high-Q resonance cavity or a high-Q resonator is loaded with the sample. The sample can be either a piece of bulk dielectric or a thin film deposited onto the dielectric substrate with known dielectric characteristics. The presence of the sample in the resonator leads to a shift of the resonance frequency (Δf_0) and to a decrease of the quality factor (ΔQ_0). The complex dielectric permittivity of the material can be evaluated from these two parameters and the sample dimensions.

Rectangular Cavity. The cavity perturbation technique was described by Altschuler in [107] and adopted

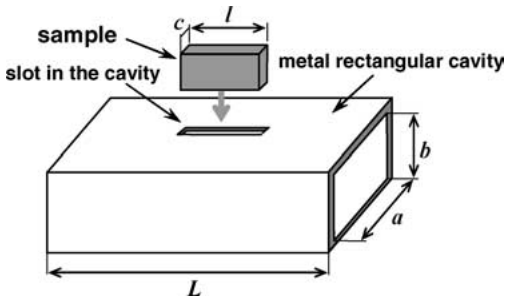

Fig. 24. Rectangular cavity with a dielectric sample to be inserted into it through the slot [120, 121].

for high dielectric permittivity materials by Dube et al. [120, 121] for the setup shown in Fig. 24.

For this setup, the real and imaginary parts of the material dielectric permittivity can be evaluated by using the following relations [121]:

$$\varepsilon = \frac{f_1 - f_2}{f_2} \frac{2V_c}{b\left[1 + \frac{L}{n\pi}\sin\left(\frac{n\pi l}{L}\right)\right]\left[c + \frac{a}{\pi}\sin\left(\frac{\pi c}{a}\right)\right]} + 1$$
$$\varepsilon'' = \frac{Q_1 - Q_2}{Q_1 Q_2} \frac{V_c}{b\left[1 + \frac{L}{n\pi}\sin\left(\frac{n\pi l}{L}\right)\right]\left[c + \frac{a}{\pi}\sin\left(\frac{\pi c}{a}\right)\right]}, \quad (4.6)$$

where f_1 and Q_1, f_2 and Q_2 are the resonance frequencies and quality factors of the cavity without and with the measured sample; a, b, and L are the dimensions of the cavity; V_c is its volume and c and l are the dimensions of the sample having the shape of a parallelepiped.

Microwave Scanning Microscopy. Recently, a new method of characterization of dielectric materials based on a near-field imaging technique, the so-called microwave scanning microscopy, has been developed. Conceptually this method is the cavity perturbation methods. A microwave scanning microscope consists of a coaxial resonator with a very sharp central conductor at the end which is used as a microwave probe tip. The dielectric sample under test plays the role of a load for the coaxial resonator (Fig. 25) [122, 123]. Comparing the resonance frequency and Q-values of the unloaded coaxial resonator with those of the resonator loaded with the ferroelectric, one can evaluate the dielectric permittivity and loss tangent of the investigated material. An important feature of this method is that it provides information of the local

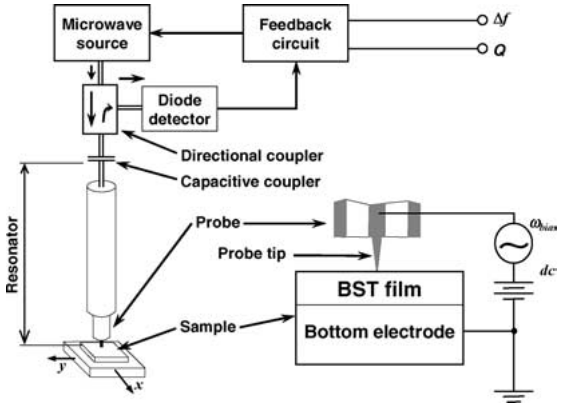

Fig. 25. A schematic description of the near-field microwave microscope [123].

values of the dielectric parameter of the material, a lateral resolution better than 1 μm being readily achieved.

Transmission-Line Resonator Methods. The most often used resonance method for the dielectric characterization of ferroelectric films is the so-called transmission-line resonator method. This method originates from the cavity perturbation method and employs transmission line resonators to characterize ferroelectric film based capacitors. Different transmission lines (microstrip lines, lines on the suspended substrate, slot lines) can be used in this method.

One practical realization of this method is a half-wavelength microstrip resonator interrupted at its center by a narrow air gap filled with the ferroelectric thin film [124] or by a ferroelectric planar capacitor mounted as a flip-chip element [125] (Fig. 26). The capacitance of the ferroelectric capacitor and loss tangent of the ferroelectric material are calculated from the measured resonance frequency and Q-value of the system by using the following formulas [125]:

$$
\begin{aligned}
C &= \left[2Z_0\omega\cot\left(\frac{\omega\sqrt{\varepsilon_{\text{eff}}}l_{\text{eff}}}{c}\right)\right]^{-1},\\
\tan\delta &= \left(\frac{1}{Q_m}-\frac{1}{Q_{\text{ref}}}\right)\cdot\zeta,\\
\zeta &= \left[\frac{1}{2}+\frac{Z_0}{X_c}\left(1+\frac{X_c^2}{4Z_0^2}\right)\right.\\
&\quad\left.\times\left(n\pi-\operatorname{arccot}\left(\frac{X_c}{2Z_0}\right)\right)\right]^{-1},\\
X_c &= \frac{1}{\omega C},
\end{aligned}
\tag{4.7}
$$

where Z_0 is the wave impedance of the microstrip resonator, ε_{eff} and l_{eff} are the effective dielectric permittivity and length of the resonator respectively, $c = 3{\cdot}10^8$ m/s, Q_m and Q_{ref} are the measured and reference unloaded quality factors (the latter can be determined by measuring the Q-factor of the resonator loaded with a low loss capacitor with known parameters), ζ is the inclusion coefficient of the ferroelectric capacitor into the resonator, n is the number of the harmonic of the resonator. The dielectric permittivity of the ferroelectric film is calculated from the obtained capacitance using Eq. (4.4).

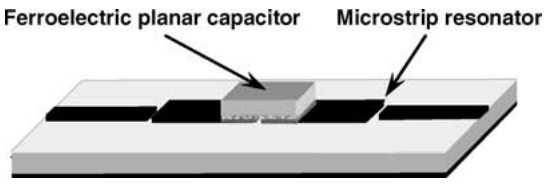

Fig. 26. Microstrip half wave resonator with the ferroelectric planar capacitor (see Fig. 19(d)) mounted as a flip-chip element with the gap centered between two parts of the resonator [125].

4.5. About the Precision and Limits of Measurement Techniques

All sources of the errors appearing in different characterization techniques can be divided into measuring errors and evaluation errors.

As described above, it is either the capacitance of the ferroelectric capacitor (at radio frequencies) or the elements of the scattering matrix of the ferroelectric containing device (at higher frequencies) that are measured by the corresponding equipment. The relative instrument error of these measurements does not exceed 1–2% and depends on the quality of calibration and calibrating standards. Table 7 contains the measurement precisions and limitation for the different measuring techniques.

The second source of errors is related to the calculation of the complex dielectric permittivity of the ferroelectric from the measured capacitance and loss of the ferroelectric capacitor or from the elements of the scattering matrix. Usually the analytical formulas used for these calculations have their own errors, which are

Table 7. Basic measurement errors and limits of the different characterization techniques. ωC [1/Ω] is the reactance of the ferroelectric capacitor.

Methods	Instrumental errors(1)	Limits(1)
Direct capacitor measurements		
Capacitance	0.05–0.1%	$10^{-17} <$ C [F] < 10
Loss tangent	0.0005–0.001%	$10^{-6} < \tan\delta < 10$
		f[Hz] $< 10^6$–10^8
Characterization of the capacitor through the measurements of the reflection coefficient		
Capacitance	2–5% (HP8722)	$0.005 < \omega C < 0.05$
Loss tangent	5–6%	$0.0005 < \omega C \tan\delta < 0.02$
Waveguide and transmission line methods (2)		
Absolute error for the phase	<5 degrees	f[GHz]> 0.5
Absolute error for the transmission coefficient	<0.02	length of the line: l[m]> $\frac{2}{f[\mathrm{GHz}]\sqrt{\varepsilon}}$
Resonance methods(3)		
Capacitance or dielectric permittivity	<1%	10^{-4}–$10^{-2} <\tan\delta < 0.1$
Loss tangent	∼ 5%	$0.05 < C$ [pF] < 1

(1) The measurement errors and limits were taken and calculated from the accuracy of the HP4284 LCR Meter and HP8722 Network Analyzer, (2) The precision of the waveguide methods is basically determined by the quality of the calibrating standards and by the possibility to separate conducting, radiative and dielectric losses; the absolute errors for the phase and transmission coefficient are to be taken into account when calculating the parameters of the ferroelectric materials using the measured transmission characteristics of the waveguide or line. (3) The limits depend on the impedance and quality factor of the non perturbed resonator.

in the range 1–2%. The source of errors is due to the inaccuracy of the measurements of the linear dimensions of the sample, which are needed for computations. This error can reach 5–6% depending on the sample size and used equipment.

The measurement techniques described in this chapter cover a large frequency range, from some tens of hertz to some tens of gigahertz. They have different limitations and precisions and their choice depends on many parameters. Figure 27 gives an idea of the frequency ranges of applicability of the main types of these measurement techniques.

4.6. *Measurements of Dielectric Permittivity and Loss as a Function of dc Electric Field*

To measure the complex dielectric permittivity of a ferroelectric under a dc bias electric field, the experimental setup including the sample itself should satisfy the three following conditions:

(i) The sample has to be coated with electrodes (the mechanical contact between the non-metallized dielectric and the metal plates of the sample fixture is not sufficient because of an air gap which always exists between two surfaces in mechanical contact).

(ii) The setup should have a possibility to apply a dc voltage to the sample without subjecting the source of the ac signal to danger and short-circuiting the ac signal with the dc voltage source.

(iii) The distribution of the dc electric field in the sample is to be homogeneous and/or well modeled; otherwise it would not be possible to evaluate the electric field acting in the material.

The first two conditions cannot be satisfied in the filled waveguide methods and in some resonance methods where the metal plates should not be in the contact

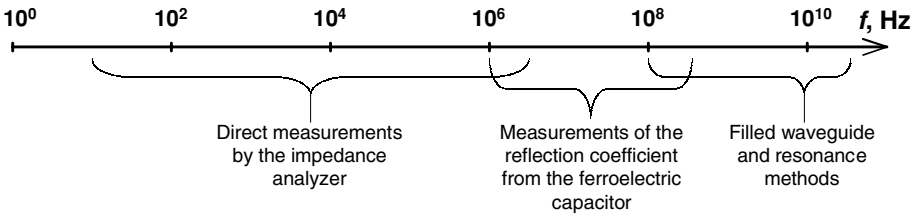

Fig. 27. Frequency range of applicability of the main types of techniques used for dielectric characterization of materials.

with the sample (Fig. 21(a), $L \gg h$ and Fig. 21(b)). Moreover, the second condition requires the use of an external blocking circuit consisting of low frequency LC or RC filters in order to isolate the dc voltage source from the ac signal and to protect the measuring equipment from high voltage.

The last condition can be satisfied, first, for the parallel plate electrode geometry of the active area of the sample (like shown in Figs. 19(a) and (b), 20(b), 21(a) (for $h = L$), 22, and 23). Second, in the planar electrode configurations (Figs. 19(c), (d) and 20(a)) in the case where the thickness of the sample (actually film) is much less than the distance between the electrodes. In such structures, the electric field can be considered as homogeneous and evaluated directly from the known values of the dc voltage applied to the sample and the distance between the electrodes. In the case, where the field in the varactor is strongly inhomogeneous (like Fig. 19(c) and (d) for the film thickness larger or comparable to the distance between the electrodes), the evaluation of the tunability requires a solution of the electrostatic problem with a field dependent permittivity, which is a very different task.

The precision of all the methods of determination of the tunability is close to that of the dielectric permittivity. This holds up to the microwave frequency range. By contrast, the situation with the field dependence of the loss tangent is very different. In the RF range, where the contribution of the conductive loss in electrodes is not essential; the precision of the determination of the loss tangent of a material with and without a dc bias field is roughly the same. However, at higher frequencies, where the contribution of the conductive loss in electrodes becomes appreciable, the measurement of the field dependence of the loss tangent of the material often becomes a much more difficult task than that of the tunability.

5. Materials for Tunable Applications

The appropriate level of tunability for tunable applications ($n \geq 1.5$ i.e. $n_r \geq 0.3$ see Section 2) is practically achievable in materials with relatively high dielectric permittivity at microwave frequencies. For non-composite bulk materials, a value of the dielectric constant exceeding some 1000 is required whereas in thin films (where the application of higher fields is possible) the dielectric constant should be lager than some 300. This limitation together with the requirement of relatively low values of the dissipation factor (below a few percent) narrows the scope of the materials of interest to the displacive type ferroelectrics (incipient or regular in the paraelectric phase). Up to now, many materials have been addressed as possible candidates for tunable applications, the most attention has being paid to $SrTiO_3$ and its solid solution with $BaTiO_3$: (Ba,Sr)TiO_3. In the present section we will address the properties of some these materials. The properties of bulk materials and thin films will be discussed separately.

5.1. *Bulk Materials*

$KTaO_3$ and $SrTiO_3$ Crystals. High quality single crystals of $SrTiO_3$ (STO) exhibit a high dielectric permittivity (up to tens of thousands) and a low loss factor at microwave frequencies (below 10^{-3}). This enables their use in tunable microwave components. As incipient ferroelectric, STO stays paraelectric down to 0 K and its dielectric constant strongly increases on cooling (see Fig. 28). STO is a cubic ($m\bar{3}m$) perovskite at $T > T_{St} = 105$ K, and undergoes at $T = T_{St}$ an antiferrodistorsive phase transition to a centrosymmetric tetragonal phase (4/mm). In its tetragonal phase, the crystal becomes dielectrically anisotropic. However, the anisotropy is apparent only at rather low temperatures, being about 3% at 80 K and more than 100% at 10 K [126]. When cooled below T_{St} without special precautions [126], STO crystals typically break into twins,

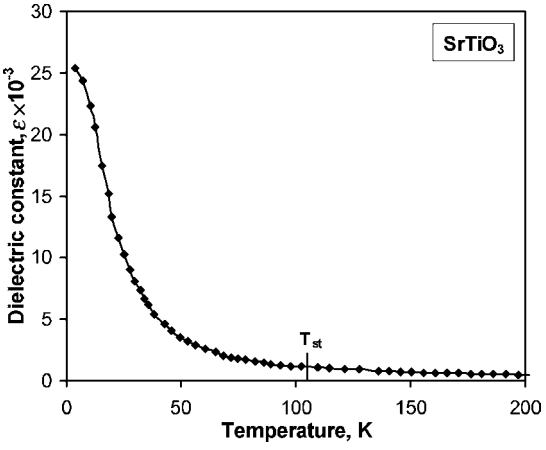

Fig. 28. Temperature dependence of the dielectric constant of $SrTiO_3$ single crystal measured at 10 kHz in the direction perpendicular to the tetragonal axis of the 4/mm phase [126].

so that their dielectric constant represents an average of its values for the different crystallographic directions. For this reason, the dielectric constant of different STO crystals measured below 30 K may substantially differ due to differences in their twin structures.

Another reason for this spread is a possible difference in the defect population in differently processed crystals; as clear from simple thermodynamic arguments, the higher the permittivity of the material, the stronger the impact of crystal imperfections on it. The temperature dependence of the dielectric permittivity of the material reasonably follows the predictions of the Landau theory [126]. For temperatures above some 50 K, it can be with good accuracy approximated by Eq. (3.12) with the parameters coming from Table 2 or, alternatively, by Eq. (3.4) and (3.6). However, there are publications reporting features of the dielectric response of STO crystals, which cannot be covered by the conventional thermodynamic approach that takes into account the polarization and the order parameter of the antiferrodistorsive phase transition. Namely, double [7, 127] and single [128] $P-E$ hysteresis loops were reported for STO crystal. Despite some hypotheses put forward, the nature of these phenomena is still unclear.

The bulk form for STO (single crystals or ceramics) exhibits a high enough tunability only at rather low temperatures whereas at room temperatures the required electric field is unrealistically large . This can be seen from the following relation for the bias field that is required to reach a given value of tunability n:

$$E_n = 0.8 \cdot 10^6 \frac{\sqrt{n-1}(2+n)}{\varepsilon^{3/2}} \left[\frac{\text{kV}}{\text{cm}}\right]. \qquad (5.1)$$

This relation readily follows from Eq. (3.11) with $\beta = 8 \times 10^9$ JC^{-4} m^{-5}. Using this relation one finds that the tunability of interest ($n > 1.5$) requires a field >30 kV/cm at 77 K ($\varepsilon \approx 1500$) and >400 kV/cm at RT ($\varepsilon \approx 300$).

In single crystals of STO the loss tangent at 10 GHz is typically about 10^{-3} [2] and, as was mentioned in Section 3, the data for the best quality crystals are consistent with the theory of the intrinsic phonon loss mechanisms (three- and four-quantum contributions in the absence of a bias electric field). Under an electric field, the theory predicts a steep rise of the intrinsic dielectric loss with increasing field (the so called field-induced quasi-Debye mechanism, see Section 3). An essential prediction is that the field corresponding to small values of the relative tunability may lead to a many-time increase of the loss tangent. This behavior was experimentally documented by Vendik et al. [115]. Figure 29(a) shows a strong decrease of the quality factor of an STO containing resonator with superconductor electrodes, which is due to the quasi-Debye mechanism.

The properties of $KTaO_3$ (KTO) crystals are very close to those of STO. This material is also a cubic incipient ferroelectric whose extrapolated instability

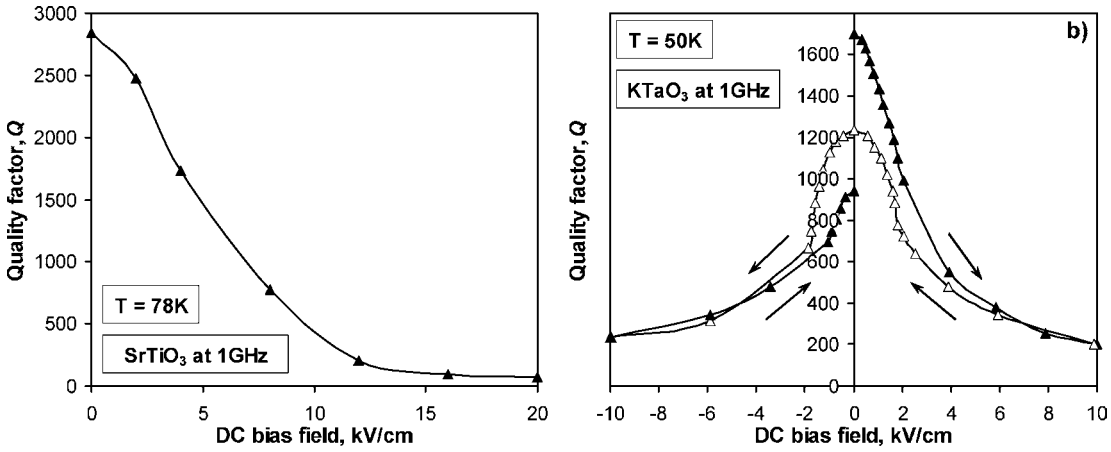

Fig. 29. Field dependences of the quality factors of the $SrTiO_3$ (a) and $KTaO_3$ (b) based bulk resonators with lossless superconducting $YBa_2Cu_3O_7$ electrodes (see Refs. [115] and [7], respectively). The directions of measurements are shown in the figure (b) by the arrows. The dc field applied to the samples resulted in a small (<20%) variation of the dielectric permittivity of material.

temperature T_0 and Curie-Weiss constant C are somewhat lower than those of STO (see Table 2), whereas the coefficient of the dielectric non-linearity[12] is slightly larger [129]. Another difference between these two crystals is that KTO remains cubic down to 0 K. Though the set of material parameters of KTO and STO are rather close, the tunablility of KTO is substantially inferior to that of STO. As it follows from the Table 2 and Eq. (3.11), for the same values of tunability n at $T = 77$ K, the tuning field in KTO should be three time larger than for STO. On the other hand the loss level exhibited in these materials is comparable. According to Gevorgian et al. [7], at $T = 77$ K @ $\omega = 1$ GHz, the crystal of KTO yields $\tan\delta = 0.5 \cdot 10^{-3}$. Under the action of a dc filed, KTO, similar to STO, exhibits an increasing field dependence of the loss consistent with the quasi-Debye contribution. The data [7] on the dc field dependence of the quality factor of a disc resonator containing $KTaO_3$, which illustrate this phenomenon, are shown in Fig. 29(b).

An important issue to discuss is the level of the extrinsic contribution to the loss at microwave frequencies in KTO and STO crystals. Though any systematic study of the problem is absent, some conclusions on STO crystals at cryogenic temperatures can be done using the available data. The analysis [54] of the data collected by Buzin [58] strongly suggests that, in STO at $T = 77$ K, the intrinsic loss corresponds to $\tan\delta \propto \omega$ with $\tan\delta/\omega = 0.7 \cdot 10^{-4}$ GHz^{-1} in the frequency range 1–30 GHz. This is to be compared to the data reported for STO crystals by other authors: at $T = 77$ K @ $\omega = 1$–2 GHz, it was reported that $\tan\delta/\omega = 3.3 \cdot 10^{-4}$ GHz^{-1} [7], $\tan\delta/\omega = 1.2 \cdot 10^{-4}$ GHz^{-1} [130], and $\tan\delta/\omega = 4.2 \cdot 10^{-4}$ GHz^{-1} [115]. The spread of the reported values, clearly exceeding the accuracy of the measurements, can be attributed to extrinsic loss contributions. Thus, $\tan\delta/\omega \cong 10^{-4}$ seems to be a reasonable estimate for these contributions at $T = 77$ K @ $\omega = 1$–2 GHz.

The presented parameters of KTO and STO crystals correspond to an excellent tunable performance of these materials at cryogenic temperatures ($T = 77$ K). Taking the tunability $n = 1.5$ and $\tan\delta = 5 \cdot 10^{-3}$ we arrive at the Commutation Quality Factor $K \approx (n-1)^2/(n \cdot \tan^2\delta) \cong 7000$, which suffices for many application (see Section 2).

(Ba,Sr)TiO₃ Crystals and Ceramics. The solid solution $Ba_xSr_{1-x}TiO_3$ (BST) is a very suitable material for tunable applications. Depending on the barium concentration this material exhibits the permittivity maxima within the temperature range 0–390 K, behavior of single crystals and ceramics being very close. The composition and temperature dependence of the permittivity of BST single crystals and bulk ceramics is illustrated in Fig. 30. As is clear from Fig. 30(b), for a given temperature, a high enough value of the dielectric permittivity can be obtained by choosing a proper barium concentration. The coefficient of the dielectric non-linearity of BST β_{BST} is expected to be smaller than that of STO because of a smaller value of β in

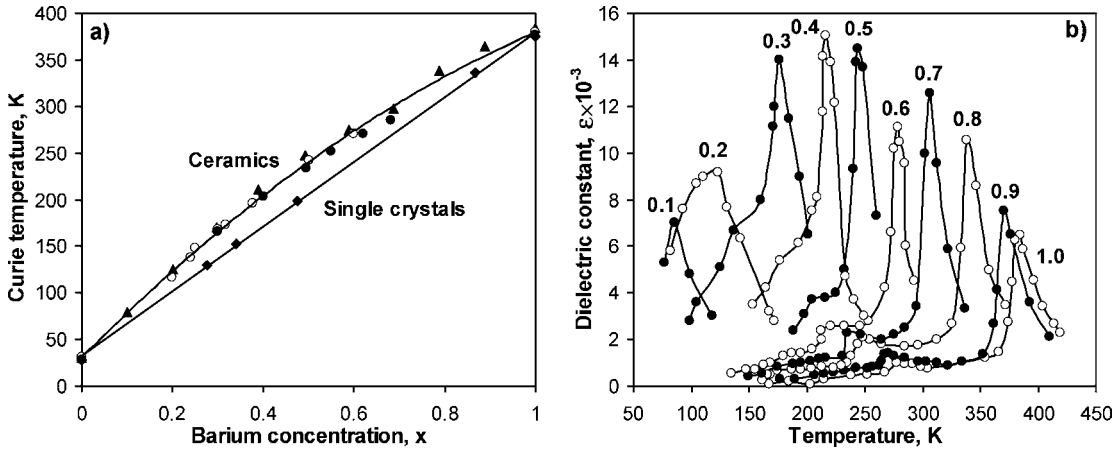

Fig. 30. (a)—Curie temperature of $Ba_xSr_{1-x}TiO_3$ ceramic and single crystal materials as a function of Ba concentration x [82]. (b)—Temperature dependences of dielectric constant of $Ba_xSr_{1-x}TiO_3$ ceramic materials for different Ba concentration x [14].

$BaTiO_3$ (BTO)[131], i.e. $\beta_{STO} \gg \beta_{BTO}$. Approximating the coefficient of the dielectric non-linearity of BST as $\beta_{BST} = (1-x)\beta_{STO} + x\beta_{BTO} \approx (1-x)\beta_{STO}$, from (3.11) and (5.1), one obtains an estimate for the bias field required for reaching the given tunability n in $Ba_xSr_{1-x}TiO_3$:

$$E_n \approx \frac{0.8 \cdot 10^6}{\sqrt{1-x}} \frac{\sqrt{n-1}(2+n)}{\varepsilon^{3/2}} \left[\frac{\text{kV}}{\text{cm}}\right]; \; x < 0.7. \quad (5.2)$$

This relation implies that, for the same permittivity, the tuning ability of $Ba_xSr_{1-x}TiO_3$ decreases with increasing barium content.

The parameter of BST single crystals important for tunable applications are given in the table (below) offered by Vendik and coworkers [2].

Parameters for BST crystal (after Vendik et al. [2])

Barium concentration	Ferroelectric instability temperature (T_0, K)	Average value of tanδ at 10 GHz in operational temperature range	Operational temperature range (K)
0.00	42	0.001	4–100
0.27	125	0.005	150–200
0.34	155	0.007	175–250
0.47	203	0.01	240–300
0.65	260	0.02	300–350
0.87	338	0.05	–
1.0	387	0.1	–

This Table illustrates several essential issues. First, the operational temperature range does not correspond to a close vicinity to T_0 where the permittivity and tunability are maximal. The reason for this[13] is the low temperature stability of the permittivity at T close to T_0. The upper limit of the operational temperature range is roughly determined by the condition $\varepsilon \approx 1000$. Second, the trend "the higher the barium concentration, the higher the microwave loss" is clearly seen. This trend is consistent with the prediction of the phonon transport theory for the dielectric loss (see Section 3). It is related to a very big difference between the damping of soft-mode phonons in the end members of the BST solid solution. This damping essentially controls the level of the intrinsic dielectric loss at microwave frequencies. In STO the soft mode is under-damped, e.g. at $T = 77$ K, $\Gamma/\Omega_{TO} \cong 0.02$ [132], whereas in BTO it is overdamped, e.g. at $T = 300$ K, $\Gamma/\Omega_{TO} \cong 2.3$ [133]. On the other hand, the intrinsic loss in cubic centrosymmetric perovskites like STO follows the estimate (3.28) that yields $\tan\delta \propto \Gamma$ as long as the soft-mode stays underdamped. Thus, for barium concentrations corresponding to this situation, the intrinsic loss in $Ba_xSr_{1-x}TiO_3$ may be expected to grow steeply with increasing "x", which is the trend clearly seen in the above table. However, for higher barium concentrations where the soft mode is overdamped, the intrinsic loss is not expected to grow with increasing Γ(this can be checked by using a simple damped oscillator model for the loss). Thus, the origin of the concentration dependence of the loss at the BTO end of the composition needs to be further clarified.

The above discussion may have important implications for the microwave applications of BST. The intrinsic loss, which steeply increases with increasing barium concentration "x", is expected to be the major part of the total loss at high barium concentrations. This actually implies that the higher the "x", the less sensitive its microwave loss to the optimization of the material. At this point one should mention one more prediction of the phonon theory. Namely, as was discussed in Section 3, in $Ba_{0.5}Sr_{0.5}TiO_3$ the field-induced quasi-Debye contribution to the loss is substantially smaller than in pure STO where it was experimentally documented. This means that, in BST with intermediate concentrations of barium, which is of interest for practical applications, one does not expect a substantial dc field induced increase of the loss like those reported for STO and KTO crystals.

Doping and Composite Effects in (Ba,Sr)TiO$_3$ Ceramics. Modification of BST by adding non-ferroelectric oxides in the range up to very high concentrations has been attempted by many workers (see e.g. [68, 134–137]). However, the full set of parameters needed to evaluate the tunable performance of the material at microwave frequencies is rarely available in the literature. A rather complete set of experimental data of BST-MgO system was reported by Sengupta and Sengupta [137], namely the permittivity, tunability (for a dc field of 20 kV/cm), and loss tangent at 10 GHz were reported for 0.45/0.55, 0.5/0.5, 0.55/0.45, and 0.6/0.4 compositions of BST with the MgO content from 0.25 to 60 Wt.% (0.4–70 vol.%). These data are presented in Figs. 31–33. Despite a substantial spread of the data and the absence of the information on their accuracy, these data can be discussed in terms of the available knowledge in the field.

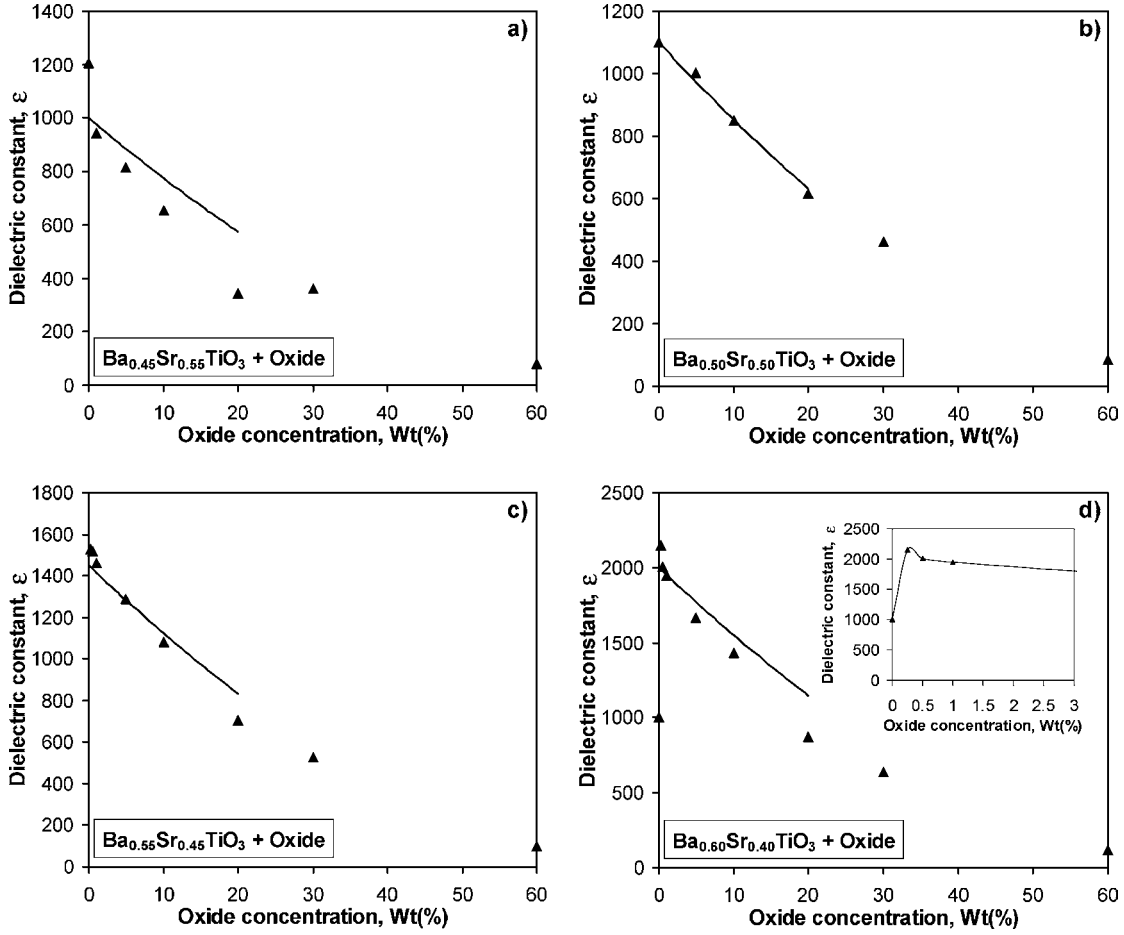

Fig. 31. Dielectric constant of ferroelectric-dielectric composite material as a function of weight concentration of the dielectric inclusions in the mixture for (a)—$Ba_{0.45}Sr_{0.55}TiO_3$/oxide, (b)—$Ba_{0.50}Sr_{0.50}TiO_3$/oxide, (c)—$Ba_{0.55}Sr_{0.45}TiO_3$/oxide, (d)—$Ba_{0.60}Sr_{0.40}TiO_3$/oxide material compositions. The black triangles are the experimental data, and the solid curves correspond to Eq. (3.24a) $\varepsilon_{\text{mix}}(q) = \varepsilon_f(1 - \frac{3}{2}q)$ with recalculated values of the concentration of dielectric inclusions q from the volume values into the percents by weight Wt(%). RT data.

As was discussed in Section 3.2.3, mixing a tunable ferroelectric with a linear dielectric may modify the electrical properties of the material due to many effects. Two of these whose physics is rather clear are (i) "doping effect",–effect of doping of the ferroelectric lattice via the substitution of the ions of the host material and (ii) "composite effect"–effects of redistribution of the electric field in the material due to the precipitation of the non-ferroelectric phase at the grain boundaries or in the bulk of the material. In addition, two more effects may be active especially in the case of the dielectric loss: (iii) effects of inter-components boundaries, and (iv) effects of mixing-induced modification of microstructure of the ferroelectric component. In a real material and possessing a limited set of experimental data, the distinction among the contributions of these effects is a difficult task. In the following discussion, we will mainly address the first two effects.

The doping effect is limited by the solubility of the additive. The main impact of this effect is the shift of the Curie-Weiss temperature T_0 of the material. In the case of the BST-MgO system, the doping effect is limited at least to the MgO concentration below 2%. This is illustrated in Fig. 34 where it is seen that, in $Ba_{0.8}Sr_{0.2}TiO_3$ with increasing MgO content, a shift of T_0 takes place for dopant concentrations below 2 mol% (0.4 wt%) [138]. Typically, the non-ferroelectric additives shift T_0 down as shown in this figure. If the non-doped material is in its ferroelectric phase, the progressive doping may lead to a non-monotonic variation of

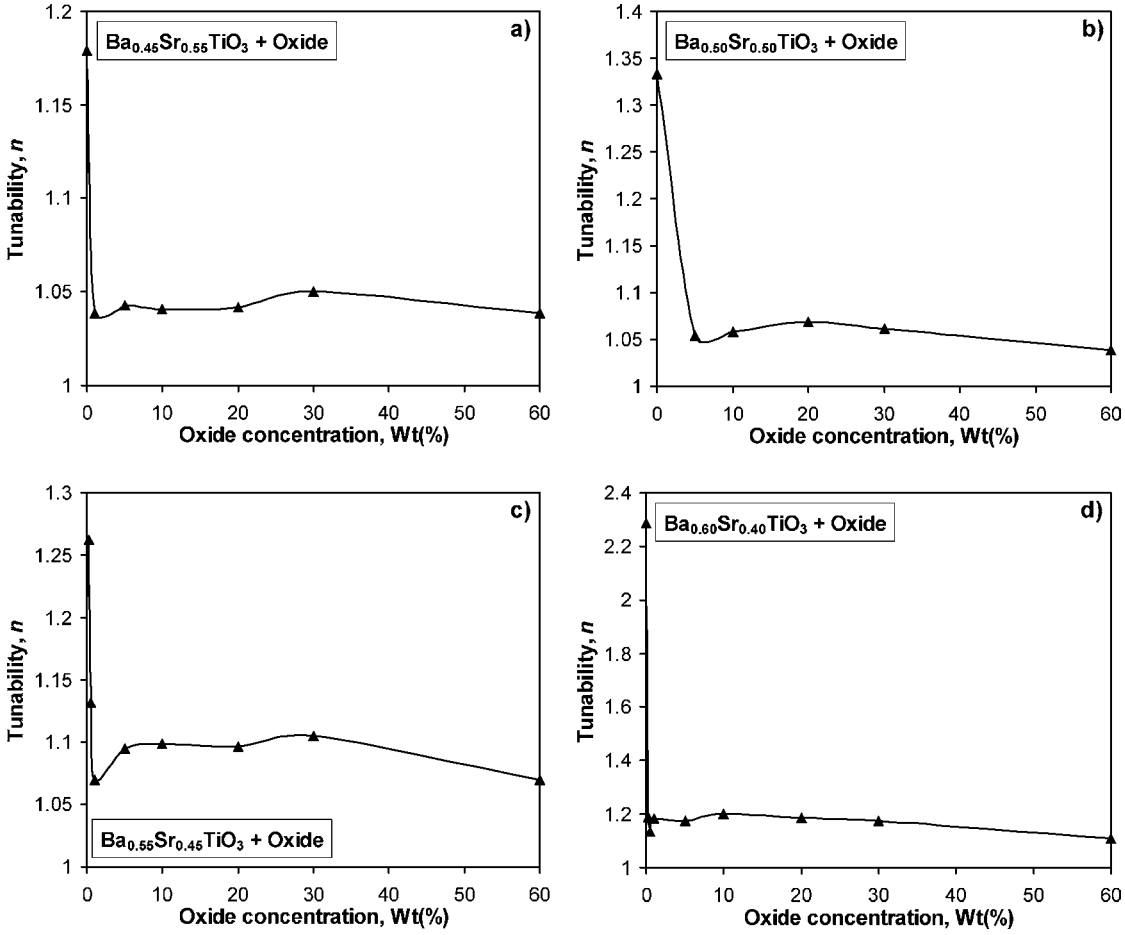

Fig. 32. Tunability of ferroelectric-dielectric composite material as a function of weight concentration of the dielectric inclusions in the mixture for (a)—$Ba_{0.45}Sr_{0.55}TiO_3$/oxide, (b)—$Ba_{0.50}Sr_{0.50}TiO_3$/oxide, (c)—$Ba_{0.55}Sr_{0.45}TiO_3$/oxide, (d)—$Ba_{0.60}Sr_{0.40}TiO_3$/oxide material compositions. RT data.

the permittivity. Such a behavior is seen in the insert in Fig. 31(d). The abrupt variation of the tunability at small MgO concentrations, which is seen in Fig. 32, can also be attributed to the doping effect. The behavior of the permittivity and tunability at higher MgO content is consistent with manifestations of the composite effect. As seen from the result of modeling for various ferroelectric/dielectric composites, the impact of the dielectric component on the permittivity and tunability of the material should be very sensitive to the geometry of its distribution in the host material. Namely, layers of the dielectric perpendicular to the direction of the electric fields impact both the permittivity and tunability much stronger than sphere-type inclusions or columns parallel to the field (see Fig. 9(a)). Comparison of the results of modeling with the experimental data on BST-MgO system (see Figs. 31 and 32) suggests that the experimental situation is close to the model of the spherical inclusion. The supporting arguments are as follows. First, the concentration dependence of the permittivity in the range of 1–30 wt% is close to that given by Eq. (3.46). Second, for not too small concentrations, the tunability is weakly concentration dependent in accordance with the prediction of the model.

The data on the concentration dependence of the loss shown in Fig. 33 cannot be fully interpreted in terms of the doping-induced shift of T_0 and composition effect. The fast drop of the loss tangent at small MgO concentrations may be at least partially attributed to the doping-induced shift of T_0 as well as to a reduction of the loss related to the transition from the ferroelectric

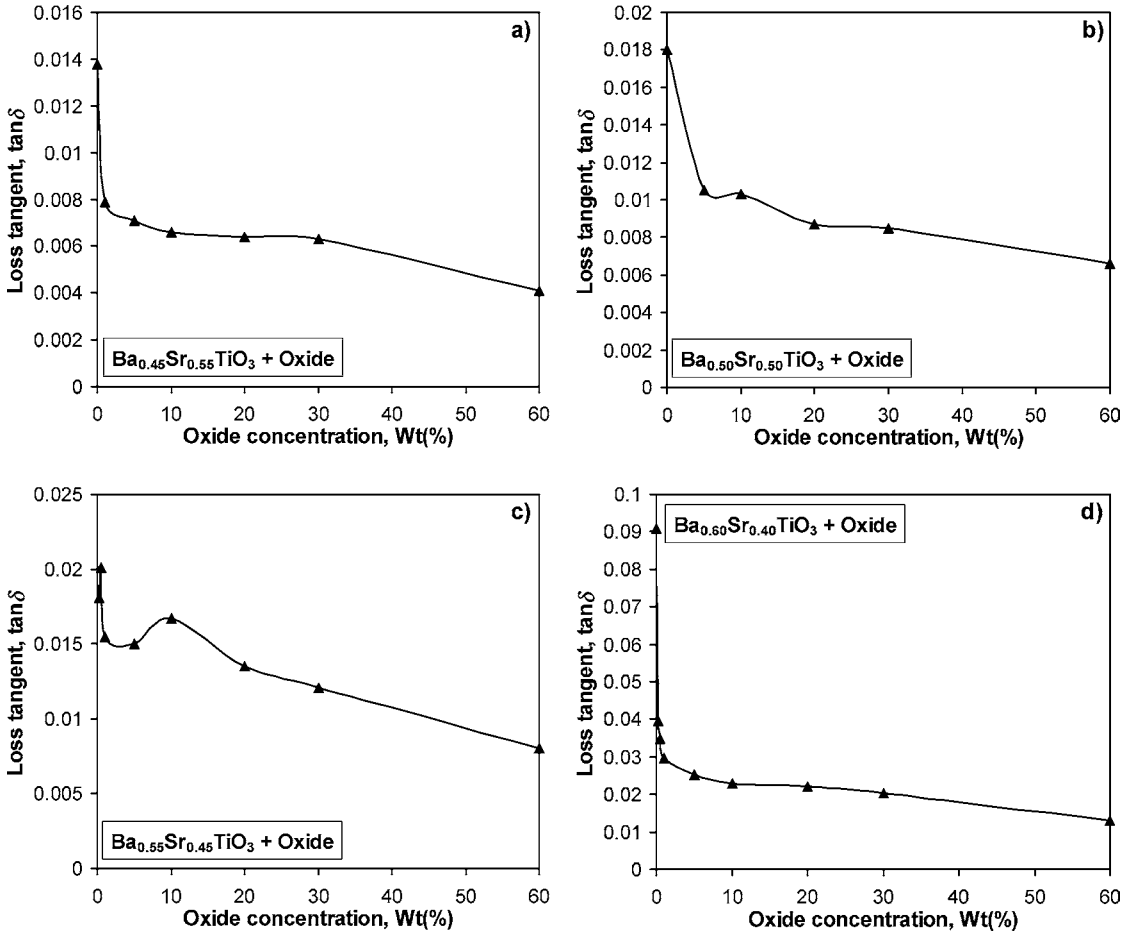

Fig. 33. Loss tangent of ferroelectric-dielectric composite material as a function of weight concentration of the dielectric inclusions in the mixture for (a)—$Ba_{0.45}Sr_{0.55}TiO_3$/oxide, (b)—$Ba_{0.50}Sr_{0.50}TiO_3$/oxide, (c)—$Ba_{0.55}Sr_{0.45}TiO_3$/oxide, (d)—$Ba_{0.60}Sr_{0.40}TiO_3$/oxide material compositions. RT data.

to paraelectric phase in the case of 0.6/0.4 BST composition.[14] However, the further reduction of the loss with increasing MgO concentration (for higher concentrations) does not look to be consistent with the flat concentration dependence of the tunability, as is clear from the comparison of Figs. 32 and 33 with the results of modeling the composite effect (Figs. 9(a) and 14(a)). The origin of this disagreement is not clear for the moment. First, the cited theory for the spherical inclusion model is strictly applicable only to the case of small oxide concentrations whereas the experimental data correspond to rather high oxide concentrations. Thus, more advance theory might be in better agreement with the experiment. Alternatively the loss reduction with increasing doping can be attributed to some non-composite mechanisms. These mechanisms may be related to a variation of the population of the point defects of the material with increasing MgO content and to the impact of the additive on the microstructure of the ceramics (e.g. grain size). The loss tangent can be sensitive to these factors. These mechanisms can also contribute to the drop of the loss tangent at the small concentrations.

The overall tunable behavior on the BST/MgO systems under consideration (data from Ref. [137]), as given by the Vendik's Commutation Quality Factor K is illustrated in Fig. 35. The presented $K-\varepsilon$ dependences of four different compositions of BST typically reveal two features. First, the initial drop of ε is accompanied by a substantial drop of the K factor, which can be associated with the shift of T_0. Second, the K factor increases on the further reduction of ε. This effect

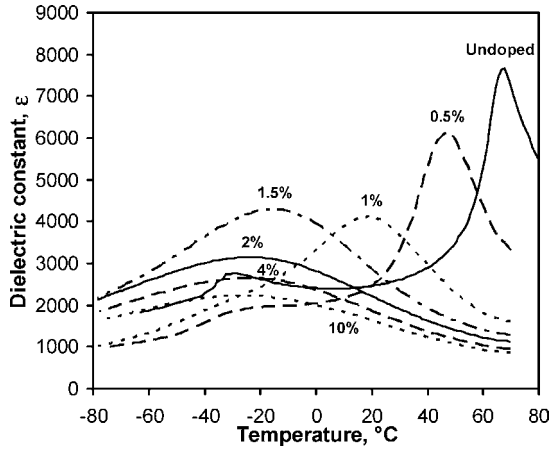

Fig. 34. Temperature dependences of the dielectric constant of $Ba_{0.8}Sr_{0.2}TiO_3$ ceramics with different levels of MgO content (indicated in mol%) [138].

is too strong to be explained by the purely composite effect at least for simple models (c.f. Fig. 16). This suggests that the change in K with increasing content of the dielectric in BST relates to other effects than the composite effect. As in the case of the concentration dependence of the loss, it may be related to a variation of the population of the point defects of the material with increasing MgO concentration and to the impact of the additive on the microstructure of the ceramics.

The data presented in Fig. 35 correspond to K factors $\leq$ 300. These values are not very far from 900 that is required from a material to be of real interest for applications in phase-shifters (Section 2). Since $K \propto 1/\tan^2 \delta$, for the bulk BST ceramic materials discussed above, a two-time reduction of the loss level is actually sufficient to reach the required level of the K factor.

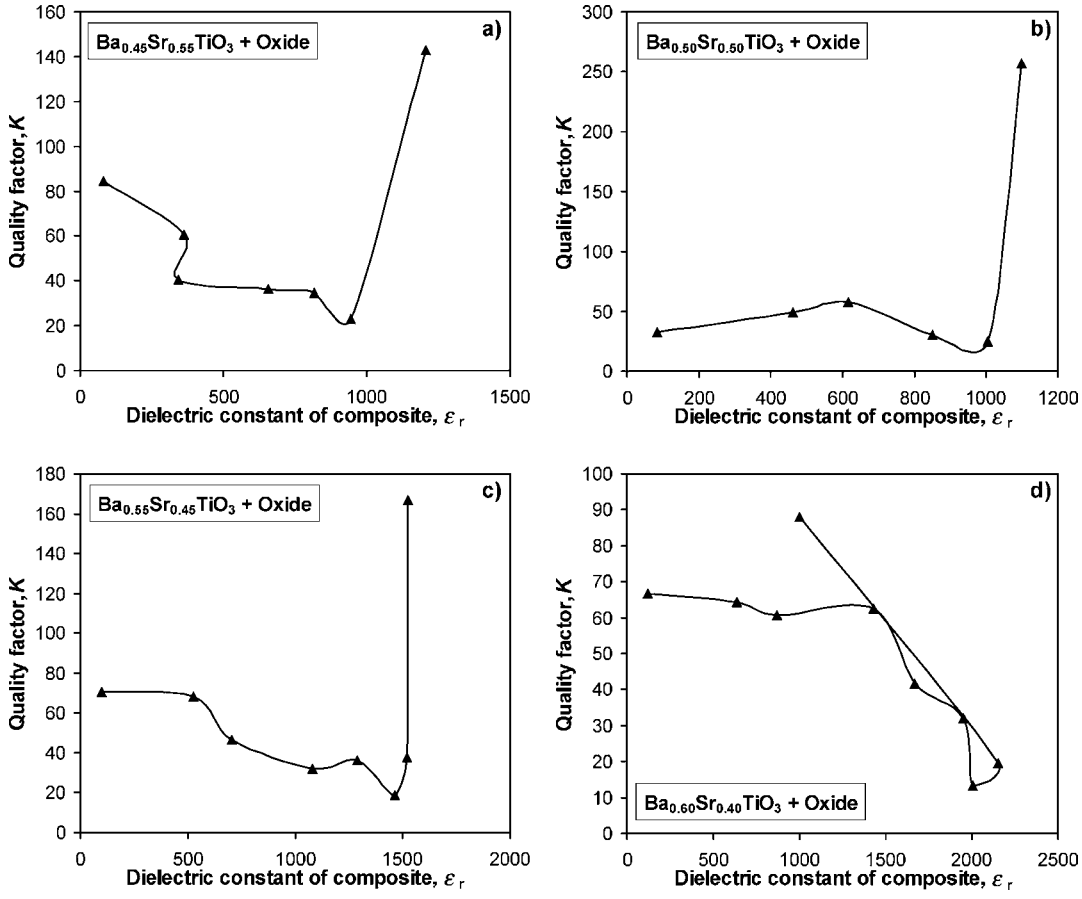

Fig. 35. Quality factor of ferroelectric-dielectric composite material as a function of dielectric constant of composite for (a)–$Ba_{0.45}Sr_{0.55}TiO_3$/oxide, (b)–$Ba_{0.50}Sr_{0.50}TiO_3$/oxide, (c)–$Ba_{0.55}Sr_{0.45}TiO_3$/oxide, (d)–$Ba_{0.60}Sr_{0.40}TiO_3$/oxide material compositions. RT data.

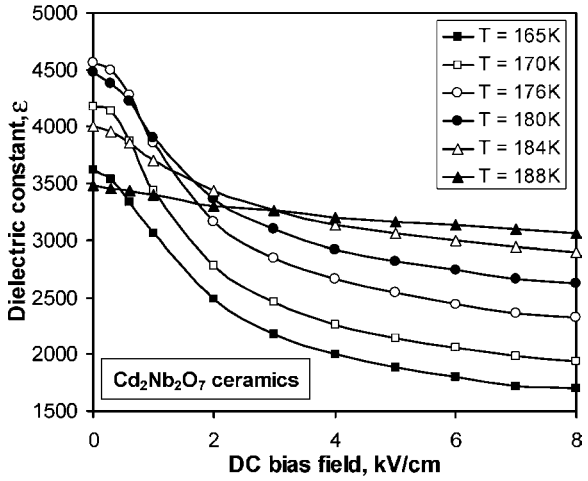

Fig. 36. dc electric field dependence of dielectric constant of $Cd_2Nb_2O_7$ ceramics measured at 5 kHz at temperatures around 180 K, the paraelectric-ferroelectric transition temperature [139].

Other Candidates for Tunable Applications. Several materials with high dielectric permittivity (>1000) were investigated as possible candidates for the tunable applications.

The compounds $Cd_2Nb_2O_7$ [139] and $(Cd_x$-$Pb_{1-x})_2Nb_2O_7$ [140] with the pyrochlore structure have been recently explored. The material exhibits a very high tunability below a diffuse dielectric anomaly at about 180 K (see Fig. 36). However, the lack of information on the dielectric loss at microwave frequencies impedes the assessment of this material as a candidate for tunable applications. Actually, the required low level of the microwave loss may not be achieved due to the relaxor nature of the main dielectric anomaly in this material.

Rather high tunability was reported for double substituted BTO: $(Ba_{(1-x)}Ln_{(x)}Ti_{(1-y)}M_{(y)}O_3$ with donor doping at A site (Ln = La^{3+}, Sm^{3+}, Gd^{3+}, Dy^{3+}) and acceptor doping at B-site (M = Al^{3+}, Fe^{3+}, Cr^{3+}) [141]. It was found that, with increasing the $LnMO_3$ content T_0 shifts downwards. With 4% substitution of $LnMO_3$ almost all the compositions show T_0 near room temperature, all have values of tunability comparable to those of $Ba_{0.6}Sr_{0.4}TiO_3$. The lack of information on the loss at microwave frequencies impedes the assessments of the Commutation Quality factor of these materials.

As a possible candidate for microwave tunable applications the solid solution K(Ta, Nb)O_3 (KTN) is worth mentioning. Being a solid solution of an incipient ferroelectric KTO (very similar to STO) and a ferroelectric $KNbO_3$ (with a sequence of phase transitions identical to that in BTO) this material represents a "direct" analog of BST. It exhibits solubility in the full range of concentrations having T_0's in the range for 0 to 700 K [142] (see Fig. 37). KTN single crystals undergo sharp first order phase transitions with dielectric permittivity as high as a few thousands in a wide temperature range (see Fig. 37). KTN ceramics exhibits a smeared dielectric anomaly with a substantial relaxor-type frequency dispersion [143–145]. The dielectric constant of the ceramics is smaller than in single crystals but still high (see Fig. 38), the tunability being even larger than in BST ceramics (for the same

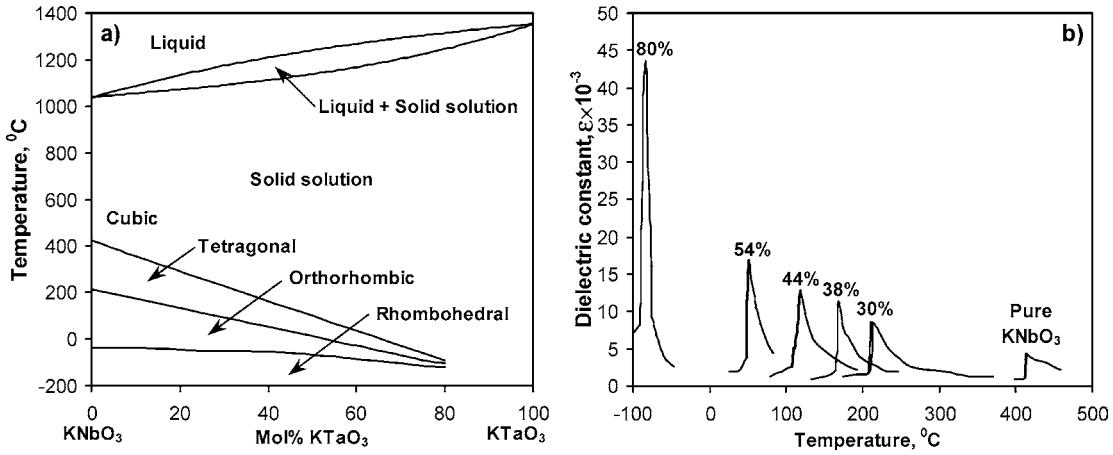

Fig. 37. (a)—Phase diagram of $KNbO_3$ – $KTaO_3$ solid solution [142]. (b)—Dielectric constant vs. temperature for solid solution single crystals of $KTaO_3$ and $KNbO_3$. The indicated percentage are in moles of $KTaO_3$. Measuring ac field is ~5 V/cm and 10 kHz [142].

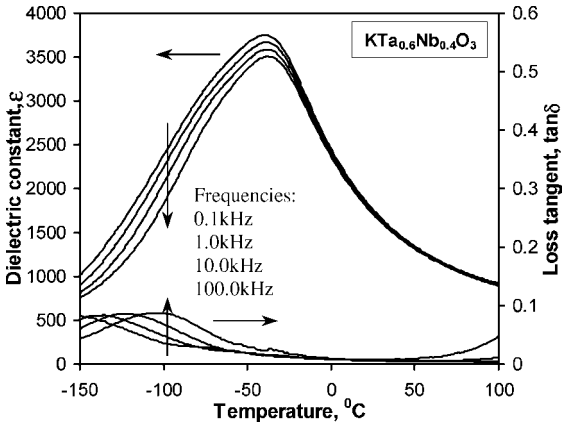

Fig. 38. Temperature dependences of the relative dielectric permittivity and loss tangent of $KTa_{0.6}Nb_{0.4}O_3$ ceramic at different frequencies [145]. The vertical arrows in the figure indicate the direction of the frequency changing (from small to high frequency).

value of the permittivity and applied field). For example, $K(Ta_{0.6}Nb_{0.4})O_3$ ceramics at RT and $\varepsilon_{RT} = 1700$ shows $n = 1.2$ at a dc bias field of 11 kV/cm [145]. On the other hand, in $Ba_{0.65}Sr_{0.45}TiO_3$ ceramics according to Eq. (5.2), the same values of the tunability and permittivity correspond to a dc bias field of 28 kV/cm. The matter of concern with KTN ceramics is the relaxor-like nature of the material, which is seemingly related to difficulty of processing high-volatility potassium-containing material. This feature of KTN ceramics may result in a dispersion of the tunability and high dielectric loss at microwave frequencies.

5.2. *Ferroelectric Thin Films*

The problem of the high bias voltage required for efficient tuning of the bulk ferroelectric based microwave components and the interest in a further miniaturization of the ferroelectric based microwave devices inspired wide investigations of the ferroelectric thin film materials since the beginning of the 1980s. The potential to produce in one technological cycle microwave integrated circuits based on ferroelectric thin films, thus reducing manufacturing costs, and the possibility to combine the microwave circuits with well developed semiconductor integrated circuits have additionally motivated an activity in the field of ferroelectric thin films.[15]

The discovery of high-temperature superconductivity (HTSC) in complex metal oxides in 1987 has stimulated a special interest in strontium titanate and potassium tantalate thin film ferroelectrics. The structural and chemical compatibility of the superconductive oxides (in particular, $YBa_2Cu_3O_7$) with STO and KTO ferroelectrics assures a high-quality interface between HTSC electrodes and ferroelectric thin films. This improves the quality of the films from the point of view of the dielectric loss and offers a substantial scope of the implementation of cryogenic microwave circuits using the unique properties of nonlinear dielectrics and superconducting materials.

On the other hand, the complexity of achieving low temperatures and the cost of the cryogenic plants necessitated the development of ferroelectric thin film materials with operating temperatures close to room temperature. This made BST films attractive. These films were found to exhibit an excellent tunable behavior even at room temperature (in the case of 40–60% concentration of barium), however, the properties of the bulk BST and BST thin films were found to be rather different. The present section addresses the dielectric properties of ferroelectric thin films with the main focus on STO and BST thin films.

The quality of the ferroelectric thin films also strongly depends on the substrates used for film deposition. The typical substrates for STO and BST thin films are single crystal sapphire, lanthanum aluminate, and magnesium oxide. These substrates have similar values of the lattice parameters with those of the aforementioned ferroelectrics, which provide the epitaxial growth of the films on the substrates, and high values of the thermal conductivity coefficient, which increase the power handling capability of the high power microwave devices based on these films [146].

Dielectric Permittivity of Ferroelectric Thin Films. The dielectric properties of ferroelectric thin films deposited onto single crystal substrate usually differ from those of bulk ferroelectric materials in relative dielectric permittivity and in tunability.

An example of direct comparison of the properties of the BST thin films deposited by RF magnetron sputtering technique and bulk ceramic samples was offered by Outzourhit et al. [147]. The films were deposited onto $LaAlO_3$ (100) substrates at 550°C and showed (100)-preferred growth orientation. It was found that the values of the dielectric constants and electrical tunability were more than an order of magnitude lower than those of bulk samples with the same composition (see Fig. 39).

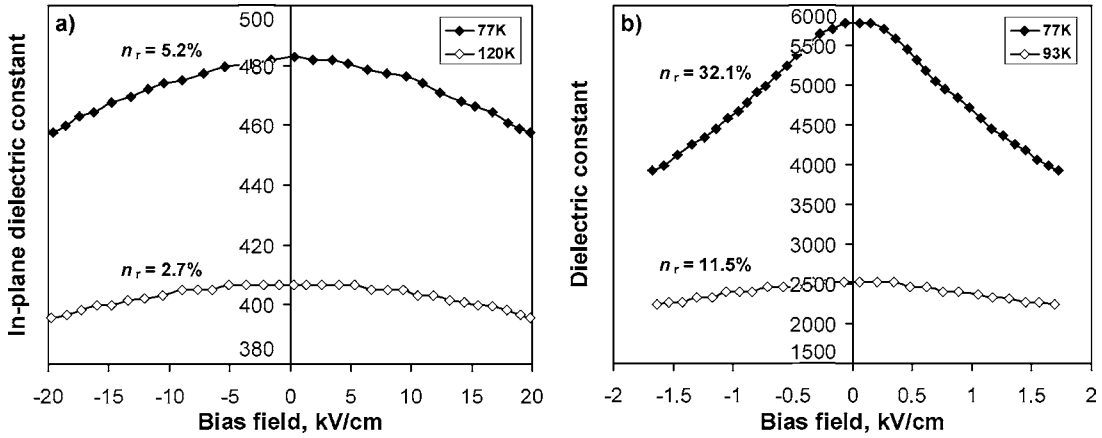

Fig. 39. Electric field dependences of the in-plane dielectric constant of (a) $Ba_{0.1}Sr_{0.9}TiO_3$ film 0.7 μm thick deposited by RF magnetron sputtering onto $LaAlO_3$ substrate; and of (b) bulk polycrystalline $Ba_{0.1}Sr_{0.9}TiO_3$ sample [147]. Measurement temperatures and maximum relative tunability achieved are indicated in the graphs.

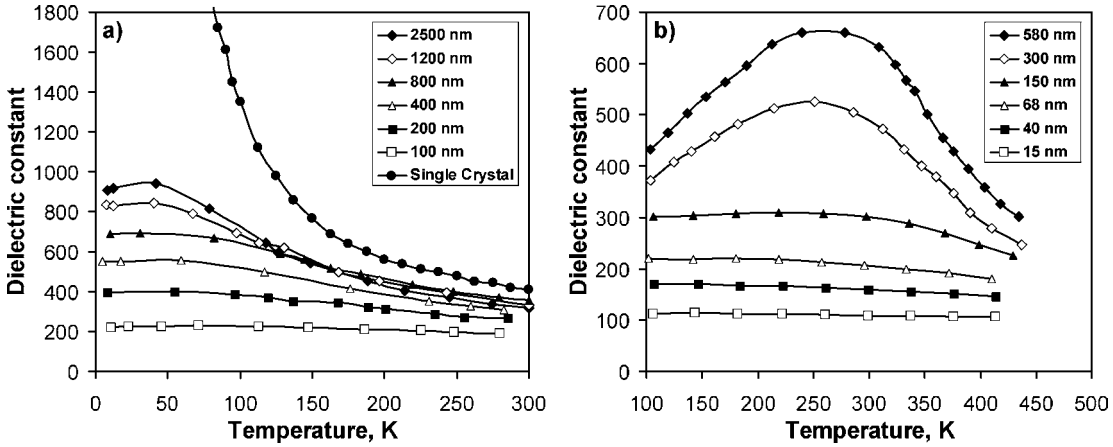

Fig. 40. (a) Out-of-plane dielectric constant as a function of temperature for $SrTiO_3$ films of difference thickness [148] grown on $SrRuO_3/LaAlO_3$ by laser pulse deposition technique and bulk dielectric constant of [100] $SrTiO_3$ single crystal sample [127]; (b) Out-of-plane dielectric constant as a function of temperature for $Ba_{0.7}Sr_{0.3}TiO_3$ films of different thickness deposited by metalorganic chemical vapour deposition technique onto $Pt/SiO_2/Si$[149] (in bulk $Ba_{0.7}Sr_{0.3}TiO_3$ material $T_c = 305$ K [14]).

One should also note that the temperature corresponding to the maximum of dielectric constant of the film was 70 K which was about 15 K smaller than that of bulk ceramics samples with the same concentration of barium (see Fig. 30(b)).

The thickness dependences of properties of ferroelectric thin films were investigated by several groups. Li et al. [148] and the group of Kingon [93, 149] investigated the influence of the film thickness on its dielectric properties. It was found that the dielectric permittivity of the films can substantially change with the thickness of the film (see Fig. 40).

The detailed analysis of the dielectric response of BST thin films of different thicknesses and different compositions has been performed by Streiffer et al. [93], Basceri et al. [150], Vendik et al. [82], and others. As has already been discussed (see Section 3.4) and in those works, one of the possible causes for the suppression of the effective dielectric constant of the ferroelectric film is the so-called passive layer effect (see Section 3.4.1). This effect corresponds to a useful formula for the inverse capacitance density, A/C of a ferroelectric film based parallel plate capacitor containing (real or effective) passive layers near to the

electrodes:

$$\frac{A}{C} = \frac{h}{\varepsilon_0 \varepsilon_f} + \frac{2\delta}{\varepsilon_0 \varepsilon_{\text{pass}}},$$

where C and A are the total capacitance and area of the capacitor, h and ε_f are the thickness and dielectric constant of the ferroelectric thin film, δ and $\varepsilon_{\text{pass}}$ are the thickness and dielectric constant of the passive layers; the formula is obtained from Eq. (3.64).

It is seen that by measuring the capacitance of the parallel plate capacitor based on ferroelectric thin film and plotting the inverse capacitance density A/C as a function of film thickness h, one can obtain the thickness to dielectric constant ration $\delta/\varepsilon_{\text{pass}}$ of the passive layer, by interpolating the A/C vs. h curve to zero film thickness. Figure 41 shows the measured inverse capacitance densities of BST film based parallel plate capacitors as a function of film thickness for different Ti contents (Fig. 41(a)) and different temperatures (Fig. 41(b)). From these figures one readily finds that in both cases the ratio $\delta/\varepsilon_{\text{pass}}$ is about 0.5 Å. This value is compatible with the result of the analysis of the dielectric properties of BST films offered by Vendik (see Ref. [82]). However, based on these data, one cannot decide which of the mechanisms for this kind of size effect (surface blocking model, "electrode" mechanism, or depletion effect, see Section 3.6.1) operates in this material since all these mechanisms deal with the values of $\delta/\varepsilon_{\text{pass}}$ of this order.

The dielectric properties of the ferroelectric thin films become somehow closer to those of bulk materials when the thickness of the films is higher than 2 micrometers (see Fig. 40). Bearing in mind microwave tunable applications of the films, an important remark should be made. These applications usually imply the planar structure of varactors (see Figs. 19(e), (d) and 20(a)), where the in-plane component of the permittivity matters. As was pointed out in Section 3, this component of the permittivity is much less sensitive to the passive layer effects than the out-of-plane one. Thus, the size effect on the out-of-plane component of the permittivity discussed above may not be relevant to the real situation in the microwave devices. To evaluate the strength of the size effect on the in-plane component of the permittivity, experimental information on the thickness dependence of this component is required. The relevant experimental information available in the literature is very scarce. Data on the thickness dependence of the in-plane tunability in BST films (h = 22–1150 nm) were recently reported by Bellotti et al. [151]. The authors found a significant reduction of the tunability with decreasing film thickness, which was also accompanied by an increase of the absolute value of the in-plane strain disregarding to its sign. The physical origin of this size effect remains unclear, since none of the presently available theories can predict such kind of behavior. Clearly, the passive layer scenario might be summoned however this scenario would require the existence of an unrealistically thick passive layer.

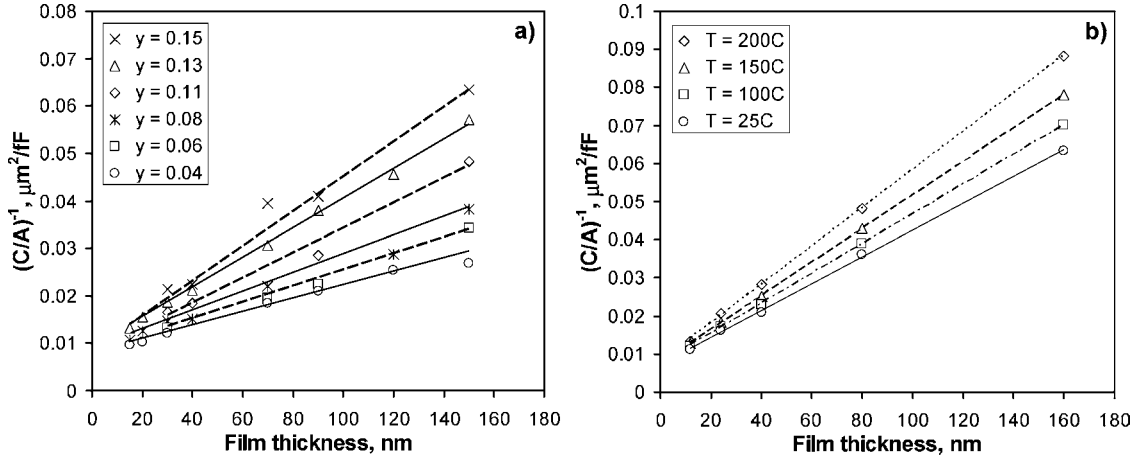

Fig. 41. (a) Film thickness dependences of the inverse zero-bias capacitance density of $(Ba_{0.7}Sr_{0.3})Ti_{1+y}O_{3+z}$ film based plate capacitors at different Ti content y [93]; (b) The inverse of the zero-bias capacitance density of $Ba_{0.7}Sr_{0.3}TiO_3$ film based parallel plate capacitors as a function of film thickness at different temperatures [150].

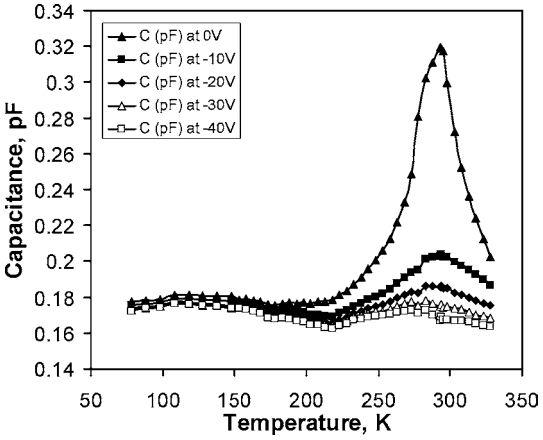

Fig. 42. Capacitance of the planar inter-digital capacitor (capacitive gap 12 μm) based on $SrTiO_3$ thin film deposited by MBE on (110) $DyScO_3$ substrate as a function of temperature under different dc bias applied [152].

Though the situation discussed above where dielectric permittivity of the films is reduced compared to its bulk counterpart is rather typical, it is not the only one possible. An example of an alternative behavior was recently reported by Schlom et al. who investigated the dielectric properties of STO thin films deposited by the molecular beam epitaxy technique onto (110) $DyScO_3$ substrates [152]. They observed a substantial shift of the phase transition temperature in the film (up to 300 K, see Fig. 42) and consequently a high tunability of planar capacitors based on this film even at room temperature ($C(0)/C(U_{max}) \approx 2$ at $T = 300$ K). These films were reported to be strongly strained exhibiting at RT an in-plane lattice constant of $a = b = 3.92$ Å (the RT bulk value of STO lattice constant is 3.905 Å), which corresponds to an in-plane misfit tensile strain of about 0.4%. This value is comparable with the in-plane misfit tensile strain of 0.7% needed to shift the transition temperature in STO films up to room temperature (see Section 3.4.3.). Thus, the effect of mechanical clamping of the film by the substrate seems to play an essential role in the change of the transition temperature and dielectric permittivity of the film compared to the bulk material.

At present, the effect of the misfit strain is often considered as the main reason for the difference between the dielectric properties of the ferroelectric films grown on different substrates and/or objected to different annealing procedures. For example, Chang et al. investigated the effect of annealing on dielectric properties of $Ba_{0.5}Sr_{0.5}TiO_3$ thin films deposited by the pulsed laser deposition technique onto (100) MgO and (100) $LaAlO_3$ substrates [153], the results are listed in Table 8.

One can see that the effect of annealing is different in the case of different substrates. For the same capacitor geometry, the as-deposited BST film on MgO shows a higher capacitance than as-deposited BST film on $LaAlO_3$, which means a higher dielectric constant. After annealing, the capacitance C and tunability of BST film on MgO decrease whereas the opposite effect is observed for films deposited onto $LaAlO_3$. The authors attributed the large difference in the dielectric behavior for the BST thin films deposited onto MgO and $LaAlO_3$ substrates to the difference in the stress in the films, which in turn is due to a difference in lattice constants and thermal expansion coefficients of the substrates.

Similar behavior of the ferroelectric film dielectric properties after post-deposition annealing has been also observed by Carlson et al. in $Ba_{0.4}Sr_{0.6}TiO_3$ thin films deposited by laser ablation on MgO and $LaAlO_3$ substrates (see Table 9) [154].

Though the explanation of the impact of annealing and the substrate material on the lines of the aforementioned "mechanical" scenario is possible, without information on the in-plane lattice constants of the films this scenario cannot be justified. A recent

Table 8. 10 GHz dielectric properties of as-deposited and low temperature ($\leq$1000°C) annealed $Ba_{0.5}Sr_{0.5}TiO_3$ films on MgO and $LaAlO_3$ substrates. (The capacitors have an interdigitated structure with eight fingers with 6 μm gap, 80 μm length, and 10 μm width) [153].

	$Ba_{0.5}Sr_{0.5}TiO_3$ on MgO		$Ba_{0.5}Sr_{0.5}TiO_3$ on $LaAlO_3$	
	As-deposited	Annealed	As-deposited	Annealed
C_0, pF	0.775	0.387	0.440	1.281
n ($E = 67$ kV/cm)	1.85	1.53	1.24	2.16
tanδ ($E = 0$)	0.14	0.07	0.05	0.17
tanδ ($E = 67$ kV/cm)	0.06	0.03	0.02	0.05

Table 9. Low-frequency (1 MHz) dielectric constants (ε) at 300 K and at the peak temperature (T_{max}) for various $Ba_{0.4}Sr_{0.6}TiO_3$ thin films [154].

Film	ε (300 K)	ε (T_{max})	T_{max}, K
As-dep. BST/MgO	2620	4130	242
Annealed BST/MgO	2290	6020	227
As-dep. BST/LAO	2960	3320	267
Annealed BST/LAO	4660	5170	277

comprehensive study [155] of similar systems actually questions the importance of the mechanical effects in this situation. In this study, the influence of annealing procedure on the dielectric properties of $SrTiO_3$ thin films deposited by laser ablation onto (100) MgO and (100) $LaAlO_3$ substrates was addressed. An example of the temperature dependences of the dielectric permittivity in these films is presented in Fig. 43.

One can see that STO thin films deposited under the same conditions onto different substrates show completely different behavior. In the case of $LaAlO_3$ substrate we can see an evident maximum in the temperature dependence of the permittivity, which suggests the appearance of ferroelectricity in STO thin films, whereas in the case of MgO substrate the STO thin films exhibit a monotonic temperature dependence of the permittivity.

As in the work of Chang et al. [153], an impact of the annealing procedure on film properties has been observed for $SrTiO_3$ thin films [155], which was qualitatively the same as that reported by Chang et al. for BST films. A post-deposition annealing at 1100°C in the oxygen atmosphere during 4 hours results in a shift of the temperature peak up in the case of $LaAlO_3$ substrate (Fig. 43(b)), which means increase of the film dielectric constant at certain temperature, and a decrease of the film dielectric constant in the case of MgO substrate (Fig. 43(a)).

To clarify the origin of the annealing-induced variation of the permittivity, in addition to dielectric measurements, the crystal cell lattice parameters of these STO thin films was measured by grazing-angle X-ray diffraction techniques [156] (see Table 10).

One can see that the annealing procedure results in an increase of the in-plane lattice constant in the case of MgO substrate[16] and in a decrease in the case of $LaAlO_3$. As it follows from the thermodynamic theory for the influence of misfit strain in the film on its dielectric properties and phase transition temperature [98, 157](see Section 3.3.3), the increase of the in-plane lattice constant should lead to an increase of the in-plane Curie-Weiss temperature and correspondingly, the decrease of the in-plane lattice constant should lead to its decrease.[17] It is clearly seen that the behavior of the dielectric permittivity in these systems, as illustrated in Fig. 43, is just opposite to this trend. This suggests that in this case the misfit strain does not play the principal role in the shift of the Curie-Weiss temperature of the films. A possible explanation for the impact of annealing and the substrate material on the dielectric properties of these films is non-stoichiometry-driven shifts of the Curie-Weiss temperature, which are sensitive to the annealing and the substrate material.

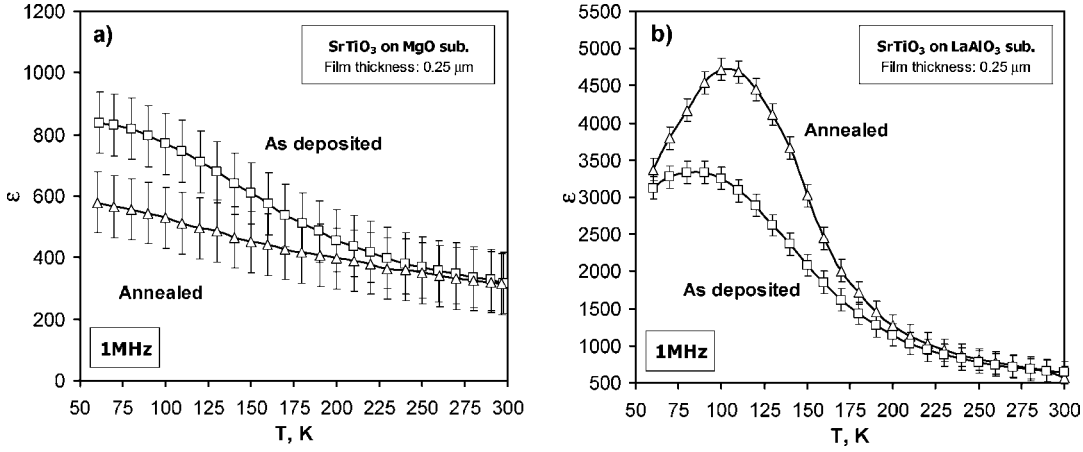

Fig. 43. Relative in-plane dielectric constant of the $SrTiO_3$ thin film deposited on MgO (a) and $LaAlO_3$ (b) substrates as a function of temperature measured at 1 MHz [155].

Table 10. The crystal cell lattice parameters for $SrTiO_3$ thin films on different substrates [155].

Crystal cell lattice parameters (Å)	$SrTiO_3$ on $LaAlO_3$		$SrTiO_3$ on MgO	
	Before annealing	After annealing	Before annealing	After annealing
a	3.903	3.903	3.894	3.899
b	3.912	3.909	3.896	3.902
c	3.905	3.905	3.909	3.909

The maxima in the temperature dependence of the permittivity mentioned in the discussion of the dielectric properties of STO films [152, 155] are strongly believed to be a manifestation of a ferroelectric phase transition. For instance, to prove the presence of ferroelectricity in the $SrTiO_3$ thin film on $LaAlO_3$ substrate [155], the hysteresis loops at room and at liquid nitrogen temperatures (the temperatures which are higher and lower than the supposed phase transition temperature) were experimentally tested (see Fig. 44). In Fig. 44 one can readily see the presence of the remanent polarization at liquid nitrogen temperature whereas at room temperature the polarization response is linear. Also, the observed value of the remanent polarization in the film is in a good agreement with the theoretical estimates which can be obtained from the Landau theory of STO films [155]. ($P_R \approx 5.6\ \mu C/cm^2$ for $(T - T_c) \approx$ 20 K). It is worth mentioning that the appearance of the ferroelectricity in STO films is not rare. For example, the presence of the ferroelectric phase in $SrTiO_3$ thin films grown by RF magnetron sputtering technique on (001)-oriented $YBa_2Cu_3O_{7-x}$ bottom electrode deposited on to an STO substrate has been observed by Fuchs et al. [158]. They reported a maximum in the temperature dependence of dielectric constant around 100 K and non-zero remanent polarization in hysteresis loops at temperatures below 120 K.

Summarizing the discussion of the present section one may identify three phenomena influencing the dielectric response of tunable thin films: (i) effects manifesting themselves in a reduction of the permittivity similar to that caused by a thin dielectric layer at the film surface (surface blocking model, "electrode" mechanism, and depletion effect), (ii) misfit-strain-driven variation of the Curie-Weiss temperature, and (iii) nonstoichiometry-driven shifts of the Curie-Weiss temperature. This list should be completed with a defect–induced suppression of the dielectric permittivity in ferroelectrics (Section 3.1.2). Being also active in bulk materials, according to the number of authors [4, 159, 160] this effect seems to be of importance for thin ferroelectric films, especially when the suppression of permittivity is large (like in Fig. 40(a) at very low temperatures).

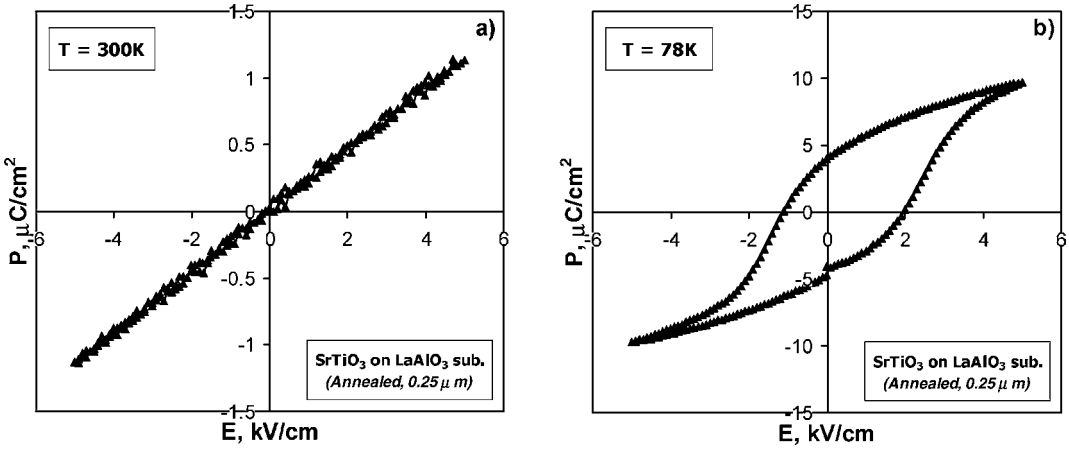

Fig. 44. Hysteresis loops for $SrTiO_3$ thin film based planar capacitors at room (a) and liquid nitrogen (b) temperatures [155].

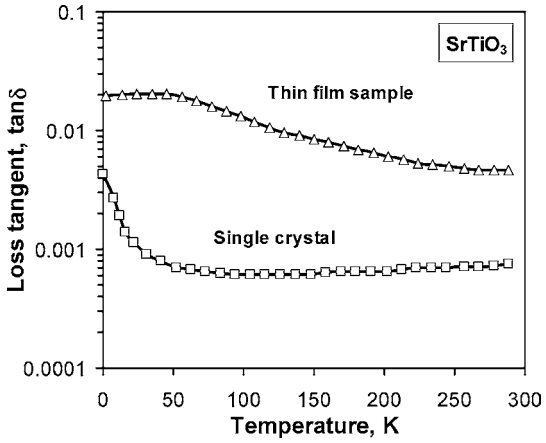

Fig. 45. Estimated loss tangent of the $SrTiO_3$ single crystal and thin film as a function of temperature at frequency $f = 10$ GHz and bias field $E = 0$ [2].

Dielectric Loss in Ferroelectric Thin Films. High values of the dielectric loss in thin films in comparison with single-crystals and bulk ceramics make a problem which sets limits to the practical application of ferroelectric thin films in microwave devices. According to Vendik et al. [2] and other experimental works [115, 161–163] the dielectric loss in the ferroelectric thin films are roughly one order of magnitude higher than those in the bulk samples (see Fig. 45).

Lemaitre et al. have investigated at microwave frequencies (2 GHz) the dc field dependences of the dielectric constant and loss tangent of the $SrTiO_3$ thin film deposited by RF magnetron sputtering onto $LaAlO_3$ substrates [163]. Plotting the loss tangent as a function of the film dielectric constant taken at the same value of the electric field, one can find that the loss tangent increases almost linearly with the dielectric constant (Fig. 46(a)). A similar behavior has been observed at radio frequencies (10 kHz) by Moeckly [30] in $SrTiO_3$ thin films deposited by laser ablation technique (see Fig. 46(b)). The data from Ref. [153] given in Table 8 also confirm the trend: the higher the permittivity, the higher the loss tangent.

The level of the microwave loss in thin films and its dependence on the permittivity is compatible with the existing knowledge on the main mechanisms of dielectric loss in ferroelectrics reviewed in the previous parts (Chapters 3.2 and 3.4). The excessive loss in the films compared to single crystals clearly attests to their mainly extrinsic origin. The observed increasing permittivity dependence of the loss tangent corresponds to the theoretical predictions for all loss mechanisms except the universal-relaxation–law, which does not look decisive at microwave frequencies. The increasing permittivity dependence of the loss tangent taken into account along with the decreasing dc field dependence of the permittivity readily suggest a decreasing dc field dependence of the loss tangent. This trend is typically observed experimentally (see e.g. [163]). However, in high quality films, it is not always observed. This situation was reported by Astafiev et al. for the loss tangent at microwave frequencies (8 GHz) in STO thin films deposited by laser pulse deposition technique

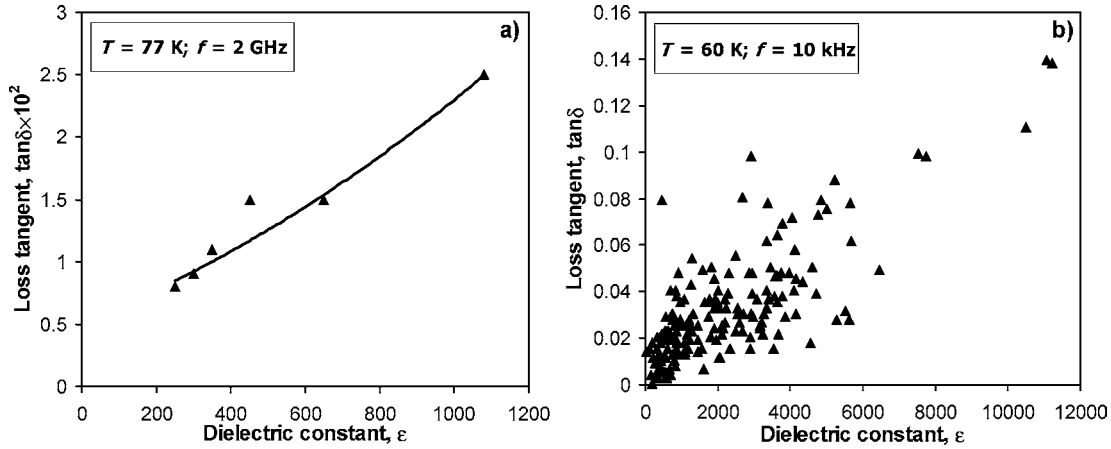

Fig. 46. (a) Loss tangent of the $SrTiO_3$ thin film at microwave frequencies (2 GHz) as a function of the in-plane dielectric constant of the film (the dielectric constant was changing by applying dc bias field to the samples) [163]. (b) Loss tangent of the $SrTiO_3$ thin film at radio frequencies (10 kHz) as a function of the film dielectric constant (the each points correspond to the different samples with different dielectric constant) [30].

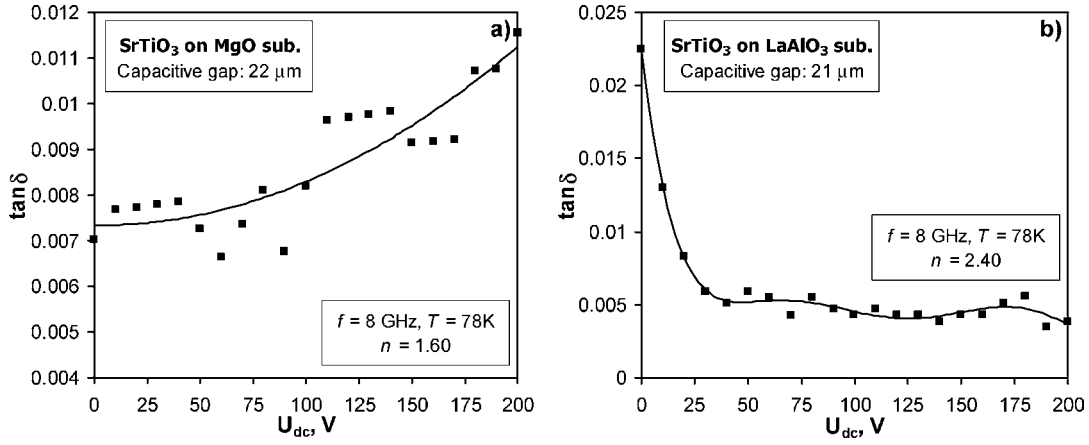

Fig. 47. Field dependences of the loss tangent of $SrTiO_3$ thin films deposited by laser ablation on to MgO (a) and $LaAlO_3$ (b) substrates [164].

onto MgO and $LaAlO_3$ substrates [164]. It has been found that when the initial value of the loss tangent (at zero bias field) is high (more than 0.01) the dielectric loss decreases with the applied field (Fig. 47(b)), at the same time, when the loss tangent is small in the absence of a bias field, one can observe field independence or an increasing field dependence of dielectric loss (Fig. 47(a)). This behavior can be attributed to a manifestation of the dc-field-induced quasi-Debye loss (see Section 3.2.1) documented for single crystals of STO and KTO (see Section 5.1): in better quality (lower loss) films the contribution of this mechanism, which rapidly increases with the increasing dc field, can be seen on the background of the extrinsic loss whereas it is impossible to detect it in the films with a higher (extrinsic) loss level.

Results on frequency dependence of the dielectric loss in thin films were offered by Baniecki et al. [75]. They found that the loss tangent of $Ba_{0.7}Sr_{0.3}TiO_3$ thin film does not depend on the frequency in the range of radio frequencies (1 Hz–100 MHz). For microwave frequencies (1–20 GHz) their data suggest an increasing frequency dependence of the loss tangent[18] (Fig. 48(a)). A similar behavior of the loss tangent at microwave frequencies was observed by Razumov et al. [165] in $Ba_{0.3}Sr_{0.7}TiO_3$ thin film deposited by RF sputtering onto ceramic alumina and single crystal sapphire substrates (Fig. 48(b)).

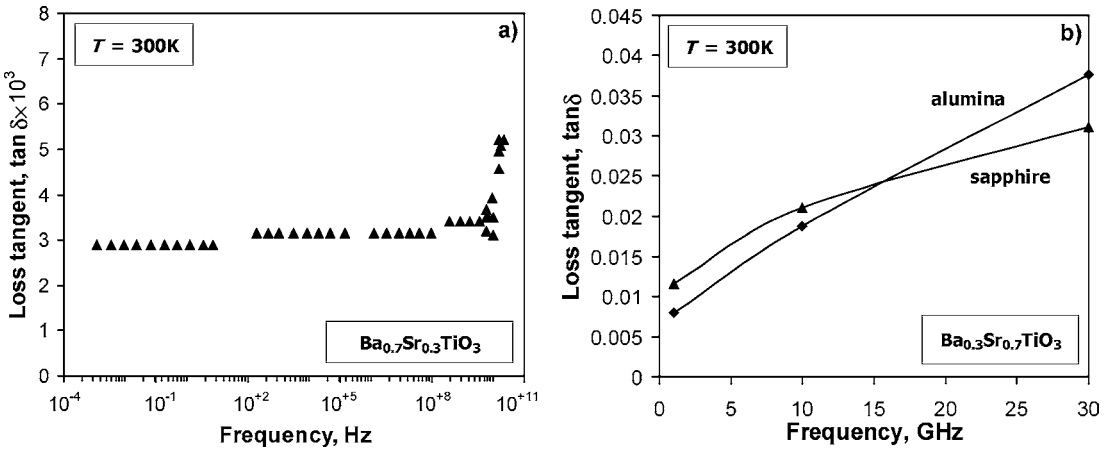

Fig. 48. Frequency dependences of the loss tangents of (a) $Ba_{0.7}Sr_{0.3}TiO_3$ thin films [75]; and (b) $Ba_{0.3}Sr_{0.7}TiO_3$ thin films deposited onto alumina and single crystal sapphire substrates [165].

The frequency dependence of the loss in thin films discussed above can be rationalized in terms of the existing knowledge on the loss mechanisms in ferroelectrics (see Section 3.2). As it has already been shown in Section 3.2, for all of the loss mechanisms (intrinsic and extrinsic) the dielectric loss tangent is almost a linear function of the frequency, except the so-called universal-relaxation-law loss mechanism. The data shown in Fig. 48(a) may be interpreted as a crossover (around $f = 1$ GHz) between the almost flat area, which probably corresponds to universal-relaxation-law loss mechanism, and an increasing frequency dependences of the loss tangent, which in turn corresponds to others loss mechanisms. In Fig. 48(b) one can see a linear frequency dependence of the loss tangent of BST thin film in the range of 1–30 GHz. It suggests that the aforementioned universal-relaxation-law loss mechanism does not contribute much to the total balance of the dielectric loss at microwave frequencies.

Dependence of the Ferroelectric Thin Film Properties on the Film Preparation Conditions and Ways to Improve the Quality of the Grown Films. Obviously, many properties of ferroelectric films strongly depend on the conditions of the film deposition. The properties relevant to tunable applications are in particularly sensitive in this respect. Razumov et al., for example, showed that the dielectric properties of the BST thin films could be substantially changed only by changing the deposition temperature (see Fig. 49) [165]. It is seen in Fig. 49 that, in the case of $Ba_{0.5}Sr_{0.5}TiO_3$ thin film, a change of the deposition temperature by 20% leads to a more than 2 times increase of the tunability, however, the loss tangent also increases more than 2 times. This behavior may be attributed to the influence of the deposition temperature on the film stoichiometry and defect population in it, which in turn affect the Curie-Weiss temperature of the material. In the case of the data presented in the Fig. 49 an increase of the deposition temperature should result in a shift of the Curie-Weiss temperature up, which according to the existing theories (see Section 3) will lead to an increase of the permittivity, loss, and tunability.

Along with the dependence of the film properties on deposition conditions there exist problems with the homogeneity of grown ferroelectric films. The dielectric response of the films can significantly differ over the area of the substrate. Steinhauer et al. investigated by scanning microwave microscopy described in Section 4.4 the distribution of the dielectric permittivity and electrical tunability of 370 nm thick $Ba_{0.6}Sr_{0.4}TiO_3$ films across the $LaAlO_3$ substrate, where the films were deposited by pulsed laser deposition technique (see Fig. 50) [123]. They found that there exist regions in the film with a reduced dielectric permittivity and tunability. This was attributed to a higher density of defects or to smaller thickness of the film in these regions. It was also shown [123] that the post-deposition annealing procedure (e.g. 650°C, in the air) lead to an improvement of the homogeneity of film properties and to a decrease of the "bad" regions with low dielectric permittivity and tunability (see Fig. 50).

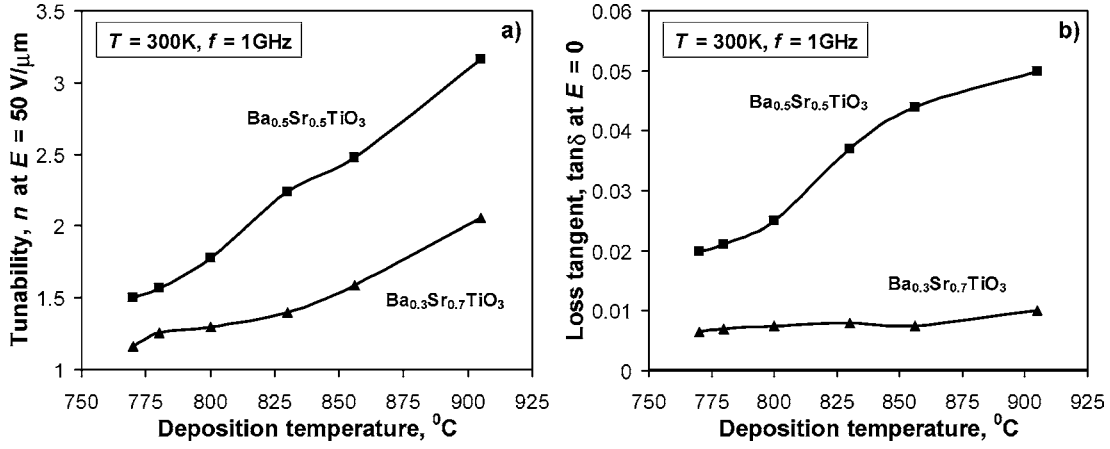

Fig. 49. Dependence of the electrical tunability (a) and loss tangent (b) of the BST thin films based planar capacitors on deposition temperature [165].

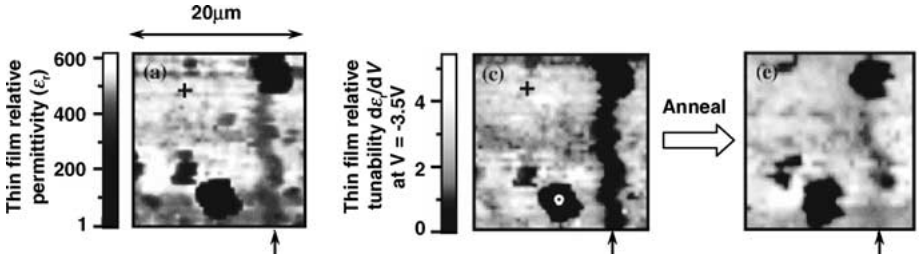

Fig. 50. Distribution of the dielectric permittivity before annealing (a) and tunability before annealing (c) and after annealing (e) of the $Ba_{0.6}Sr_{0.4}TiO_3$ thin film along the surface of substrate measured at frequency 7.2 GHz [123].

Another possible way to improve the quality of ferroelectric thin films from the point of view of its dielectric properties is doping of the film by different dopants like magnesium or manganese. Joshi et al. have reported the microstructural and dielectric properties of Mg-doped $Ba_{0.6}Sr_{0.4}TiO_3$ thin films prepared by the metalorganic solution deposition technique [166]. They observed an increase of the quality factor at 5 mol% content of Mg in the mixture, and a decrease of that factor with further increasing the Mg content in the mixture up to 20 mol% (see Table 11).

This behavior substantially differ from that of the bulk ceramics of the same composition discussed in Section 5.1 and it can not be interpreted in terms of simple doping and composite effects.

A different behavior of a multicomponent ferroelectric film was recently reported by Jain et al. [80] (see Table 12) for a layered structure of sol-gel-derived $Ba_{0.5}Sr_{0.5}TiO_3$ thin films and MgO thin layers (four layers of BST each 70 nm thick and three layers of MgO, 40 nm each). A planar capacitor sturucture was used for the characterization so that, electrically, the system was equivalent to the columnar (parallel) composite model (see Sections 3.1.3 and 3.2.3). The composite film yielded a three times higher value of the quality factor K than an identically processed pure BST film. At the same time, a shift of phase transition temperature was not practically observed. This behavior by no means can be attributed to a manifestation of the composite effect which predicts for the parallel composite a weakly decreasing ε-dependence of the K-factor. Specifically, the observed reduction of the loss is too large to be explained by the composite effect. Two mechanisms can be invoked to rationalize the reported behavior of the K factor and loss: a small mutual doping effect at the borders of layers and an improvement of the film morphology (e.g, grain size). Indeed, Jain et al. indicated a better densification of the composite films.

Table 11. Effect of Mg doping on the dielectric properties of $Ba_{0.6}Sr_{0.4}TiO_3$ thin films. (Film thickness: ~0.26 μm, room temperature measurements at 100 KHz).

Mg (mol%)	ε	tanδ	n ($E = 20$ V/μm)	K
0	450	0.013	1.39	650
5	386	0.007	1.21	730
20	205	0.009	1.09	84

Table 12. Dielectric properties of pure and multilayer MgO:BST thin films at 1 MHz and room temperature [80].

Film	ε	tanδ	n	T_{max}, K	K
Pure BST	2714	0.0215	2.08	267	1213
MgO:BST layered	1729	0.0049	1.34	258	3593

New Technologies and Alternative Thin Film Ferroelectric Materials for Tunable Microwave Applications. The desire to combine the advantages of the thin films with the high quality of single-crystals has inspired the development of a completely new technique of thin ferroelectric layer production: a single-crystal separation by hydrogen implantation or so-called "Smart-Cut" process [167]. The typical "Smart-Cut" process procedure consists of a few main steps:

- Ion implantation of hydrogen ions in a single-crystal STO wafer;
- A bonding at room temperature of the STO wafer to another wafer, for example to an insulating glass substrate;
- Two-step heat treatment of the two bonded wafers: During the first step (400–600°C), the implanted STO wafer splits into two parts: a thin layer of monocrystalline strontium titanate remaining

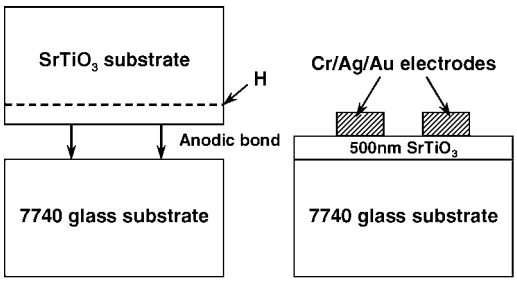

Fig. 51. Interdigitated finger capacitor fabrication approach using separation by hydrogen ion implantation [168].

bonded to glass substrate and the rest of STO wafer. The second high temperature treatment phase (>1000°C) aims to strengthen the chemical bonds;

– Polishing: after splitting, the thin monocrystalline layers exhibit a microroughness which makes chemo-mechanical polishing of the surface necessary.

Recently, Kub et al. characterized interdigitated planar capacitors based on a 500 nm thick monocrystalline strontium titanate layers produced by this technique [168]. Planar interdigitated finger capacitors were fabricated on the as-hydrogen-split surface with no further cleaning or processing steps (see Fig. 51). The metal electrodes for the interdigitated finger capacitors consisted of a 20 nm thick chromium adhesion layer, 1.5 μm thick silver layer, and a 50 nm gold cap layer to ensure a good probe contact and to prevent tarnishing. A capacitor contained six finger pairs with 10 μm finger width, 6 μm finger gaps, and 80 μm overlap length.

The properties of the obtained thin ferroelectric layer based planar capacitor are presented in Fig. 52. The reported rather low tunability of the planar capacitor ($n_{cr} \approx 0.3\%$) (Fig. 52(a)) is compatible with the dielectric properties of STO bulk crystals at RT. On the other hand, the dielectric loss is much higher than that in STO bulk crystals and the expected increase in dielectric loss with bias and frequency (like in the bulk material) is not observed (Fig. 52(b)). The origin of the elevated loss level in the "smart cut" STO films remains unclear: it may be an effect of the hydrogen splitting or a manifestation of the loss induced by the electrode-ferroelectric interface.

A possible application of materials other than BST and STO as a part of microwave tunable devices has been also pursued in the last decade. Shareef et al. have reported on the effect of dc field on the dielectric properties of $Pb(Zr,Ti)O_3$ and BTO thin film materials grown on Al_2O_3 and $LaAlO_3$ substrates [169]. Even though the data reported on tunability is promising (up to 50%), large hysteresis has been observed in the dielectric constant versus electric field characteristics, which is disadvantageous for the tunable applications. The loss tangent of the film at high frequencies (>1 GHz) were not presented so that one can not assess the suitability of these materials for microwave tunable components.

The room temperature phase is monoclinic. One of the interesting properties exhibited by these

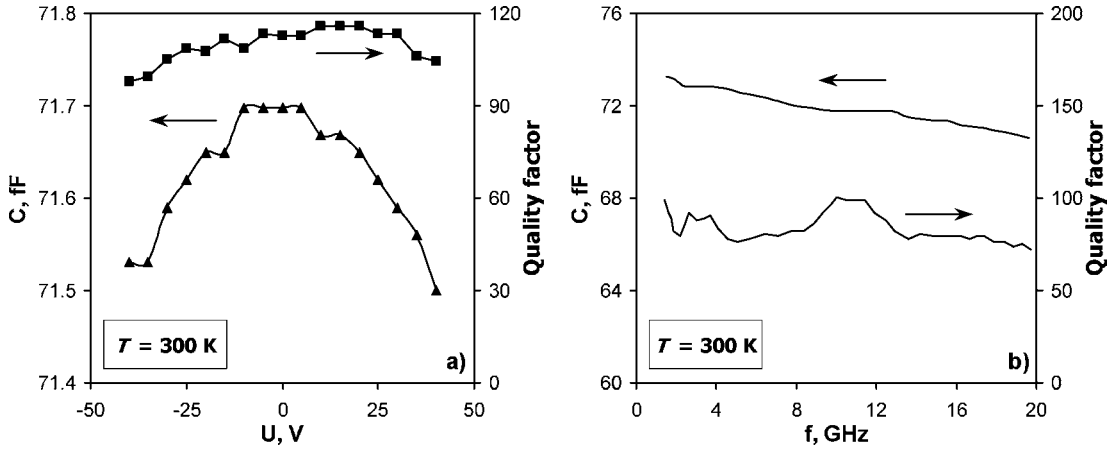

Fig. 52. Field (a) and frequency (b) dependences of the capacitance and quality factor of the interdigitated planar capacitors based on 500 nm thick monocrystalline $SrTiO_3$ layer [168].

compounds is their relatively low dielectric loss ($\tan\delta < 0.002$ at 1 MHz) in the ferroelectric phase [170]. A recent report on ATN films grown on MgO and $LaAlO_3$ substrates reveals that tunability measured at 1 kHz is around 6% and the loss tangent varies between 0.0025 and 0.0034 at 1 MHz [171]. However, the suitability of these materials for microwave tunable components still cannot be assessed because of the lack of data on microwave dielectric loss.

6. Conclusions

This paper reviewed and analyzed the properties of ferroelectric materials that are relevant to tunable devices at microwave (MW) frequencies. We centered on effects that can be analyzed in terms of physical mechanisms related to ferroelectricity and in terms of interaction of the material with electric field. Although very important, chemical effects such as the inter-diffusion between different components of the material, or the mechanisms which relate the processing conditions to the microstructure were out of the scope of this paper. Yet, experimental results on 'imperfect' materials both from the literature and from authors' laboratory were analyzed in light of the theory and often showed a reasonable agreement with it. However, one should recognize that the descriptive ability of the existing theory is limited. The theory for the tunability available in the literature is adequate for the description of real materials, except for the tunability of composites where only limited amount of results is reported. The theory of the dielectric loss is properly developed for the case of intrinsic phonon loss whereas the available models for the extrinsic microwave loss do not seem to cover the spectrum of the loss mechanisms operating in real materials. More detailed conclusions that can be drawn from the critical analysis offered in this paper can be summarized as follows.

Which Materials are Suitable for Tunable MW Applications? The most interesting materials for tunable ferroelectric applications are the paraelectric phases of displacive ferroelectrics (or incipient ferroelectrics). The high Curie-Weiss constant of displacive ferroelectrics implies high values of dielectric permittivity and tunability even far above the Curie temperature. This also reduces the sensitivity of the permittivity to temperature changes. The absence of ferroelectric domains helps in keeping the loss level low.

The Relation Between Tunability and Permittivity. In both the ferroelectric and the paraelectric phases, the tunability strongly depends on the permittivity: At low fields the tunability varies cubically with the permittivity, and at higher fields this is reduced to a linear dependence (Fig. 7).

Real ferroelectric ceramics can be modeled as composites containing a minor dielectric (non ferroelectric) phase. In the case of a layered composite, e.g. a passive layer at the ferroelectric-electrode interface, the permittivity and the tunability can be strongly suppressed. This is particularly important for thin films. In fact, the behavior of a layered ferroelectric composite is very close to that of a pure ferroelectric with a decreased Curie temperature. Two more cases are of interest. The columnar composite, e.g. a columnar microstructure of thick films with a passive layer at the grain boundary (in the case of out-of-plane component of the permittivity) and a composite of a ferroelectric material with dielectric spherical inclusions, e.g. a parasitic phase at the triple points. A remarkable feature of both cases is that while the permittivity can be strongly reduced, the tunability is much less affected (Fig. 9), though for the spherical inclusion model this statement should be taken with a reservation for the roughness of the approximation used in the calculations.

Intrinsic and Extrinsic Dielectric Loss in 'Ideal' and in 'Real' Ferroelectrics. At microwave frequencies, in contrast to lower frequencies, the intrinsic and extrinsic contributions to the losses in tunable ferroelectrics can be of the same order of magnitude.

The intrinsic dielectric loss of ferroelectrics in the paraelectric phase increases with the dielectric permittivity. This loss originates from the interaction of the ac field with the phonons in the material through 3-quantum and 4-quantum mechanisms. The contribution to losses by the 3-quantum mechanism is expected to be of a higher importance. In the so-called high-K dielectrics (low loss paraelectrics with relative permittivity in the 20–100 range), it has been shown both theoretically and experimentally that $\tan\delta$ due to the 3-quantum mechanism increases by power of 3–4 with the dielectric permittivity. In $SrTiO_3$ this power law has an exponent of 1.5.

Electric field induces an additional loss mechanism in paraelectrics, the quasi-Debye loss, due to the breaking of the center of symmetry. At the frequencies of interest (<100 GHz) this loss mechanism can be substantially higher than 3- and 4-quantum mechanisms.

It varies with the electric field in a complex manner—having a quadratic dependence on the field at low fields, and flattening at higher fields. At the higher MW frequency range, a slowing down of the loss dependence of frequency is expected. As an order-of-magnitude estimate, an intrinsic loss of 0.02 was calculated for BST (60:40) at 25 GHz and 100 kV/cm (see Section 3.2.1).

Extrinsic losses emanating from charged defects (which are expected to be stronger in thin films) are directly dependent on the permittivity and inversely dependent on applied field. Local polar regions induced by defects will also contribute to the losses, with a strong dependence on the permittivity and on the value of the local polarization.

Altogether, for the materials of interest, the quasi-Debye mechanism is the only mechanism that leads to a higher loss under field, while the other mechanisms, intrinsic and extrinsic alike are more severe in the zero field situation where the permittivity is at maximum. In this way, the quasi-Debye mechanism imposes an upper limit on the tunable performance as a function of dc field (Fig. 15). However, it should be kept in mind that the importance of Quasi-Debye loss varies from material to material, depending on the phonon damping and the strength of the fletoelectric coupling. Because of this, the losses are less field dependent in BST than in pure STO.

The effect of the addition of a second phase of a lower permittivity and loss was analyzed in terms of various composite configurations, layered structure, columnar structure, and spherical inclusions of the dielectric phase into the ferroelectric matrix. The electric field redistribution due to the introduction of the second phase was considered, while possible chemical modifications such as inter-diffusion were ignored. While the layered composite undergoes a strong reduction in the loss upon addition of a small fraction of dielectric material, the loss in the columnar and the spherical inclusion configurations are much less sensitive to the second phase addition.

Can the Commutation Quality Factor be Increased by the Addition of a Dielectric Phase? Combining the composite effects on the permittivity and the dielectric loss it was found that, the Vendik's commutation quality factor, K, cannot be appreciably increased by the introduction of a dielectric phase. On the other hand, it was found that the columnar configuration and spherical inclusions lead to a substantial reduction of the permittivity, without essential impact on the K factor (for spherical inclusion model this statement should be taken with a reservation for the limitations of the approximations used in the calculations). This may be advantageous in applications where a lower permittivity is desired. An important conclusion of the analysis is that if an improvement in the K factor is gained by adding a dielectric to the ferroelectric, the reason for that should probably be sought in chemical or microstructure effects rather than in the composite effect. To be more specific concerning this issue, one is to possess a better theory on the dielectric non-linearity of ferroelectric composites.

Dielectric Response of Tunable Ferroelectric Thin Films. The dielectric response of tunable ferroelectric thin films differs from that of bulk materials: their permittivity is often lower and the loss is higher. Not all the differences are accounted for so far.

Size effects are responsible for some differences. The ferroelectric lattice is harder near the surface in comparison to the bulk. The ferroelectric film can be therefore considered as a composite of a ferroelectric layer sandwiched between two dielectric layers of a very small thickness. The thickness of this effective dielectric layer varies depending on the measurement configuration (in-plane or out-of-plane), and it may also be sensitive to the electrode material. Depletion effects are also important in thin films. Depletion effects can be described too in terms of a layer composite model, though the in-plane and out-of-plane dielectric response will not be the same as in the previous situations. The depletion effect has not been studied yet in detail. Another competing scenario for the explanation of the size effect in films is related to the finite screening length in the electrodes ("electrode effect"). The dielectric-layer, depletio and "electrode" effects all of them can explain the thickness dependence of the out-of-plane component of dielectric permittivity of thin films, however, the reported experimental results do not suffice for the discrimination between these three possible scenarios.

Misfit strain may substantially shift the Curie temperature and modify the permittivity. This has been proven theoretically and experimentally. The effect can be as strong as to make the normally incipient ferroelectric STO be ferroelectric at room temperature. In addition, the Curie temperature for the in-plane and out-of-plane components of the permittivity should remarkably differ. Another important conclusion is that the influence of strain on losses and on the tunability

is expected to be limited to that obtained indirectly through the modification in the dielectric permittivity.

The dielectric loss in thin films is roughly one order of magnitude higher than in bulk materials. This is believed to be of extrinsic origin. A more detailed investigation revealed that, in well-prepared films (that have low loss at zero dc field), an increase of loss under dc field is observed, compatible with the Debye-loss mechanism.

Additional Practical Conclusions and Needed Work. The last but not least interesting question is how to proceed in order to evaluate the potential of ferroelectrics that have not been studied so far. For displacive type ferroelectrics the permittivity and tunability at low frequencies are indicative of these properties at MW frequencies—this eases the characterization problem. However, this is not correct for relaxor ferroelectrics which exhibit a strong frequency dispersion.

In general, the losses measured at rf are not indicative for the loss in high frequencies since the mechanisms involved are different. More information about MW loss in various ferroelectrics is needed. Thickness dependence of dielectric properties are needed for both in-plane and out-of-plane configurations. Finally very little is reported about the field dependence of MW loss—these experiments are complex to carry but are valuable for further development of the subject.

Acknowledgments

The Swiss National Science Foundation is acknowledged for financial support. Part of the work has been done within the European project MELODY—The Swiss Office of Science and Education is acknowledged for the financial support of the authors' participation in this project.

The authors are indebted to Dr. Stephen K. Streiffer for his numerous suggestions on the improvement of the manuscript.

Notes

1. The dielectric anomaly in order-disorder ferroelectrics suffers from very strong frequency dispersion already in the radio frequency range.
2. In this article we do not discuss the critical phenomena which may impact the linear temperature dependence of α very close to T_0 since the available experimental data do not suggest that this effect is substantial in ferroelectrics.
3. A comprehensive overview of the linear dielectric response of ferroelectric composites was offered by Hudak et al. [42]. The problem of the tunability of ferroelectric composite was theoretically approach by Liou and Chiou [43]. However, the analysis offered in this paper is based on many approximation and assumptions. For these reason in the present paper, we will not discuss the results of this work.
4. In Section 3.1.1. the difference $\varepsilon_b - 1$ was neglected because for the situation treated in that Section this approximation leads only to a small (about $\varepsilon_b/\varepsilon_f \ll 1$) inaccuracy in the results. In Eqs. (3.15) and (3.23) the contribution of ε_b is also neglected to within the same accuracy.
5. Actually, the ε-dependence in Eq. (3.28) was derived only for the two aforementioned cases of strong and vanishing dispersion of the optical mode; for the case of an arbitrary dispersion, the dependence $A \propto \varepsilon^x$ with $2.5 < x < 5$ should be considered as an interpolation.
6. This does not contradict the expected leading role of the 3-quantum contribution in this frequency range. The point is that, in this range, the these functional dependences for the 3-quantum and 4-quantum contributions (including Vendik's model) are very close, though the 3-quantum one is expected to be numerically larger.
7. This is not the only way to address this problem, for an alternative description see Ref. [42].
8. To within $h/g \ll 1$.
9. Actually the correlation length is anisotropic, in other words the parameter κ (from Eq. (3.52)) is different for different orientations of the polarization and its gradient. Since here we are interested in an estimate, this anisotropy will be neglected.
10. This can also be shown by considering Eq. (3.59) with the nonlinear term βP^3.
11. The misfit strain may be also be affected by the formation of the misfit dislocation in the already crystallized film (see e.g. the work by Speck and Pompe [92]. We will not address this issue in the paper, since this effect does not seem to be of practical importance for the tunable thin films.
12. This statement holds for the case where both ac and dc fields are parallel to a cubic axis of the material, in the general situation it may not be the case. Detailed information on the anisotropy of the dielectric non-linearity can be found in Ref. [129].
13. Elevated values of the loss in the vicinity of T_0 does not look to be a limiting factor for applications of the material in tunable devices. One can show that, in this temperature range, elevated values of the tunability will probably compensate the loss increase.
14. Judging from the non-monotonic concentration dependence of the permittivity shown in Fig. 31(d), at RT, the samples of pure BST 60/40 studied in this work were in the ferroelectric phase whereas some Wt.1% mixing with the oxide shifts the transition temperature below RT. This explains a high loss level in pure material and a strong reduction of the loss with doping, which are shown in Fig. 33(d).
15. Here and further the term "*thin film*" means the film which is thinner than 2–3 μm.
16. The origin of the anisotropy of the in-plane lattice constants ($a \neq b$) of the films deposited onto cubic MgO substitutes remains unclear.

17. This can be readily checked using Eq. (3.74) and the materials parameters of STO listed in Section 3.4.3.
18. The interpretation of these data is not clear. According to the authors of the paper the measured increasing frequency dependence of the loss tangent may be an artifact of the measurement setup.

References

1. M.D. Domenico, D.A. Johnson, and R.H. Pantell, *Journal of Applied Physics*, **33**, 1697 (1962).
2. O.G. Vendik, E.K. Hollmann, A.B. Kozyrev, and A.M. Prudan, *Journal of Superconductivity*, **12**, 325 (1999).
3. M.J. Lancaster, J. Powell, and A. Porch, *Supercund. Sci. Technol.*, **11**, 1323 (1998).
4. X.X. Xi, H.C. Li, W.D. Si, A.A. Sirenko, I.A. Akimov, J.R. Fox, A.M. Clark, and J.H. Hao, *Journal of Electroceramics*, **4**, 393 (2000).
5. F.A. Miranda, F.W. Van Keuls, R.R. Romanofsky, C.H. Mueller, S. Alterovitz, and G. Subramanyam, *Integrated Ferroelectrics*, **42**, 131 (2001).
6. V.L. Gurevich and A.K. Tagantsev, *Adv. Phys.*, **40**, 719 (1991).
7. S. Gevorgian, E. Carlsson, E. Wikborg, and E. Kollberg, *Intergrated Ferroelectrics*, **22**, 245 (1998).
8. S.A. Wolf and D. Treger, *Integrated Ferroelectrics*, **42**, 39 (2001).
9. O.G. Vendik, *Ferroelectrics at Microwaves (in Russian)* (Sovyetskoye Radio, Moscow, 1979).
10. N.M. Alford, S.J. Penn, A. Templeton, X. Wang, J.C. Gallop, N. Klein, C. Zuccaro, and P. Filhol, *IEE Colloquium on Electro-Technical Ceramics—Processing, Properties and Applications*, 9/1 (1997).
11. S.J. Penn, N. McNAlford, A. Templeton, N. Klein, J.C. Gallop, P. Filhol, and X. Wang, *IEE Colloquium on Advances in Passive Microwave Components*, 6/1 (1997).
12. G. Rupprecht and R.O. Bell, *Physical Review*, **135**, A748 (1964).
13. A. Linz, *Physical Review*, **91**, 753 (1953).
14. G.A. Smolenskii and V.A. Isupov, *Zhurnal Tekhnicheskoi Fiziki*, **24**, 1375 (1954).
15. G.S. Khizha, I.B. Vendik, and E.A. Serebryakova, *Microwave Phase Shifters Based on p-i-n Diodes (in Russian)* (Radio i Svyas, Moscow, 1984).
16. I. Vendik, O. Vendik, and E. Kollberg, *IEEE Trans. Microwave Theory and Techniques*, **48**, 802 (2000).
17. A. Deleniv, A. Eriksson, and S. Gevorgian, *2002 IEEE MTT-S Digest*, 197 (2002).
18. J. Rao, D. Patel, and V. Krichevsky, *IEEE Trans. Antennas and Propagation*, **47**, 458 (1999).
19. F.D. Flaviis, N.G. Alexopoulos, and O.M. Stafsudd, *IEEE Trans. Microwave Theory Tech.*, **45**, 963 (1997).
20. O.G. Vendik, L.T. Ter-Martirosyan, A.I. Dedyk, S.F. Karmanenko, and R.A. Chakalov, *Ferroelectrics*, **144**, 33 (1993).
21. A. Kozyrev, V. Osadchy, A. Pavlov, and L. Sengupta, *IEEE MTT-S Digest*, 1355 (2000).
22. B. Acikel, T.R. Taylor, P.F. Hansen, J.S. Speck, and R.A. York, *IEEE Microwave and Wireless Components Letters*, **12**, 237 (2002).
23. A. Kozyrev, A. Ivanov, A. Prudan, O. Soldatenkov, E. Hollmann, V. Loginov, D.S. Ginley, and T. Rivkin, *Integrated Ferroelectrics*, **24**, 287 (1999).
24. V. Sherman, K. Astafiev, N. Setter, A. Tagantsev, O. Vendik, I. Vendik, S. Hoffmann-Eifert, U. Bottger, and R. Waser, *IEEE Microwave and Wireless Components Letters*, **11**, 407 (2001).
25. O.G. Vendik, I.B. Vendik, and V.O. Sherman, *Integrated Ferroelectrics*, **43**, 81 (2002).
26. I. Vendik, O. Vendik, E. Kollberg, and V. Sherman, *IEEE Transactions on Microwave Theory and Techniques*, **47**, 1553 (1999).
27. F.A. Miranda, G. Subramanyam, F.W.V. Keuls, R.R. Romanofsky, J.D. Warner, and C.H. Mueller, *IEEE Trans. on Microwave Theory and Techniques*, **48**, 1181 (2000).
28. A. Kozyrev, A. Ivanov, V. Keis, M. Khazov, V. Osadchy, T. Samoilova, A. Pavlov, G. Koepf, C. Mueller, D. Galt, and T. Rivkin, *IEEE MTT-S Digest*, **2**, 985 (1998).
29. V. Keis, A. Kozyrev, M. Khazov, J. Sok, and J. Lee, *Electronics Letters*, **34**, 1107 (1998).
30. B.H. Moeckly and Y. Zhang, *IEEE Transaction on Applied Superconductivity*, **11**, 450 (2001).
31. I. Vendik, O. Vendik, V. Pleskachev, A. Svishchev, and R. Woerdenweber, *IEEE MTT-S Digest*, **3**, 1461 (2001).
32. T.B. Samoilova, K.F. Astafiev, T. Rivkin, and D.S. Ginley, *Journal of Applied Physics*, **90**, 5703 (2001).
33. J.G. Colom, R.A. Rodrigues-Solis, J. Almodovar, and M. Castaneda, *Integrated Ferroelectrics*, **42**, 313 (2001).
34. C. Weil, P. Wang, H. Downar, J. Wenger, and R. Jakoby, *Frequenz*, **54**, 250 (2000).
35. J.O. Gentner, P. Gerthsen, N.A. Schmidt, and R.E. Send, *J. Appl. Phys.*, **49**, 4585 (1978).
36. V.G. Vaks, *Introduction to the Microscopic Theory of Ferroelectrics* (Nauka, Moscow, 1973).
37. J.H. Barrett, *Phys. Rev.*, **86**, 118 (1952).
38. O.G. Vendik, L.T. Ter-Martirosyan, and S.P. Zubko, *J. Appl. Phys.*, **84**, 993 (1998).
39. O.G. Vendik, *Sov. Phys. Solid State*, **14**, 849 (1972).
40. O.G. Vendik and S.P. Zubko, *J. Appl. Phys.*, **82**, 4475 (1997).
41. O.G. Vendik, S.P. Zubko, and M.A. Nikol'ski, *J. Appl. Phys.*, **92**, 7448 (2002).
42. O. Hudak, I. Rychetsky, and J. Petzelt, *Ferroelectrics*, **208**, 429 (1998).
43. J.W. Liou and B.S. Chiou, *Journal of Physics-Condensed Matter*, **10**, 2773 (1998).
44. M. Vollman and R. Waser, *J. Am. Ceram. Soc.*, **77**, 235 (1994).
45. K.F. Astafiev, V.O. Sherman, A.K. Tagantsev, and N. Setter, *Journal of the European Ceramic Society*, **23**, 2381 (2003).
46. L.D. Landau, E.M. Lifshitz, and L.P. Pitaevskii, *Electrodynamics of Continuous Media* (Butterworth-Heinemann, 1995).
47. V. Sherman, A. Tagantsev, K. Astafiev, and N. Setter, (2004) to be published.
48. J.E. Sipe and R.W. Boyd, *Physical Review A*, **46**, 1614 (1992).
49. K.W. Yu, P.M. Hui, and D. Stroud, *Physical Review B*, **47**, 14150 (1993).
50. V.S. Vinogradov, *Fiz. Trerd. Tela*, **4**, 712 (1962).
51. V.L. Gurevich, *Fiz. Tverd. Tela*, **21**, 3453 (1979).
52. A.K. Tagantsev, *Sov. Phys. JETP*, **53**, 555 (1981).

53. K.A. Subbaswamy and D.L. Mills, *Phys. Rev. B*, **33**, 4213 (1986).
54. A.K. Tagantsev, *Sov. Phys. JETP*, **59**, 1290 (1984).
55. A.K. Tagantsev, J. Petzelt, and N. Setter, *Solid State Commun*, **87**, 1117 (1993).
56. V.L. Gurevich, *Transport in Phonon Systems* (North-Holland, Amsterdam, 1986).
57. R. Zurmulen, J. Petzelt, S. Kamba, G. Kozlov, A. Volkov, B. Gorshunov, D. Dube, A. Tagantsev, and N. Setter, *J. Appl. Phys*., **77**, 5351 (1995).
58. I.M. Buzin, *Vestn. Mosk. Univ. Fiz. Astron*., **18**, 70 (1977).
59. R. Stolen and K. Dransfeld, *Phys. Rev*., **139**, 1295 (1965).
60. B.Y. Balagurov, V.G. Vaks, and B.I. Shklovskii, *Fiz. Tverd. Tela*, **12**, 89 (1970).
61. O.G. Vendik, *Sov. Phys. Solid State*, **17**, 1096 (1975).
62. G.J. Cooms and R.A. Cowley, *J. Phys. C*, **6**, 121 (1973).
63. A.K. Tagantsev, *Sov. Phys. JETP*, **50**, 948 (1979).
64. C. Kittel, *Introduction to Solid State Physics* (John Wiley & Sons, Inc., New York, London, 1971).
65. A. Tagantsev, *Appl. Phys. Lett*., **76**, 1182 (2000).
66. A.K. Tagantsev and K.F. Astafiev, *Integrated Ferroelectrics*, **39**, 251 (2001).
67. K.F. Astafiev and A.K. Tagantsev, *Proc. of St. Petersburg Electrotech. Univ., Ser. Solid State Phys. And Electronics [Izvestiya LETI]*, 204 (2002).
68. L.C. Sengupta, S. Stowell, E. Ngo, M.E. O'Day, and R. Lancto, *Integrated Ferroelectrics*, **8**, 821 (1995).
69. E. Schlöman, *Phys. Rev*., **135**, A413 (1964).
70. O.G. Vendik and L.M. Platonova, *Sov. Phys. Solid State*, **13**, 1353 (1971).
71. B.M. Garin, *Sov. Phys. Solid State*, **32**, 1917 (1990).
72. C.J. Brennan, *Integrated Ferroelectrics*, **7**, 93 (1995).
73. J.G. Simmons, *J. Phys. Chem. Solids*, **32**, 2581 (1971).
74. A.K. Jonscher, *Universal Relaxation Law* (Chelsea Dielectrics Press, London, 1996).
75. J.D. Baniecki, R.B. Laibowitz, T.M. Shaw, P.R. Duncombe, D.A. Neumayer, D.E. Kotecki, H. Shen, and Q.Y. Ma, *Appl. Phys. Lett*., **72**, 498 (1998).
76. R. Waser, in *Science and Technology of Electroceramic Thin Films*, vol. 284, *NATO ASI; Series E:Applied Science*, edited by O. Auciello and R. Waser (1995), p. 223.
77. Y. Fukuda, K. Numata, K. Aoki, and A. Nishimura, *Jpn. J. Appl. Phys*., **35**, 5178 (1996).
78. J. Petzelt, T. Ostapchuk, I. Gregora, I. Rychetsk, S. Hoffmann-Eifert, A.V. Pronin, Y. Yuzyuk, B.P. Gorshunov, S. Kamba, V. Bovtun, J. Pokorn, M. Savinov, V. Porokhonskyy, D. Rafaja, P. Vanek, A. Almeida, M.R. Chaves, A.A. Volkov, M. Dressel, and R. Waser, *Phys. Rev. B*, **64**, 184111 (2001).
79. L.C. Sengupta, S. Stowell, E. Ngo, and S. Sengupta, *Integrated Ferroelectrics*, **13**, 203 (1996).
80. M. Jain, S.B. Majumder, R.S. Katiyar, D.C. Agrawal, and A.S. Bhalla, *Applied Physics Letters*, **81**, 3212 (2002).
81. R. Kretschmer and K. Binder, *Phys. Rev. B*, **20**, 1065 (1979).
82. O.G. Vendik and S.P. Zubko, *J. Appl. Phys*., **88**, 5343 (2000).
83. I.P. Batra and B.D. Silverman, *Solid State Communications*, **11**, 291 (1972).
84. R.D. Tilley and B. Zeks, *Ferroelectrics*, **134**, 313 (1992).
85. J.M. Ziman, *Principles of the Theory of Solids* (Cambridge University Press, Cambridge, 1972), p. 435.
86. A.K. Tagantsev, E.Courtens, and L. Arzel, *Phys. Rev. B*, **64**, 224107 (2001).
87. Y. Yamada, G. Shirane, and A. Linz, *Phys. Rev*., **177**, 848 (1969).
88. A.K. Tagantsev and I.A. Stolichnov, *Appl. Phys. Lett*., **74**, 1326 (1999).
89. A.K. Tagantsev, C. Pawlaczyk, K. Brooks, and N. Setter, *Integrated Ferroelectrics*, **4**, 1 (1994).
90. A.M. Bratkovsky and A.P. Levanyuk, *Phys. Rev. B*, **61**, 15042 (2000).
91. R. Waser and M. Klee, *Integrated Ferroelectrics*, **2**, 23 (1992).
92. J.S. Speck and W. Pompe, *J. Appl. Phys*., **76**, 466 (1994).
93. S.K. Streiffer, C. Basceri, C.B. Parker, S.E. Lash, and A.I. Kingon, *J. Appl. Phys*., **86**, 4565 (1999).
94. N.A. Pertsev, A.G. Zembilgotov, S. Hoffman, R. Waser, and A.K. Tagantsev, *J. Appl. Phys*., **85**, 1698 (1999).
95. Landolt-Bornstein, *Numerical Data and Functional Relationships in Science and Technology* (Springer, New York, 1981), Vol. New Series Vol. III/29a,b.
96. N.A. Pertsev, A.G. Zembilgotov, and A.K. Tagantsev, *Phys. Rev. Lett*., **80**, 1988 (1998).
97. A.K. Tagantsev, N.A. Pertsev, P. Muralt, and N. Setter, *Phys. Rev. B*, **65**, 012104 (2002).
98. N.A. Pertsev, A.K. Tagantsev, and N. Setter, *Phys. Rev. B*, **61**, R825 (2000).
99. R.E. Collin, *Fondations for Microwave Engineering* (McGraw-Hill, New York, 1992), p. 924.
100. D.C. Dube, J. Baborowski, P. Muralt, and N. Setter, *Applied Physics Letters*, **74**, 3546 (1999).
101. A. Tombak, J.P. Maria, F. Ayguavives, Z. Jin, G.T. Stauf, A.I. Kingon, and A. Mortazawi, *IEEE Microwave and Wireless Components Letters*, **12**, 3 (2002).
102. T. Ayguavives, A. Tombak, J.P. Maria, G.T. Stauf, C. Ragaglia, J. Roeder, A. Mortazawi, and A. Kingon, *Proc. 12th ISAF*, **1**, 365 (2000).
103. S. Li, J. Sheen, Q.M. Zhang, S.-J. Jang, A.S. Bhalla, and L.E. Cross, *Proc. 8th ISAF*, 480 (1992).
104. S.S. Gevorgian, T. Martinsson, P.L.J. Linner, and E.L. Kollberg, *IEEE Trans. on Microwave Theory And Techniques*, **44**, 896 (1996).
105. O. Vendik, S. Zubko, and M. Nikolski, *Technical Physics*, **44**, 349 (1999).
106. A.N. Deleniv, *Technical Physics*, **44**, 356 (1999).
107. M. Sucher and J. Fox, *Handbook of Microwave Measurements* (Interscience, New York, 1963), vol. 2.
108. C. Krowne, S. Kirchoefer, and J. Pond, *IEEE MTT-S Digest*, 1193 (2000).
109. E. Carlsson and S. Gevorgian, *IEEE Transactions on Microwave Theory and Techniques*, **47**, 1544 (1999).
110. A.T. Findikoglu, Q.X. Jia, C. Kwon, B.J. Gibbons, K.O. Rasmussen, Y. Fan, D.W. Reagor, and A.R. Bishop, *Materials Research Sosiety Symposium Proceedings*, **603**, 27 (2000).
111. A.T. Findikoglu, D.W. Reagor, K.O. Rasmussen, A.R. Bishop, N. Gronbech-Jensen, Q.X. Jia, Y. Fan, C. Kwon, and L.A. Ostrovsky, *Journal of Applied Physics*, **86**, 1558 (1999).
112. B.W. Hakki and P.D. Coleman, *IRE Trans. on Microwave Theory and Technique*, 402 (1960).
113. J. Krupka, *5th International Conference on Dielectric Materials, Measurements and Applications*, 322 (1988).

114. J. Delaballe, P. Guillon, and Y. Garault, *AUE, Electronics and Communication*, **35**, 80 (1981).
115. O.G. Vendik, E. Kollberg, S.S. Gevorgian, A.B. Kozyrev, and O.I. Soldatenkov, *Electronics Letters*, **31**, 654 (1995).
116. A. Eriksson, P. Linner, and S. Gevorgian, *IEE Proc.-Microw. Antennas and Propag.*, **148**, 51 (2001).
117. J. Watkins, *Electronics Letters*, **5**, 524 (1969).
118. D. Kajfez, *IEEE Trans. on Microwave Theory And Techniques*, **42**, 1149 (1994).
119. S. Gevorgian, E. Carlsson, P. Linner, E. Kollberg, O. Vendik, and E. Wikborg, *IEEE Trans. on microwave Theory And Techniques*, **44**, 1738 (1996).
120. R. Thomas and D.C. Dube, *Electronics Letters*, **33**, 218 (1997).
121. D.C. Dube, *Ferroelectrics*, **225**, 141 (1999).
122. Y.G. Wang, M.E. Reeves, W. Chang, H.J.S., and W. Kim, *Materials Research Sosiety Symposium Proceedings*, **603**, 289 (2000).
123. D.E. Steinhauer, C.P. Vlahacos, F.C. Wellstood, S.M. Anlage, C. Canedy, R. Ramesh, A. Stanishevsky, and J. Melngailis, *Appl. Phys. Lett.*, **75**, 3180 (1999).
124. D. Galt, J. Price, J. Beall, and T. Harvey, *IEEE Trans. on Applied Superconductivity*, **5**, 2575 (1995).
125. A.B. Kozyrev, V.N. Keis, G. Koepf, R. Yandrofski, O.I. Soldatenkov, K.A. Dudin, and D.P. Dovgan, *Microelectronic Engineering*, **29**, 257 (1995).
126. T. Sakudo and H. Unoki, *Phys Rev Lett*, **26**, 851 (1971).
127. M.A. Saifi and L.E. Cross, *Phys. Rev. B*, **2**, 677 (1970).
128. J. Hemberger, P. Lunkenheimer, R. Viana, R. Bohmer, and A. Loidl, *Phys. Rev. B*, **52**, 13159 (1995).
129. G.V. Belokopytov, *Ferroelectrics*, **168**, 69 (1995).
130. J. Krupka, R.G. Geyer, M. Kuhn, and J.H. Hinken, *IEEE Transactions on Microwave Theory and Techniques*, **42**, 1886 (1994).
131. F. Jona and G. Shirane, *Feroelectric Crystals* (Macmillan, New York, 1962).
132. L. Arzel, PhD thesis, University of Montpellier II, Montpellier, 2001.
133. J. Harada, J. Axe, and G. Shirane, *Phys. Rev. B*, **4**, 155 (1971).
134. E. Ngo, P.C. Joshi, M.W. Cole, and C.W. Hubbard, *Appl. Phys. Lett.*, **79**, 248 (2001).
135. L. Wu, S. Wu, F.-C. Chang, Y.-T. Shen, and Y.-C. Chen, *J. of Materials Science*, **35**, 5945 (2000).
136. D.M. Potrepka, S.C. Tidrow, and A. Tauber, *Integrated Ferroelectrics*, **42**, 97 (2002).
137. L.C. Sengupta and S. Sengupta, *Mat. Res. Innovat.*, 278 (1999).
138. B. Su, J.H. Holmes, and T.W. Button, *J. Am. Ceram. Soc.* (2003) (submitted).
139. C. Ang, A.S. Bhalla, R. Guo, and L.E. Cross, *J. Appl. Phys.*, **90**, 2465 (2001).
140. M. Daglish, M. Presland, and S. Batbedat, *Integrated Ferroelectrics*, **39**, 339 (2001).
141. D. Li and M.A. Subramanian, *Soild State Science*, **2**, 507 (2000).
142. S. Triebwasser, *Phys. Rev.*, **114**, 63 (1959).
143. B. Cristopher, C.B. DiAntonio, and S.M. Pilgrim, *J. Am. Ceram. Soc.*, **84**, 2547 (2001).
144. P. Debely, P. Gunter, and H. Arend, *Am. Ceram. Soc. Bull.*, **58**, 606 (1979).
145. J. Venkatesh et al. (unpublished).
146. A. Kozyrev, A. Ivanov, T. Samoilova, O. Soldatenkov, K. Astafiev, and L.C. Sengupta, *Journal of Applied Physics*, **88**, 5334 (2000).
147. A. Outzourhit, J.U. Trefny, T. Kito, B. Yarar, A. Naziripour, and A.M. Hermann, *Thin Solid Films*, **259**, 218 (1995).
148. H.-C. Li, W. Si, A.D. West, and X.X. Xi, *Appl. Phys. Lett.*, **73**, 464 (1998).
149. C.B. Parker, J.P. Maria, and A.I. Kingon, *Applied Physics Letters*, **81**, 340 (2002).
150. C. Basceri, S.K. Streiffer, A.I. Kingon, and R. Waser, *Journal of Applied Physics*, **82**, 2497 (1997).
151. J. Bellotti, E.K. Akdogan, A. Safari, W. Chang, and S. Kirchoefer, *Integrated Ferroelectrics*, **49**, 113 (2002).
152. D. Schlom (2003) (unpublished).
153. W. Chang, J.S. Horwitz, A.C. Carter, J.M. Pond, S.W. Kirchoefer, C.M. Gilmore, and D.B. Chrisey, *Appl. Phys. Lett.*, **74**, 1033 (1999).
154. C.M. Carlson, T.V. Rivkin, P.A. Parilla, J.D. Perkins, D.S. Ginley, A.B. Kozyrev, V.N. Oshadchy, and A.S. Pavlov, *Appl. Phys. Lett.*, **76**, 1920 (2000).
155. K.F. Astafiev, V.O. Sherman, A.K. Tagantsev, N. Setter, P.K. Petrov, T. Kaydanova, D.S. Ginley, S. Hoffmann-Eifert, U. Bottger, and R. Waser, *Integrated Ferroelectrics* (2003) (submitted).
156. P.K. Petrov, Z.G. Ivanov, and S.S. Gevorgyan, *Materials Science and Engineering a-Structural Materials Properties Microstructure and Processing*, **288**, 231 (2000).
157. Z.G. Ban and S.P. Alpay, *Journal of Applied Physics*, **91**, 9288 (2002).
158. D. Fuchs, C.W. Schneider, R. Schneider, and H. Rietschel, *J. Appl. Phys.*, **85**, 7362 (1999).
159. O.G. Vendik and L.T. Ter-Martirosyan, *J. Appl. Phys.*, **87**, 1435 (2000).
160. J.H. Chen, C.L. Lia, K. Urban, and C.L. Chen, *Applied Physics Letters*, **81**, 1291 (2002).
161. G. Rupprecht and R.O. Bell, *Physical Review*, **125**, 1915 (1962).
162. M.J. Dalberth, R.E. Stauber, J.C. Price, C.T. Rogers, and D. Galt, *Appl. Phys. Lett.*, **72**, 507 (1998).
163. Y. Lemaitre, B. Marcilhac, D. Mansart, J. Siejka, and J.C. Mage, *Physica C*, **372**, 667 (2002).
164. K.F. Astafiev et al. (2003) (unpublished).
165. S. Razumov, A. Tumarkin, O. Buslov, M. Gaidukov, A. Gagarin, A. Ivanov, A. Kozyrev, Y.W. Song, and C.S. Park, *Integrated Ferroelectrics*, **39**, 1317 (2001).
166. P.C. Joshi and M.W. Cole, *Appl. Phys. Lett.*, **77**, 289 (2000).
167. M. Bruel, *Electronics Letters*, **31**, 1201 (1995).
168. F.J. Kub, K.D. Hobart, J.M. Pond, and S.W. Kirchoefer, *Electronics Letters*, **35**, 477 (1999).
169. H.N. Al-Shareef, D. Dimos, M.V. Raymond, and R.W. Schwartz, *Journal of Electroceramics*, **1**, 145 (1997).
170. M. Hafid, G.E. Kugel, A. Kania, K. Roleder, and M.D. Fontana, *Journal of Physics-Condensed Matter*, **4**, 2333 (1992).
171. J.H. Koh and A. Grishin, *Applied Physics Letters*, **79**, 2234 (2001).